Chapter 5

Results and Discussion

5.1. HPLC analytical method

As the HPLC method used for quantification of RSV in our study is well established, we are reporting only correlation coefficient (R^2) value, accuracy and precision [174]. The HPLC calibration curve of RSV in rat plasma was found to be linear from 10 to 5000 ng/ml with the regression equation of y = 49.264x - 889.57 and correlation coefficient (R^2) value of 0.9991. The precision and accuracy results are shown in Table 5.1. Intra-day and inter-day precision of the methods were less than 15%. The values of precision and accuracy were acceptable as per the international recommendations [174]. Calibration curves in mobile phase, brain, lungs, liver, spleen and kidney homogenates of rat were also found to be linear over 100 to 5000 ng/mL. HPLC chromatogram of RSV in rat plasma and calibration curve in plasma, mobile phase, brain, lungs, liver, spleen and kidney homogenates of rat are shown in Figure 5.1.

Table 5.1. Accuracy and precision of RSV spiked in rat plasma samples (n=6)

Spiked concentration	Measured concentration (Mean±SD)		Accuracy %		Precision (%RSD)	
10	9.5±1.34	9.25±2.76	95	92.5	8.31	9.83
2000	1972.5±49.16	1912.67±76.94	98.625	95.6335	2.49	4.02
5000	4897±102.49	4768.94±143.67	97.94	95.3788	2.09	3.01

% RSD (relative standard deviation) = (SD/mean) x 100

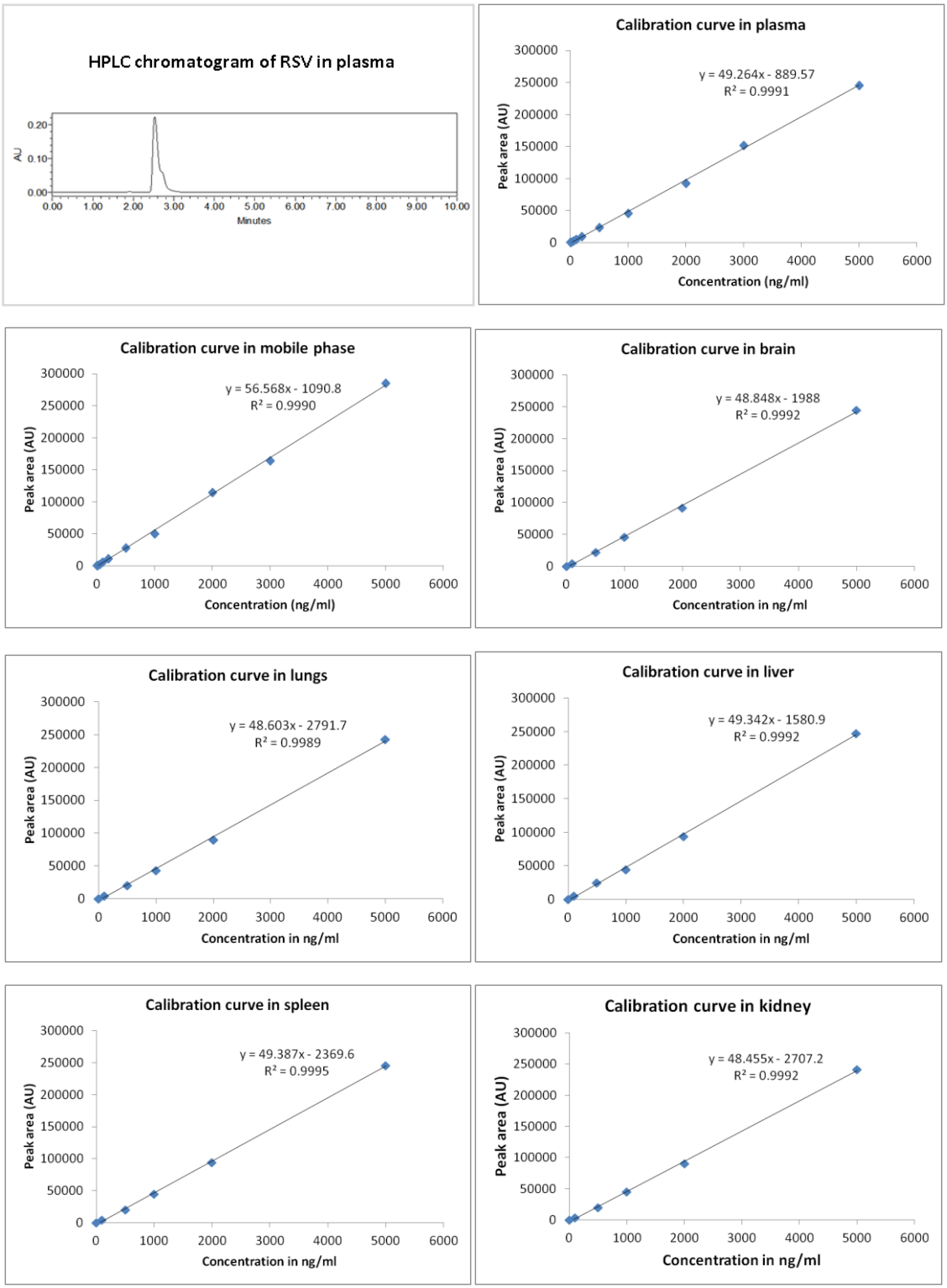

Figure 5.1. HPLC chromatogram of RSV in plasma and calibration curve in plasma, mobile phase, brain, lungs, liver, spleen and kidney

5.2. Solid lipid nanoparticles

RSV is highly lipophilic and poorly water soluble in nature (solubility in water = 30 mg/L; log P = 3.06). SLN are the nanocarriers made up of biocompatible lipids (lipophilic). RSV molecules can be accommodated in to SLN due to lipophilic nature. The effect of TPGS and DSPE PEG 2000 on pharmacokinetics and brain distribution potential and cytotoxicity of RSV loaded SLN through intravenous administration was not investigated. Therefore, RSV loaded TPGS and DSPE PEG 2000 coated SLN formulations were formulated for improving biological half life and passive brain accumulation.

5.2.1. Particle size, polydispersity index and zeta potential

The mean particle sizes of various RSV-TPGS-SLN batches varied from 128.6±16.11 nm to 429.1±24.75 nm as shown in Figure 5.2. As the drug to lipid ratio varied from 1:5 to 1:15, particle size was statistically increasing in all levels of sonication time ($p<0.05$). For instance, particle size of drug to lipid ratio of 1:5, 1:10 and 1:15 at 1 min of sonication time (RSV-TPGS-SLN batches 1, 4 and 7) was found to be 196.3±13.79, 265.4±17.18 and 423.9±25.09 nm, respectively. As the sonication time increased from 1 to 3 min, the particle size was decreased significantly at all sets of drug to lipid ratio (1:5, 1:10 and 1:15) ($p<0.05$). The decrease in particle size is due to sonication energy which breakdown nanostructures during preparation. While further increasing sonication time from 3 to 5 min, particle size was found to be increased significantly ($p<0.05$). The increase in particle size may be due to coalescence or aggregation of lipids resulted from excess of sonication time [183]. Polydispersity index of RSV-TPGS-SLN batches were

varied from 0.241±0.11 to 0.486±0.12. Zeta potential varied from -6.07±1.49 to -19.64±2.03 mV. No trend was observed in polydispersity index and zeta potential (Table 5.2).

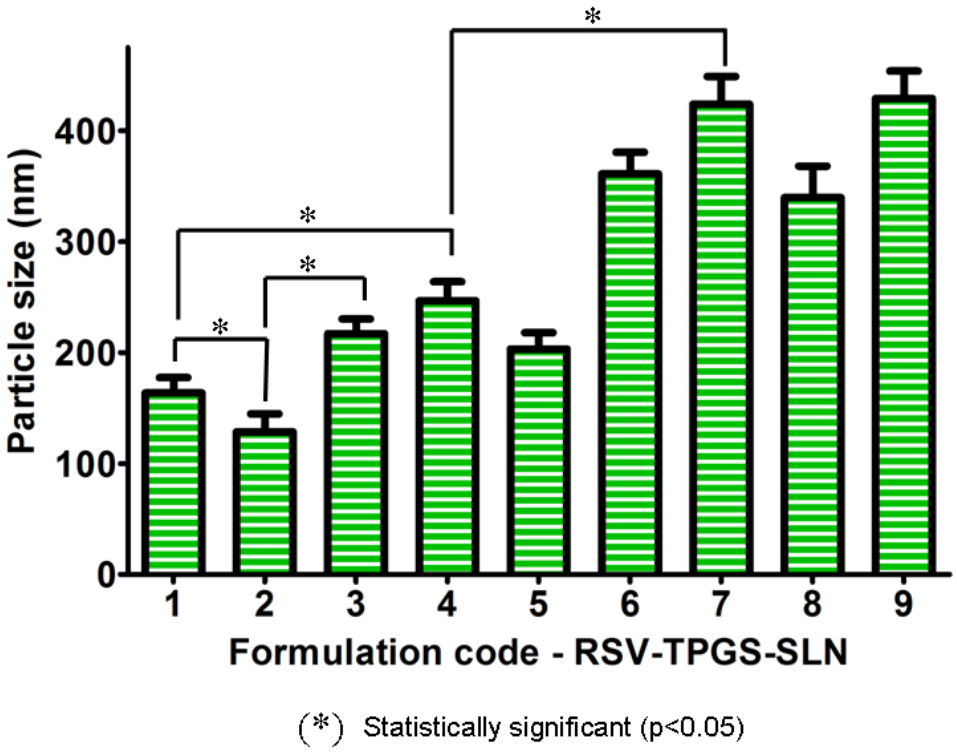

Figure 5.2. Particle size of various batches of RSV-TPGS-SLN. Values are represented as mean±SD (n=3).

Table 5.2. Polydispersity index and zeta potential of various batches of RSV-TPGS-SLNs

Formulation code	Polydispersity index	Zeta potential (mV)
RSV-TPGS-SLN 1	0.486±0.12	-10.77±1.02
RSV-TPGS-SLN 2	0.43±0.09	-10.59±0.94
RSV-TPGS-SLN 3	0.241±0.11	-9.4±1.24
RSV-TPGS-SLN 4	0.462±0.15	-11.78±1.03
RSV-TPGS-SLN 5	0.263±0.12	-10.5±2.94
RSV-TPGS-SLN 6	0.358±0.76	-9.44±1.59
RSV-TPGS-SLN 7	0.311±0.14	-19.64±2.03
RSV-TPGS-SLN 8	0.277±0.09	-11.91±0.97
RSV-TPGS-SLN 9	0.347±0.15	-6.07±1.49

5.2.2. Entrapment efficiency

Entrapment efficiency of RSV-TPGS-SLN formulations varied from 38.75±5.64 to 74.42±7.67% as shown in Figure 5.3. As the drug to lipid ratio varied from 1:5 to 1:10, the entrapment efficiency was found to be increased at all levels of sonication times ($p<0.05$). For an instance, when the drug to lipid ratio was varied from 1:5 to 1:10, the entrapment efficiency was found to be increased from 49.28±2.67 to 70.18±5.19% at 3 min sonication time. Further increase in concentration of lipid (drug to lipid ratio varied from 1:10 to 1:15) did not show such increment in entrapment efficiency. For example, entrapment efficiency was changed from 70.18±5.19 to 71.75±5.67% at 3 min of sonication. These results suggest that the drug to lipid ratio 1:10 is sufficient enough to

accommodate maximum number of RSV molecules in SLN matrix. The higher entrapment efficiency may be due to the high lipid concentration that resulted in housing of more RSV molecules (lipophilic in nature) at the interspaces of hydrophobic lipid matrix. The lesser entrapment efficiency of RSV-TPGS-SLN formulations having 1:5 drug to lipid ratio may be due to saturation of lipid matrix interspaces with lesser number of RSV molecules. The formulations having drug to lipid ratio 1:15 failed to improve the partition of RSV molecules in to lipid matrix during formation of nanoparticles which may be the reason for insignificant increase in entrapment efficiency from the formulations having drug to lipid ratio 1:10. With increase in sonication time, entrapment efficiency did not changed significantly in all levels of drug to lipid ratio ($p>0.05$).

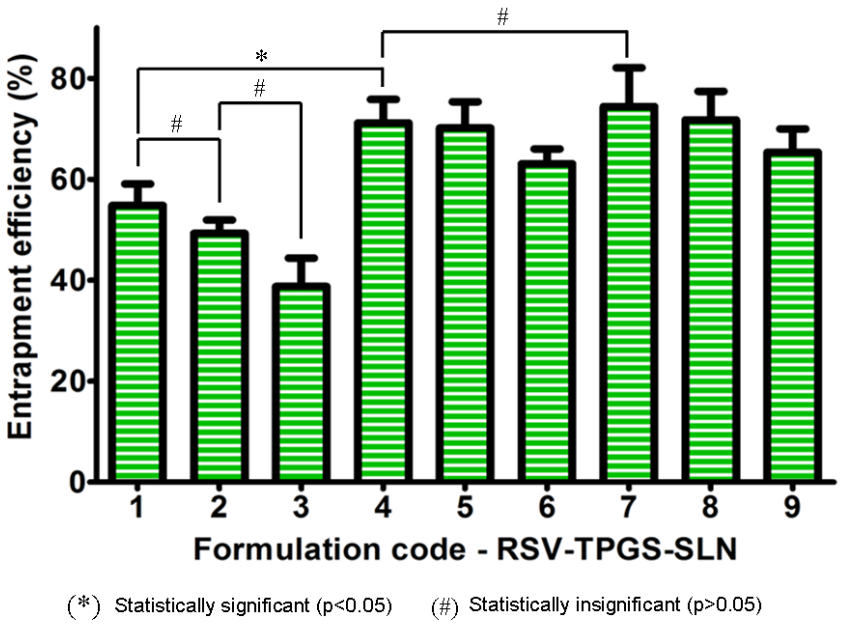

Figure 5.3. Entrapment efficiency of various batches of RSV-TPGS-SLN. Values are represented as mean±SD (n=3).

5.2.3. Selection of best formulation

RSV-TPGS-SLN 5 having lower particle size of 203.1±14.91 nm, narrow polydispersity index of 0.263±0.12 and higher entrapment efficiency of 70.18±5.19% was selected as optimized formulation for further investigations. RSV-PEG-SLN prepared using similar composition of RSV-TPGS-SLN 5 by replacing TPGS with DSPE PEG 2000 showed particle size of 125.95±12.09 nm, polydispersity index of 0.386±0.04 and entrapment efficiency of 74.67±4.76%. Zeta potential of optimized RSV-TPGS-SLN 5 and RSV-PEG-SLN was found to be -10.5±2.94 and -24.43±3.27 mV, respectively.

5.2.4. Shape of SLN formulations

TEM micrographs of both RSV-TPGS-SLN and RSV-PEG-SLN showed spherical shape (Figure 5.4. (a) and (b), respectively). As the RSV-TPGS-SLN and RSV-PEG-SLN were proposed to be used in the treatment of brain cancer, the mean particle size was optimized to be suitable for passive brain targeting. Intercellular gap between the cancer cells in most of the solid tumours was found to be between 380 and 780 nm. Accordingly, nanoparticles of 100 to 300 nm in size can be easily extravasate through these intercellular gaps [184]. The size of optimized RSV-TPGS-SLN and RSV-PEG-SLN will be suitable for extravasation through these passageways and accumulate at tumour site via enhanced permeability and retention (EPR) effect.

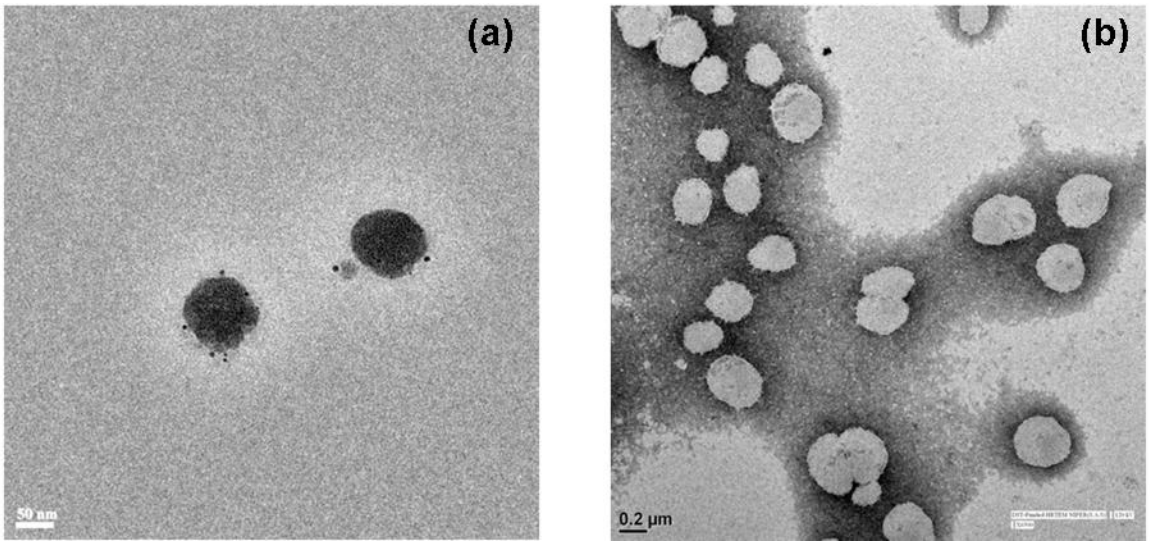

Figure 5.4. Transmission electron microscope images of optimized batch of (a) RSV-TPGS-SLN (b) RSV-PEG-SLN.

5.2.5. *In vitro* drug release

In vitro drug release profile of RSV-TPGS-SLN and RSV-PEG-SLN is shown in Figure 5.5. Both the SLN formulations showed sustained release without any burst release. The cumulative percentage of drug release of RSV-TPGS-SLN and RSV-PEG-SLN was found to be 69.87±6.97 and 66.12±4.82% after 48 h, respectively. Absence of burst release may be due to lack of free RSV molecules at the surface of SLN or in the dispersion medium of formulation. As the lipophilic RSV molecules housed at intermolecular spaces of SLN matrix, the drug release may be sustained which depends on strong affinity of drug-lipid, concentration gradient and depletion of drug molecules from lipid matrix. Higuchi kinetics was shown to be the best fit model for RSV-TPGS-SLN and RSV-PEG-SLN (Table 5.3). Therefore, the drug release mechanism of both SLN formulations was found to be diffusion. The release exponent (n) value of RSV-

TPGS-SLN and RSV-PEG-SLN calculated by Korse-Meyer Peppas model was found to be 0.6307 and 0.8982, respectively. Therefore, the mechanism of release of both SLN formulations was found to be 'anomalous transport' which indicates non-linear diffusion of RSV molecules with respect to time.

Table 5.3. Correlation co-efficient (R^2) and release exponent (n) value of *in vitro* drug release kinetics from RSV-TPGS-SLN and RSV-PEG-SLN

Kinetics/Parameter	**RSV-TPGS-SLN**	**RSV-PEG-SLN**
Zero order	0.8282	0.7681
First order	0.9422	0.8635
Higuchi model	0.9854	0.9400
Korsmeyer–Peppas model	0.9511	0.9287
Release exponent (n)	0.6307	0.8982
Best fit	**Higuchi kinetics**	
Mechanism of RSV release	**Anomalous transport**	

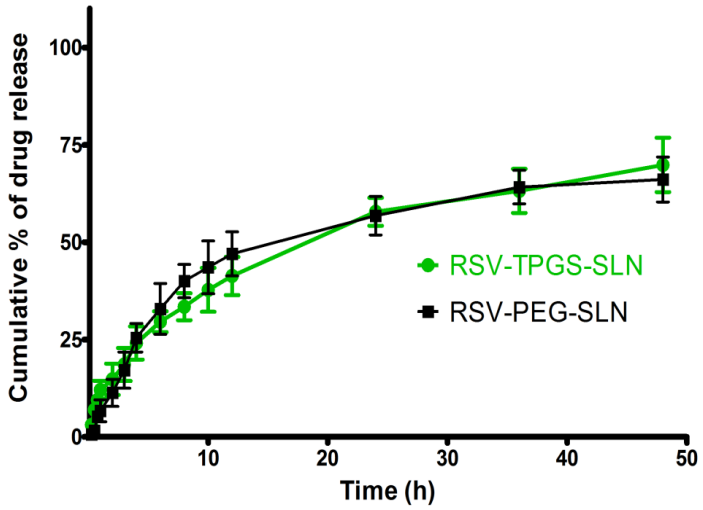

Figure 5.5. *In vitro* release profile of RSV-TPGS-SLN and RSV-PEG-SLN. Values are represented as mean±SD (n=3).

5.2.6. Drug excipient compatibility studies

FT-IR spectrum of RSV, RSV-TPGS-SLN and RSV-PEG-SLN are shown in Figure 5.6 (a), (b) and (c), respectively. RSV showed its characteristic absorption bands at 3288.7 $cm^{-1}$for O-H stretching due to alcoholic group, 1606.7 cm^{-1} for C-C stretching of olefinic group, 1442.8 cm^{-1} and 1587.4 cm^{-1} for C=C stretching of aromatic ring, 1153.4 cm^{-1} for C-O stretching and 964.4 cm^{-1} for *trans* olefinic bond (Figure 5.6 (a)). RSV-TPGS-SLN showed all the characteristic peaks of RSV with minor shift in absorption bands (Figure 5.6 (b)). Alcoholic O-H stretching at 3184.58 cm^{-1}, C-C stretching of olefinic group at 1635.69 cm^{-1}, C=C stretching of aromatic ring at 1464.02 cm^{-1} and 1587.47 cm^{-1}, C-O stretching at 1147.68 cm^{-1} and *trans* olefinic band at 966.37 cm^{-1} were observed in RSV-TPGS-SLN.

RSV-PEG-SLN also showed all the characteristic peaks of RSV with minor shift in absorption bands (Figure 5.6 (c)). Alcoholic O-H stretching at 3196.1 cm^{-1}, C-C stretching of olefinic group at 1645.3 cm^{-1}, C=C stretching of aromatic ring at 1471.4 cm^{-1} and 1587.47 cm^{-1}, C-O stretching at 1147.6 cm^{-1} and *trans* olefinic band at 966.3 cm^{-1} were observed in RSV-PEG-SLN. The presence of all characteristic absorption bands of RSV in RSV-TPGS-SLN and RSV-PEG-SLN confirmed that there is no potential chemical interaction between RSV and other formulation excipients.

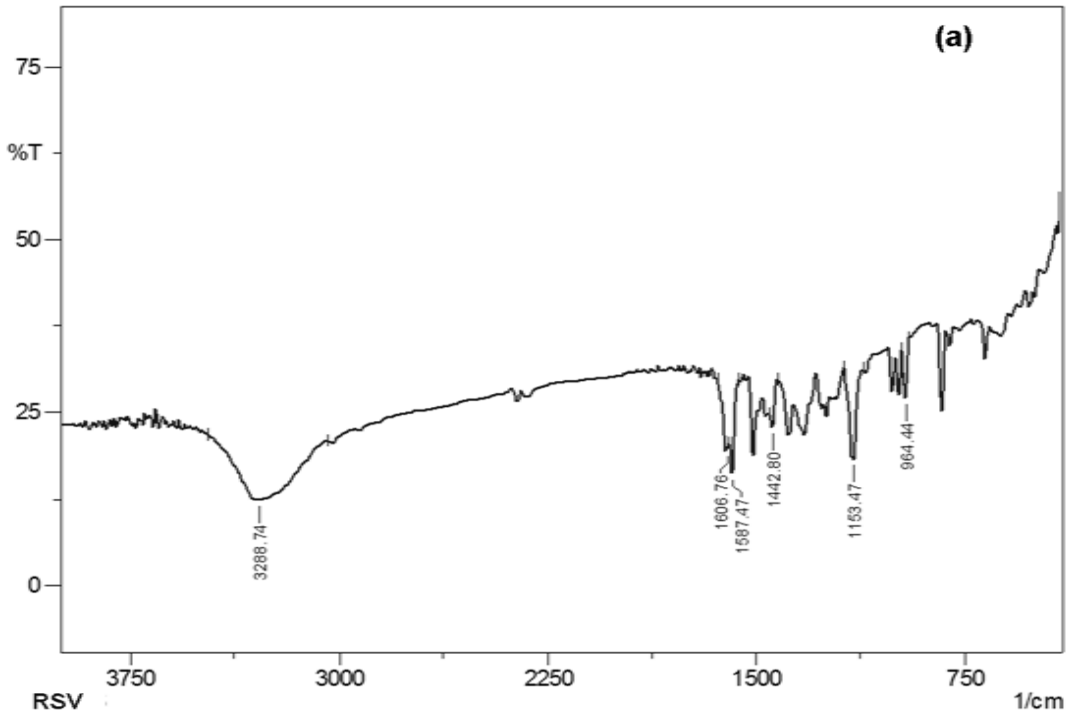

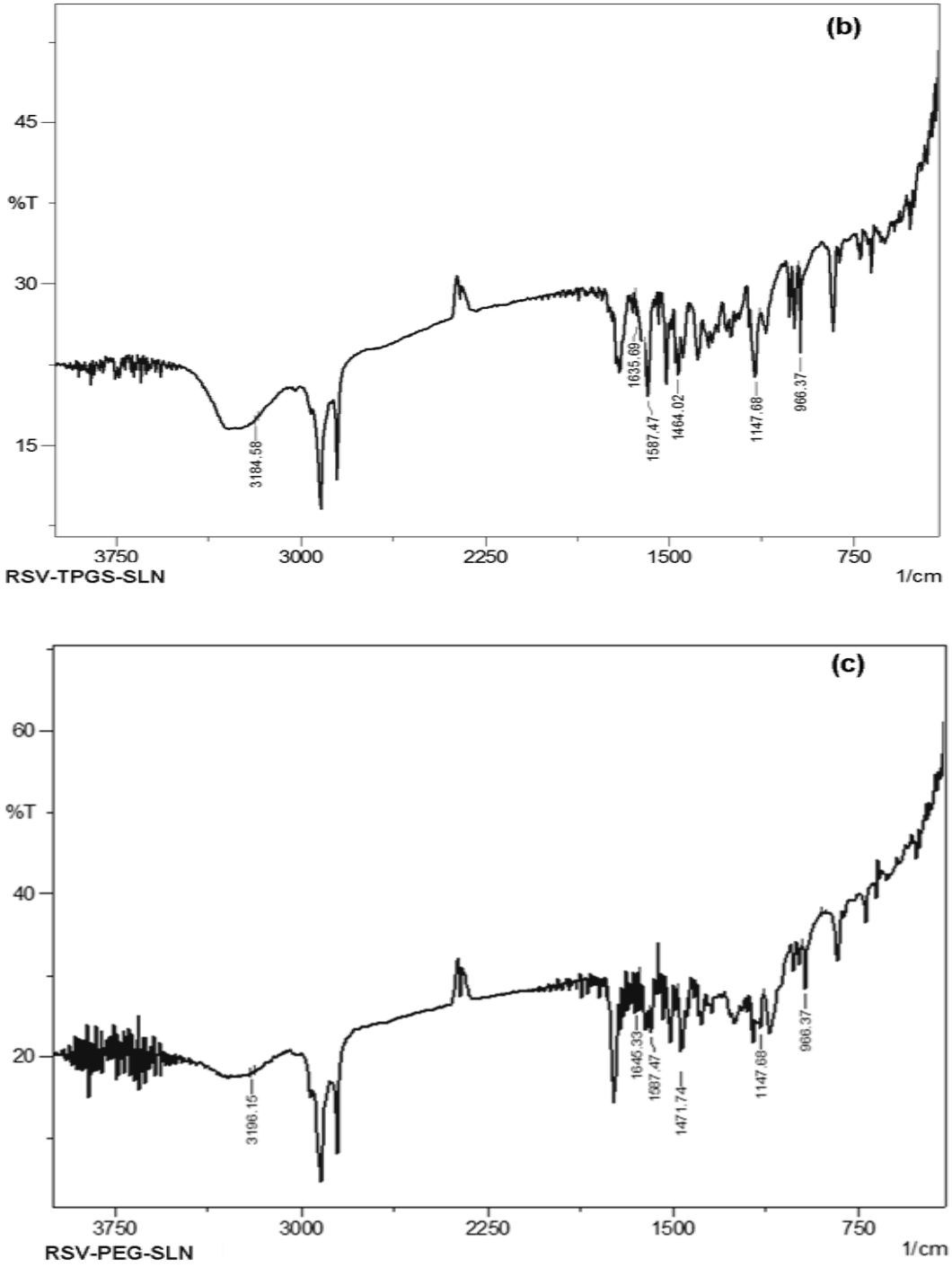

Figure 5.6. Fourier transformed infra red (FT-IR) spectra of (a) RSV (b) RSV-TPGS-SLN and (c) RSV-PEG-SLN

5.2.7. DSC analysis

DSC thermograms of RSV, phosphatidylcholine, tristearin, TPGS, DSPE PEG 2000, RSV-TPGS-SLN and RSV-PEG-SLN are shown in Figure 5.7. RSV showed a sharp endothermic peak at 267.71 °C which corresponds to its melting point. Phosphatidylcholine showed two blunt peaks at 68.12 and 79.04 ^{o}C. Tristearin, TPGS and DSPE PEG 2000 showed sharp endothermic peaks at 59.23, 35.11 and 57.68 ^{o}C, respectively, corresponding to their respective melting points. RSV-TPGS-SLN showed a sharp peak at 69.71 °C which corresponds to the merged peaks of tristearin and phosphatidylcholine with minor shift in their positions. RSV-PEG-SLN showed a sharp peak at 57.83 °C which corresponds to the merged peaks of tristearin and DSPE PEG 2000 with minor shift in their positions. Absence of RSV melting peak at 267.71 °C in the thermograms of RSV-TPGS-SLN and RSV-PEG-SLN suggest that RSV is dispersed in amorphous form.

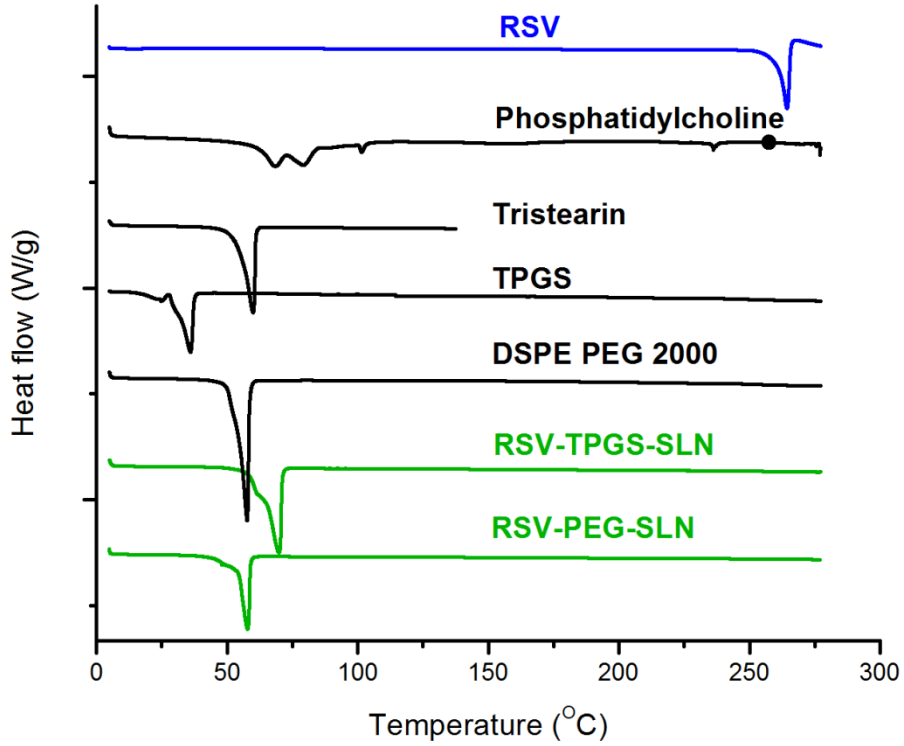

Figure 5.7. Differential scanning calorimetric thermograms of RSV, phosphatidylcholine, tristearin, TPGS, DSPE PEG 2000, RSV-TPGS-SLN and RSV-PEG-SLN.

5.2.8. X-Ray diffraction analysis

XRD pattern of RSV, RSV-TPGS-SLN and RSV-PEG-SLN are shown in Figure 5.8. RSV showed sharp diffraction peaks at 6.62°, 13.2°, 16.36°, 19.18°, 22.28°, 23.54°, 25.18°, 28.26°, 31.6°, 38.32° and 45.18° in 2θ scale. These results indicate that RSV is of crystalline in nature. In contrast, RSV-TPGS-SLN showed only two small peaks at 6.38 and 7.46 in 2θ scale and did not show other characteristic intense sharp peaks. RSV-PEG-SLN also showed only one small peak at 6.36 in 2θ scale. These results suggest that RSV is converted from crystalline to amorphous form in the lipid matrix of RSV-TPGS-SLN

and RSV-PEG-SLN. XRD results were correlated well with the DSC results, which confirm the conversion of RSV from crystalline form to amorphous form.

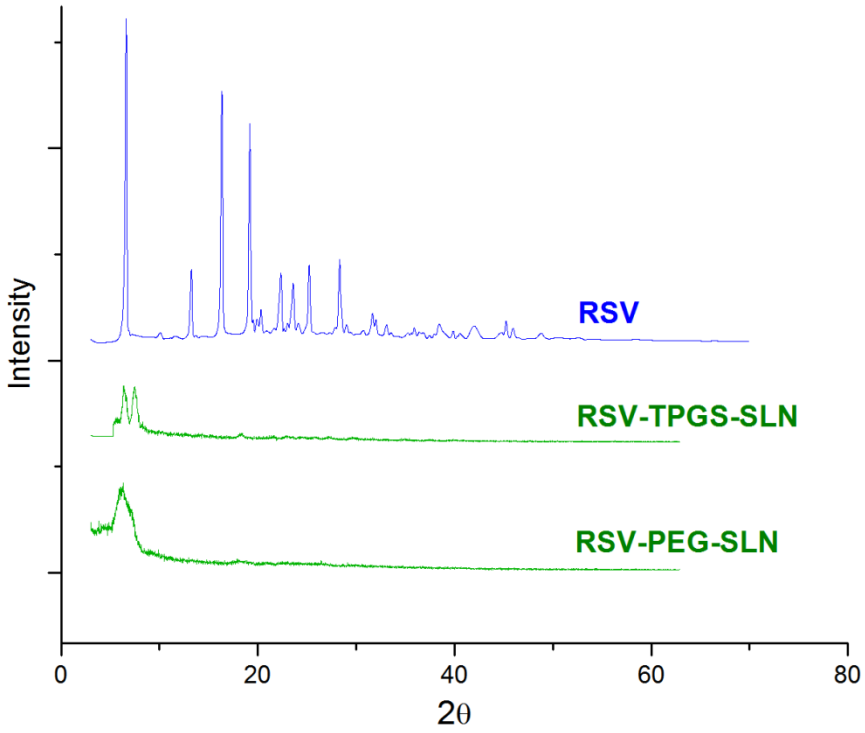

Figure 5.8. X-ray diffraction pattern of RSV, RSV-TPGS-SLN and RSV-PEG-SLN.

5.2.9. Cytotoxicity against C6 glioma cells

Cytotoxicity study was performed to assess the efficacy of RSV, RSV-TPGS-SLN and RSV-PEG-SLN against C6 glioma cell lines. Cytotoxicity of pristine RSV, RSV-TPGS-SLN, RSV-PEG-SLN, Placebo-TPGS-SLN and Placebo-PEG-SLN is shown in Figure 5.9. RSV-TPGS-SLN showed significantly higher cytotoxicity than RSV in all individual concentrations ($p<0.05$). The additional cytotoxic potential can be explained from the cytotoxicity of placebo formulations. Placebo-TPGS-SLN showed statistically significant increase in cytotoxicity in each increment of its concentrations ($p<0.05$) whereas

equivalent concentration of lipid components of Placebo-TPGS-SLN dispersed in water without TPGS did not show any cytotoxicity (not shown in figure). These results evidently indicate that the cytotoxicity of Placebo-TPGS-SLN is due to TPGS. The cytotoxic potential of TPGS has been proved for several types of cancer both *in vitro* and *in vivo* [185-188]. TPGS was more effective at 40 µM concentration by inducing apoptosis in A549 cells as measured by DNA fragmentation [188]. TPGS induced apoptosis in androgen receptor negative (AR^-) DU145, PC3 and androgen receptor positive (AR+) LNCaP prostate cancer cells [185]. TPGS induced G1/S cell cycle arrest and apoptosis in breast cancer cell lines MCF-7 and MDA-MB-231 at 20 µM. The induction of G1/S phase cell cycle arrest by TPGS was associated with upregulation of P21, P27Kip1 proteins, phospho-AKT and downregulation of antiapoptotic proteins survivin and Bcl-2 [187]. Essentially, TPGS did not affect the nontumourigenic cells (MCF-10A and MCF-12F) suggesting its efficacy specifically against cancer cells. Therefore, the additive cytotoxicity of RSV-TPGS-SLN formulation in our study is due to presence of TPGS. The added cytotoxic potential of RSV-TPGS-SLN will be more beneficial in the treatment of glioma without any toxicity to the normal cells.

Cytotoxicity of RSV-PEG-SLN was found to be statistically similar with RSV and lower than RSV-TPGS-SLN in all individual concentrations ($p<0.05$). These results suggest that the cytotoxic potential of RSV is preserved after being entrapped in RSV-PEG-SLN which is beneficial for the treatment of glioma. The lower cytotoxicity of RSV-PEG-SLN than RSV-TPGS-SLN may be due to absence of TPGS and nontoxic nature of DSPE PEG 2000.

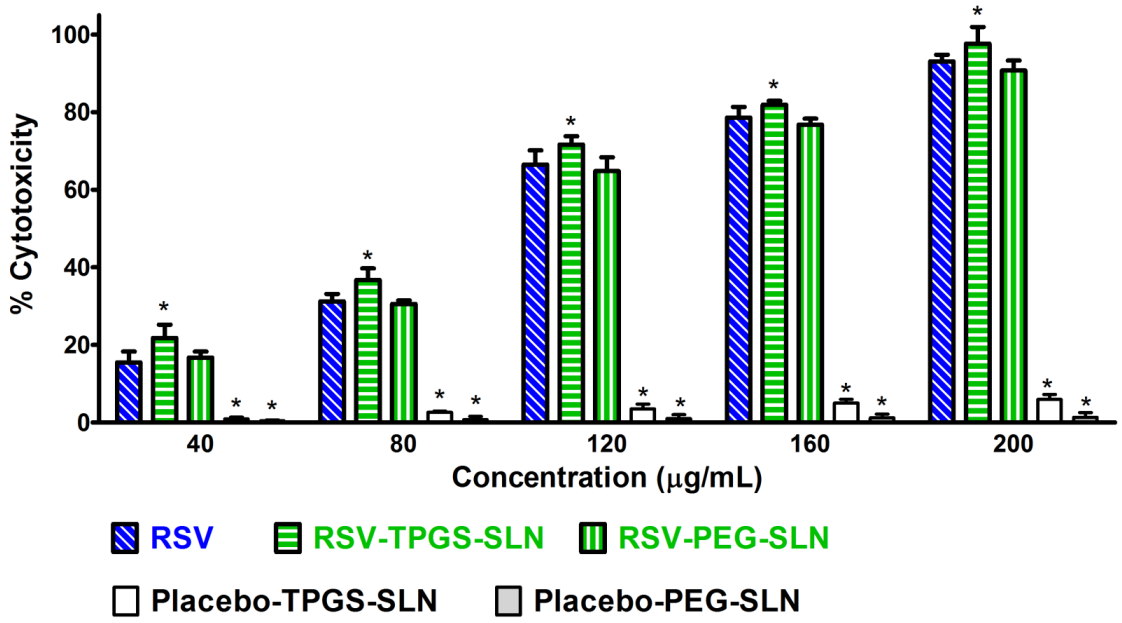

Figure 5.9. *In vitro* cytotoxicity of RSV, RSV-TPGS-SLN, Placebo-TPGS-SLN. RSV-PEG-SLN and Placebo-PEG-SLN. Values are represented as mean±SD (n=3). *Mark indicates significant difference from RSV ($p<0.05$).

5.2.10. Cellular uptake of Coumarin-6 loaded SLN

Figure 5.10 shows the CLSM images of C6 glioma cells after treating with COU-TPGS-SLN and COU-PEG-SLN after counter stained by DAPI to visualize the nucleus. Figure 5.10 (a) and (b) are showing CLSM images of FITC and DAPI channels of COU-TPGS-SLN captured using appropriate filters. Cellular uptake of images of COU-TPGS-SLN (green colour) was visualized by superimposing the FITC channel and DAPI channel (blue colour) (Figure 5.10 (c)). Similarly, Figure 5.10 (d) and (e) are CLSM images of FITC and DAPI channels of COU-PEG-SLN captured using suitable filters, respectively. Cellular uptake of images of COU-PEG-SLN (green colour) was visualized by

superimposing the FITC channel and DAPI channel (blue colour) as shown in Figure 5.10 (f).

Both COU-TPGS-SLN and COU-PEG-SLN showed excellent cell internalization in C6 glioma cells after 2 h of incubation. Nanoparticles were found to be highly concentrated at cytoplasm. Cytoplasm is the major site of several apoptotic mechanisms of RSV which includes upregulation of p53, Bax and Bak, downregulation of Bcl-2 for release of cytochrome c, increased expression of caspase-3 mRNA and caspase-3 activation, inhibiting matrix metalloproteinases (MMPs) and deactivation of IAP [8]. Therefore, the present design of RSV-TPGS-SLN and RSV-PEG-SLN can be applied as potential tool to exert cytotoxic potential of RSV at cytoplasm.

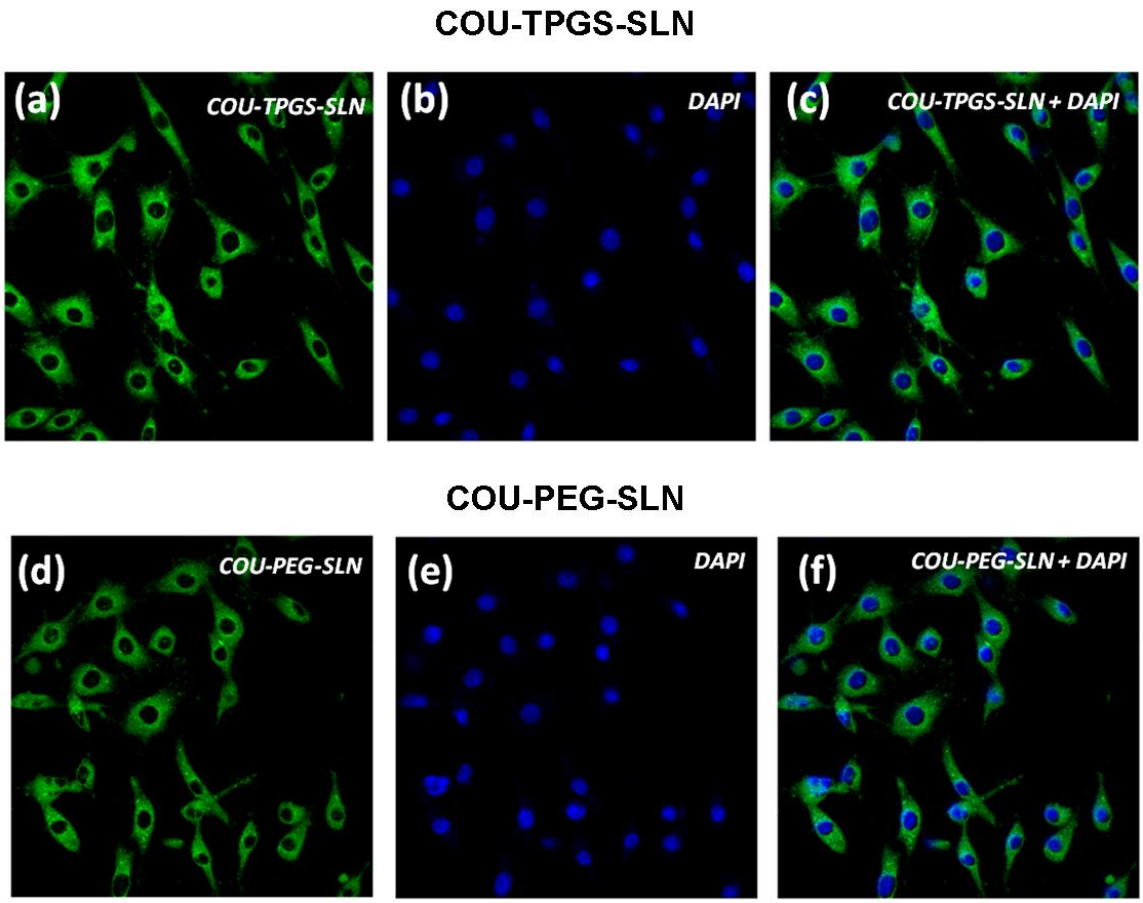

Figure 5.10. Cellular internalization of COU-TPGS-SLN (a, b and c) and COU-PEG-SLN (d, e and f) in C6 glioma cancer cells assessed by confocal laser scanning microscopy (CLSM).

5.2.11. Evaluation of haemolysis

The nanoparticle formulations should not cause haemolysis during and after intravenous infusion. Haemolysis of RSV, RSV-TPGS-SLN and Placebo-TPGS-SLN at 10, 50 and 100 µg/mL concentrations are shown in Figure 5.11 (a), (b) and (c), respectively. Haemolysis of RSV, RSV-PEG-SLN and Placebo-PEG-SLN at 10, 50 and 100 µg/mL concentrations are shown in Figure 5.11 (d), (e) and (f), respectively. As per international

standards, the spontaneous haemolysis limit is 10% to preserve the functionality of erythrocytes in blood [189]. Despite RSV, RSV-TPGS-SLN, Placebo-TPGS-SLN, RSV-PEG-SLN and Placebo-PEG-SLN showed disparate haemolysis values, all formulations are within the haemolysis limit of less than 10%. Therefore, RSV-TPGS-SLN and RSV-PEG-SLN are safe for *i.v.* administration in terms of haemolysis. Moreover, RSV is reported for other antioxidative mechanisms such as reduction of glutathione (GSH) and membrane sulphydryl groups (-SH) in erythrocytes which thereby strongly exhibit protective effect [7]. In addition, RSV is also proved for protective effect on erythrocytes by decreasing malondialdehyde (MDA) level and protein carbonyl group content [7]. All these protective mechanisms of RSV will prevent the degradation of erythrocytes. Thus, intravenous administration of RSV-TPGS-SLN and RSV-PEG-SLN will be safe for glioma chemotherapy.

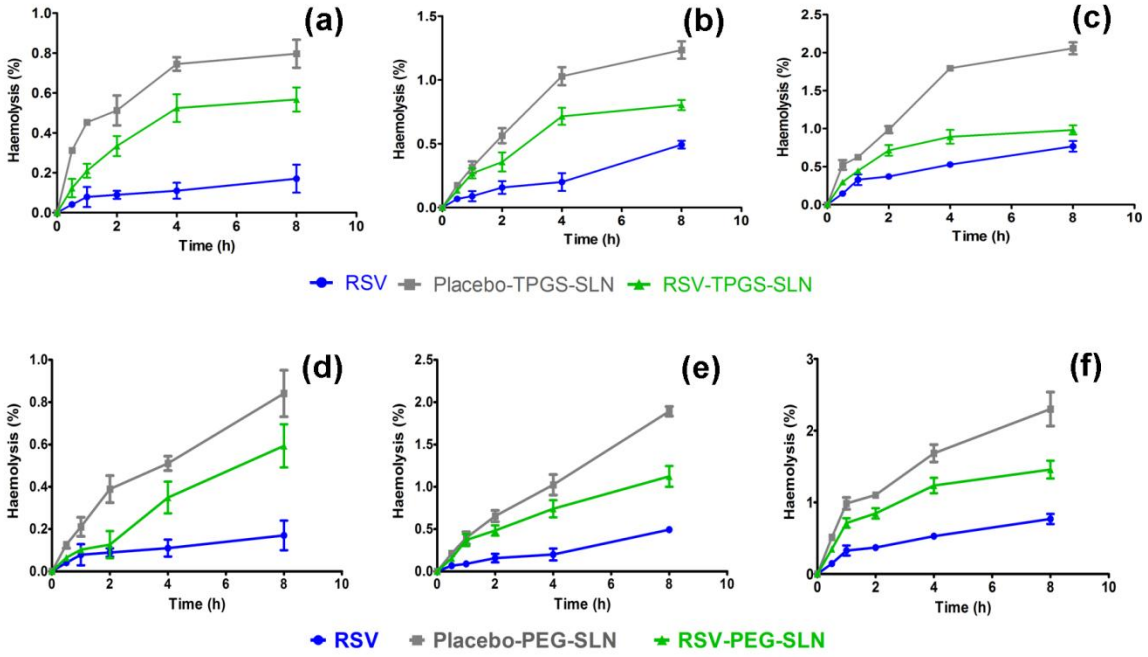

Figure 5.11. Percentage of haemolysis at different time intervals in whole blood samples after addition of (a) 10 (b) 50 (c) 100 µg/mL RSV-TPGS-SLN and (d) 10 (e) 50 (f) 100 µg/mL of RSV-PEG-SLN. Values are represented as mean±SD (n=3).

5.2.12. Evaluation of erythrocyte membrane integrity

As the structural disturbance in erythrocytes membrane integrity results in elevated level of LDH release, evaluation of membrane integrity was assessed by LDH enzyme quantification. Amount of LDH release after treating 1 mL of erythrocyte suspension with RSV, RSV-TPGS-SLN (equivalent to 10, 50 and 100 μg/mL of RSV) and Placebo-TPGS-SLN (equal to the volume of RSV-TPGS-SLN) are shown in Figure 5.12 (a), (b) and (c), respectively. Similarly, amount of LDH release after treating 1 mL of erythrocyte suspension with RSV, RSV-PEG-SLN (equivalent to 10, 50 and 100 μg/mL of RSV) and Placebo-PEG-SLN (equal to the volume of RSV-PEG-SLN) are shown in Figure 5.12

(d), (e) and (f), respectively. RSV, RSV-TPGS-SLN, Placebo-TPGS-SLN, RSV-PEG-SLN and Placebo-PEG-SLN did not show significant increase in LDH release in comparison to spontaneous enzyme release observed in PBS treated samples after 1, 4 and 8 h of incubation at all concentrations. These results suggest that membrane integrity of erythrocyte will not be affected at these concentrations of test samples. Therefore, RSV, RSV-TPGS-SLN and RSV-PEG-SLN formulations in blood at 10, 50 and 100 μg/mL concentrations will not damage erythrocyte membrane integrity and therefore safe for *i.v.* administration.

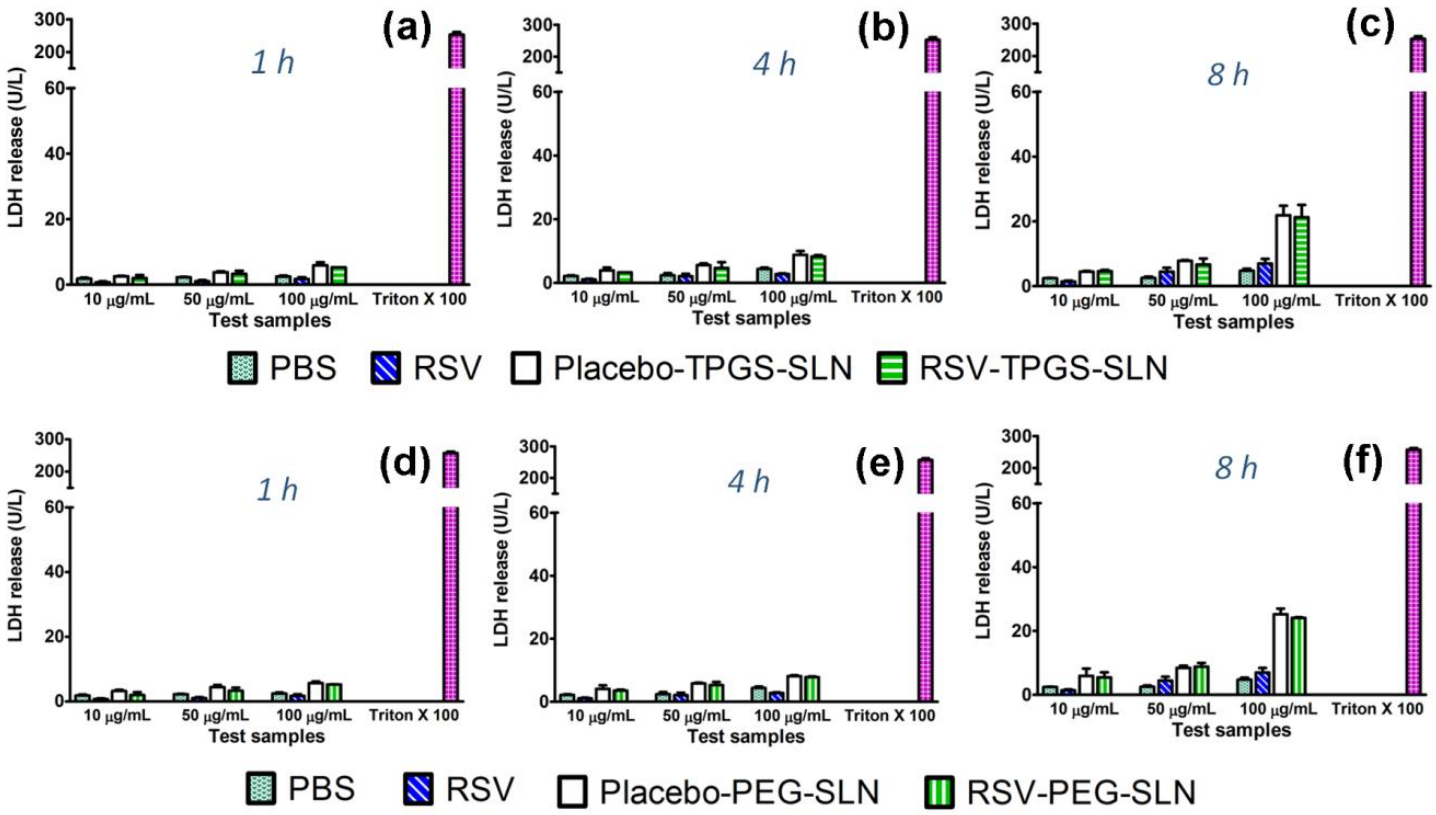

Figure 5.12. Amount of LDH release after treating with RSV-TPGS-SLN at (a) 1, (b) 4 and (c) 8 hours and RSV-PEG-SLN at (d) 1, (e) 4 and (f) 8 hours. Values are represented as mean±SD (n=3).

5.2.13. Platelet aggregation

Excessive or inappropriate aggregation of platelets upon intravenous infusion of SLN formulation can lead to thrombus formations in blood vessels that result in transient ischaemia, myocardial infarction or stroke. Therefore, assessment of platelet aggregation upon *i.v.* administration of SLN formulations is essential. Platelet aggregation results of RSV, RSV-TPGS-SLN and Placebo-TPGS-SLN are shown in Figure 5.13 (a). RSV treated samples did not show any significant difference in platelet count than PBS treated samples at all the three concentrations. These results suggest that RSV is not involved in platelet aggregation. Placebo-TPGS-SLN showed significantly lower ($p<0.05$) platelet count than that of PBS treated samples. The lower platelet count observed in Placebo-TPGS-SLN may be due to the effect of SLN components. Though all components of Placebo-TPGS-SLN are present in RSV-TPGS-SLN, it showed higher platelet count than Placebo-TPGS-SLN and similar platelet count as of PBS treated samples.

Platelet aggregation results of RSV, RSV-PEG-SLN and Placebo-PEG-SLN are shown in Figure 5.13 (b). RSV-PEG-SLN and Placebo-PEG-SLN showed significantly lower platelet count than that of PBS treated samples in all concentration ranges ($p<0.05$); however, RSV-PEG-SLN treated samples showed statistically higher platelet counts than that of Placebo-PEG-SLN ($p<0.05$). Lower platelet count observed in RSV-PEG-SLN and Placebo-PEG-SLN may be due to the effect of its formulation components. Though all components of Placebo-PEG-SLN are present in RSV-PEG-SLN, RSV loaded SLN formulation showed significantly higher platelet count. This may be due to antiplatelet aggregation property of RSV.

Systemic administration of RSV is proved to obstruct the increase in platelet aggregation in rabbits induced by hypercholesterolaemic diet [7]. Moreover, RSV is proved for anti platelet aggregation effect *in vitro* [20]. Thromboxane A2 (TxA2) is a potent inducer of platelet aggregation. TxA2 is synthesized by COX1 in platelets. Prostacyclin is an antiplatelet aggregator which is synthesized by COX2 in vascular endothelial cells. RSV is proved for selective inhibition of COX1 which causes decrease in TxA2 and thereby prevents platelet aggregation [7]. RSV also showed to decrease the size of thrombus generated by laser-induced damage to endothelium in genetically hypercholesterolaemic mice [7].

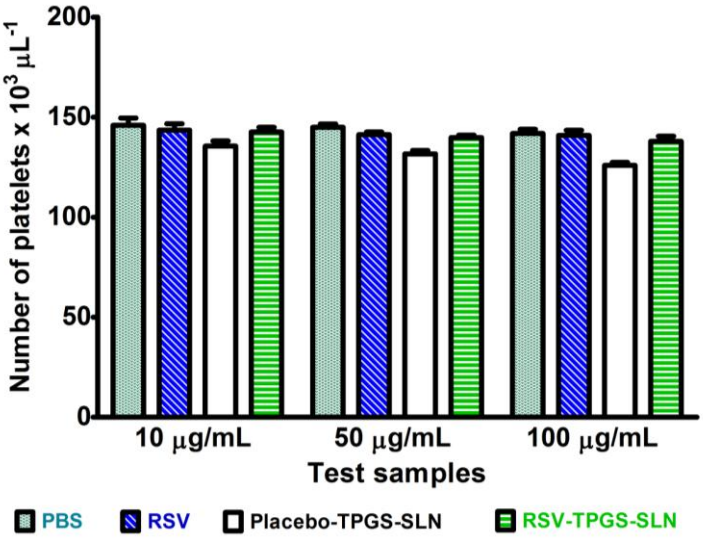

Figure 5.13. (a) Number of platelets after addition of PBS, RSV, Placebo-TPGS-SLN and RSV-TPGS-SLN at 10, 50 and 100 µg/mL. Values are represented as mean±SD (n=3).

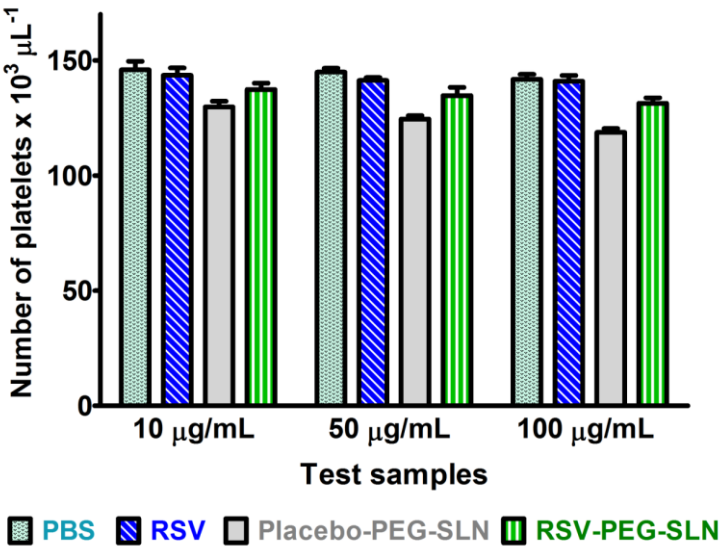

Figure 5.13. (b) Number of platelets after addition of PBS, RSV, Placebo-PEG-SLN and RSV-PEG-SLN at 10, 50 and 100 µg/mL. Values are represented as mean±SD (n=3).

In addition to platelet count, the platelet aggregation in whole blood was observed by optical microscopy after incubation. Erythrocytes, leucocytes and platelets were visualized and the platelets are indicated by arrow marks on the microphotographs. Supportively, no platelet aggregation was seen in all samples (RSV, RSV-TPGS-SLN, Placebo-TPGS-SLN, RSV-PEG-SLN and Placebo-PEG-SLN) at all concentrations (Figure 5.14). Though slight decrease in platelet count was observed with Placebo-TPGS-SLN, RSV-PEG-SLN and Placebo-PEG-SLN in quantitative measurements, platelets were distributed evenly throughout the blood smears upon microscopic observations. All these observations indicated that RSV, RSV-TPGS-SLN and RSV-PEG-SLN are nontoxic, haemocompatible and safe for intravenous administration.

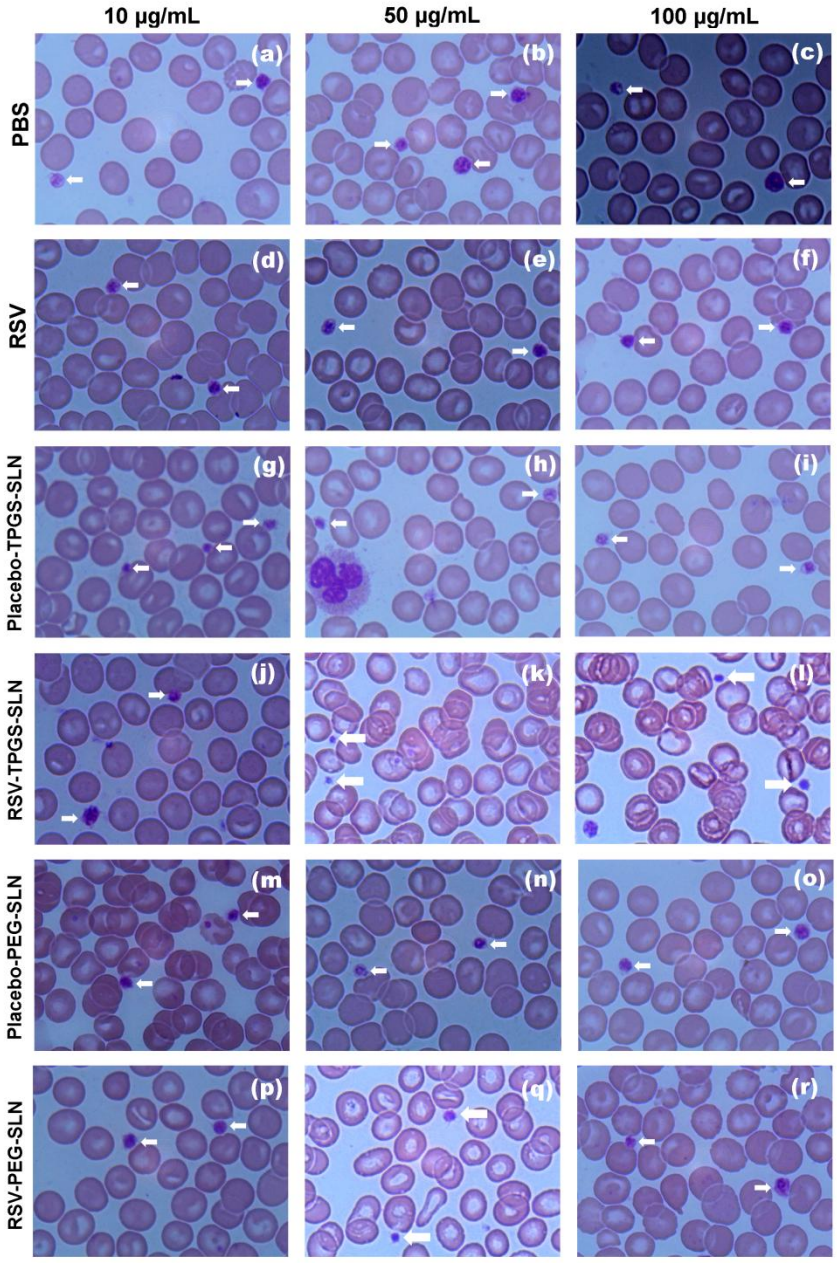

Figure 5.14. Light microscopy images of Leishman's stained whole blood samples after treating with (a) PBS equivalent volume to 10 µg/mL of test samples (b) PBS equivalent volume to 50 µg/mL of test samples (c) PBS equivalent volume to 100 µg/mL of test samples (d) 10 µg/mL RSV (e) 50 µg/mL RSV (f) 100 µg/mL RSV (g) 10 µg/mL Placebo-TPGS-SLN (h) 50 µg/mL Placebo-TPGS-SLN (i) 100 µg/mL

Placebo-TPGS-SLN (j) 10 µg/mL RSV-TPGS-SLN (k) 50 µg/mL RSV-TPGS-SLN (l) 100 µg/mL RSV-TPGS-SLN (m) 10 µg/mL Placebo-PEG-SLN (n) 50 µg/mL Placebo-PEG-SLN (o) 100 µg/mL Placebo-PEG-SLN (p) 10 µg/mL RSV-PEG-SLN (q) 50 µg/mL RSV-PEG-SLN (r) 100 µg/mL RSV-PEG-SLN. Images were captured at magnification of 100x.

5.2.14. Pharmacokinetic studies

Comparative plasma concentration time profiles of RSV-TPGS-SLN and RSV-PEG-SLN with RSV up to 24 h are shown in Figure 5.15 (a) and (b), respectively. The pharmacokinetic parameters are presented in Table 5.4. Plasma concentration time curve of RSV solution showed a rapid decline up to 0.5 h, slight increment at 1 h (a small second peak), declined again up to 2 h and remain undetectable after 2 h. RSV-TPGS-SLN showed marked decline at 1 h, again rose to give second peak concentration at 2 h and declined up to 8 h. The plasma concentration increased again to the small extent at 12 h and continuous decline up to 24 h, after which the concentration was undetectable. Similarly, RSV-PEG-SLN showed marked decline at 2 h and again rose to give a peak at 8 h, continuously declined and was undetectable after 24 h. Formation of additional peaks (increment in plasma concentration) in RSV, RSV-TPGS-SLN and RSV-PEG-SLN is due to enterohepatic recirculation of drug. Enterohepatic circulation of RSV was due to conversion of RSV into glucuronide/sulfate conjugates and secretion to small intestine via breast cancer resistance protein and multidrug resistance protein 2 [190]. Enterohepatic circulation of RSV observed in our study was well correlated with the earlier reports of different research groups [190]. Initial plasma concentration (C_0) of

RSV (2625.33±366.74 ng/mL) after *i.v.* administration was found to be significantly higher than that of RSV-TPGS-SLN formulation (2162.39±193.21 ng/mL) ($p<0.05$). C_0 of RSV-PEG-SLN was found to be 2313.31±394.83 ng/mL, which is statistically insignificant with RSV. Area under the curve (AUC) and plasma half life ($t_{1/2}$) after *i.v.* administration of RSV-TPGS-SLN was found to be approximately 11.12 and 9.37 times higher than RSV, respectively. Similarly, RSV-PEG-SLN showed 5.41 times higher AUC and 13.7 times higher $t_{1/2}$ than that of RSV solution, respectively. The higher AUC and $t_{1/2}$ values revealed that RSV-TPGS-SLN and RSV-PEG-SLN significantly enhanced systemic availability and increase the stay in circulation in comparison to RSV. The improved pharmacokinetics profile of SLN formulations may be due to presence of TPGS or DSPE PEG 2000 at the surface of nanoparticles. The plasma half life ($t_{1/2}$) of RSV obtained in this study was higher than earlier reported value (0.13±0.02 h) at 15 mg/kg and well correlated with the value (0.55 h, calculated by Bayesian estimations) of population pharmacokinetic study at 2, 10 and 20 mg/kg of RSV after *i.v.* administrations in rats [17, 18]. Short $t_{1/2}$ of RSV can be attributed to its higher clearance (CL) value (1679.48±460.73 mL/h/kg). In contrast, higher half life of RSV-TPGS-SLN and RSV-PEG-SLN is due to lower CL value (151.99±11.44 286.42±13.64 mL/h/kg, respectively). The volume of distribution (V_d) of RSV (1383.18±177.36 mL/kg) and RSV-TPGS-SLN (1212.87±159.04 mL/kg) were found to be same ($p>0.05$). V_d of RSV-PEG-SLN (3378.03±387.09 mL/kg) was found to be 2.38 times lower than that of RSV. V_d of RSV, RSV-TPGS-SLN and RSV-PEG-SLN were found to be exceptionally higher than the total body water of a rat (150 mL/kg for a body weight of 0.25 kg) [17]. Therefore, RSV and SLN formulations undergo extensive tissue binding after *i.v.* administration. Mean

residence time (MRT) of RSV-TPGS-SLN and RSV-PEG-SLN was found to be approximately 11.4 and 11.98 times higher than that of RSV solution which confirmed their long circulation potential. TPGS or DSPE PEG 2000 present at the surface of SLN formulations prevents the adhesion of plasma proteins and thereby avoids recognition of SLNs by reticulo endothelial system which ultimately resulted in prolonged systemic circulation. The overall observation of higher AUC, $t_{1/2}$ and MRT and lower CL of RSV-TPGS-SLN and RSV-PEG-SLN than pristine RSV clearly indicate that the present design of SLN formulations will be the potential tool for improving systemic availability, prolonging systemic circulation and extend the half life of RSV.

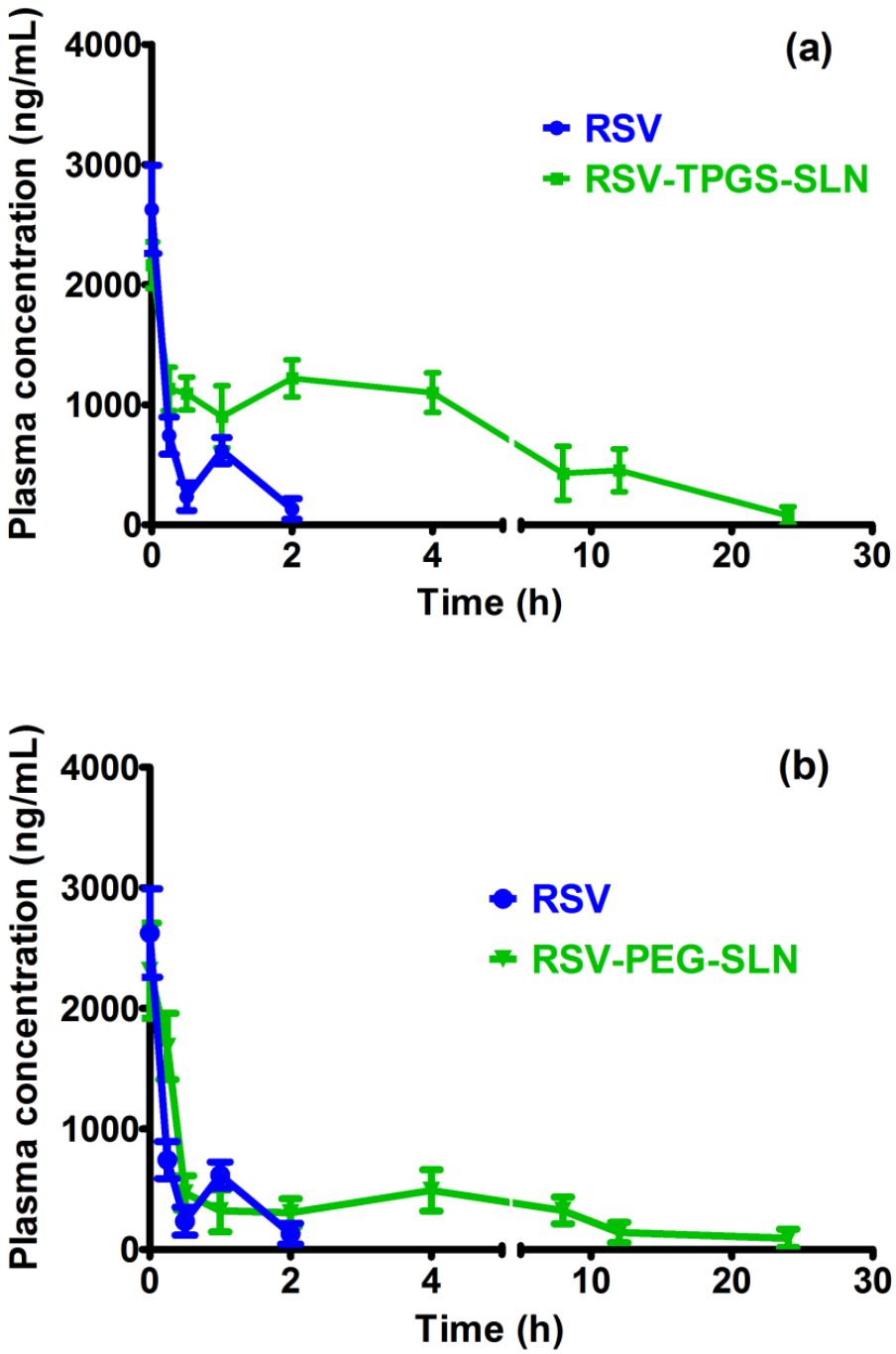

Figure 5.15. Comparative plasma concentration time profile of (a) RSV-TPGS-SLN and (b) RSV-PEG-SLN with RSV up to 24 hours after *i.v.* administration of 2 mg/kg dose; Each data point is the representation of mean±SD (n=6).

Table 5.4. Pharmacokinetic parameters of RSV, RSV-TPGS-SLN and RSV-PEG-SLN after *i.v.* administration of 2 mg/kg dose.

PK parameters	RSV	RSV-TPGS-SLN	RSV-PEG-SLN
C_0 (ng/mL)	2625.33±366.74	2162.39±193.21	2313.31±394.83
AUC (ng*h/mL)	1130.96±245.50	12574.95±1074.95*	6090.90±107.84*
$t_{1/2}$ (h)	0.59±0.11	5.53±0.55*	8.22±1.36*
CL (mL/h/kg)	1679.48±460.73	151.99±11.44*	286.42±13.64*
V_d (mL/kg)	1383.18±177.36	1212.87±159.04	3378.03±387.09*
MRT (h)	0.60±0.04	6.84±0.23*	7.19±0.69*

Data is presented as mean±SD (n=6); *Mark indicates significant difference from RSV ($p<0.05$).

5.2.15. Tissue distribution studies

The bio-distribution of RSV, RSV-TPGS-SLN and RSV-PEG-SLN is shown in Figure 5.16. RSV-TPGS-SLN and RSV-PEG-SLN showed highest brain accumulation of 7.48±1.69 and 6.962±1.08 µg/g, respectively. Brain distribution of RSV-TPGS-SLN and RSV-PEG-SLN was approximately 9.23 and 8.60 times higher than that of RSV solution

(0.81±0.48) ($p<0.05$). Colloidal nanocarrier having 200 and 250 nm were well reported for crossing blood brain barrier (BBB) [191-193]. Passive brain targeting efficiency of such nanoparticles is proved in healthy and diseased conditions both *in vitro* and *in vivo* experiments [191-194]. Therefore, RSV-TPGS-SLN and RSV-PEG-SLN having particle size of 203.1±14.91 and 125.95±12.09 nm can be expected to be effectively crossing BBB to deliver RSV in brain. Kidney is the major elimination organ of RSV. Total excretion of RSV after *i.v.* administration was calculated to be 42.3 to 83.2% [16]. The distribution of RSV-TPGS-SLN and RSV-PEG-SLN in kidney was found be significantly lower than that of RSV solution ($p<0.05$). The lower distribution of SLN formulations in kidney would be expected to decrease the elimination of RSV. Lungs and spleen distribution of both SLN formulations and RSV was found to be statistically similar ($p>0.05$). Liver distribution of RSV-PEG-SLN was found to be 8.40 times lower than that of RSV ($p<0.05$). Lower liver accumulation of RSV-PEG-SLN may be due to presence of DSPE PEG 2000 at the surface of lipid nanoparticle. Liver is one of the major organs of reticulo endothelial system (RES). RES is also comprised of macrophages and monocytes, liver kupffer cells and lymphatic vessels. This system is responsible for removing foreign materials from the systemic circulation. Adsorption of plasma at the surface of any foreign materials that enters the systemic circulation called opsonization. Consequently, the opsonised foreign materials are taken up by the macrophages and transport them to liver or spleen for metabolism and excretion. Hydrophobic particles are more susceptible to opsonisation and RES uptake. Phagocytic macrophages permanently located in liver (also known as Kupffer cells) also trap such hydrophobic materials in liver and metabolize them. In our case, hydrophilic PEG chain

of DSPE PEG 2000 is present at the surface of RSV-PEG-SLN which reduces opsonisation and thereby prevents recognition by monocytes, macrophages and Kupffer cells. This resulted in lower accumulation in liver and facilitated RSV-PEG-SLN to remain in blood pool for longer period of time. The reduction of liver distribution also minimizes the rate of biotransformation of RSV-PEG-SLN. Moreover, RSV molecules entrapped inside RSV-PEG-SLN will not readily available for metabolism like free RSV in liver which further delays biotransformation process. The lower liver accumulation is well correlated with higher AUC and $t_{1/2}$ of RSV-PEG-SLN observed in pharmacokinetic studies. Liver distribution of RSV-TPGS-SLN was found to be statistically similar as that of RSV. The overall review of bio distribution results showed that the brain distribution of RSV-TPGS-SLN and RSV-PEG-SLN were found to be significantly higher than that of RSV solution. Therefore, both SLN formulations can be applied as effective tool for potential brain targeting of RSV which is useful in the treatment of glioma.

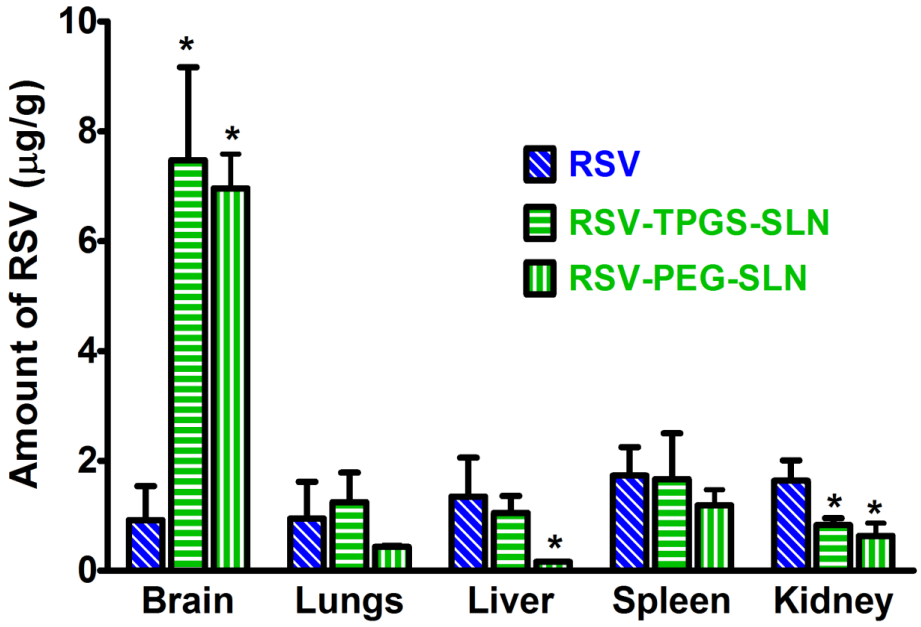

Figure 5.16. Comparative *in vivo* biodistribution of RSV, RSV-TPGS-SLN and RSV-PEG-SLN in brain, lungs, liver, spleen and kidney after *i.v.* administration of 2 mg/kg dose; Values are represented as mean±SD (n=3). (*) Statistically significant difference from RSV ($p<0.05$).

5.2.16. Comparative results of RSV-TPGS-SLN and RSV-PEG-SLN

Parameters	**RSV-TPGS-SLN**	**RSV-PEG-SLN**
Particle size	203.1±14.91 nm	125.95±12.09 nm
Polydispersity index	0.263±0.12	0.386±0.04
Zeta potential	-10.5±2.94 mV	-24.43±3.27 mV
Shape	Spherical	
Entrapment efficiency	70.18±5.19%	74.67±4.76%
In vitro release studies	Sustained, Higuchi, anomalous	
Interaction analysis (DSC/FTIR)	No potential chemical interaction	
Analysis of crystallinity (XRD)	Crystalline to amorphous	
Cytotoxicity in C6 glioma cells (in comparison to RSV)	Higher cytotoxicity (due to TPGS)	Similar cytotoxicity
Cellular uptake	Excellent cellular internalization	
Haemolysis	Less than limit (10%), safe for *i.v.*	
Erythrocyte membrane integrity	Less than limit (10%) , safe for *i.v.*	
Platelet aggregation	No aggregation and safe for *i.v.*	
Pharmacokinetic studies	Higher AUC, $t_{1/2}$ (5-8 h); present in blood up to 24 h	
Brain distribution (than RSV)	9.23 times higher	8.60 times higher

5.3. Blend nanoparticles

In our previous study, all pharmacokinetic parameters and brain distribution of SLN formulations are significantly improved in comparison to that of RSV solution. However, the biological half life of RSV-TPGS-SLN and RSV-PEG-SLN were found to be only 5.53±0.55 and 8.22±1.36 h, respectively. The lower biological half life of SLN formulations indicates that multiple doses are required to maintain the therapeutic concentration in plasma. Therefore, attempts can be made to improve the biological half life and to reduce the number of dose per day. Polymeric nanoparticles are potential nanocarrier for prolonged systemic circulation and higher biological half life [25-29]. They are capable of opening tight junctions of BBB, effectively mask barrier limiting characteristics of drug molecules. They also reported for sustained drug release, prolonged the systemic circulation and protection of entrapped molecules from enzymatic degradation. Poly (D,L-lactide-co-glycolide) (PLGA) is a FDA-approved biodegradable polymer useful for chemotherapeutic applications of anticancer drugs. As PLGA is hydrophobic in nature, nanoparticles prepared using this polymer may be taken up by RES and reduces systemic circulation, which becomes major limitation for achieving required RSV concentration in plasma. Surface coating of PLGA nanoparticles with hydrophilic materials such as poly (ethylene glycol) (PEG) prevents adsorption of plasma proteins (opsonisation), prolongs systemic circulation and thereby allows them to target the site of action. In recent literature, PLGA:Poloxamer blend nanoparticles were reported for providing protective environment and preventing structural alteration of entrapped drug/biological molecules [30]. The poloxamer molecules are covering the

surface of nanopaticles and thereby render hydrophilic surface. Addition of hydrophilic substances in blend nanoparticles significantly reduced opsonisation/uptake by RES system and thereby prolonged systemic circulation. PLGA:Poloxamer blend nanoparticles were also reported to deliver tetanus toxoid vaccine, peptides or peptidomimetic derivatives, proteins such as bovine serum albumin (BSA) and immuno-γ-globulin (IgG), gene delivery, chemotherapeutic molecules such as paclitaxel, etc [30]. In the present literature, preparation of blend nanoparticles using TPGS for prolonged systemic circulation was not yet focussed. Therefore, RSV-PLGA-BNPs were developed for prolonged systemic circulation, improving biological half life and brain accumulation.

5.3.1. Particle size, polydispersity index and zeta potential

PLGA: TPGS blend ratio and organic to aqueous ratio were varied to get lower particle size and higher zeta potential. Particle size results are shown in Figure 5.17. Polydispersity index and zeta potential results are shown in Table 5.5. When PLGA: TPGS blend ratio was increased from 1:0.5 to 1:0.75, the particle size decreased significantly ($p<0.05$) and further increment to 1:1 did not show further decrease in particle size ($p>0.05$) at all levels of organic to aqueous ratio as shown in Figure 5.17. For instance, particle size of RSV-PLGA-BNPs 1 and 2 prepared using PLGA: TPGS blend ratio of 1:0.5 and 1:0.75 at organic to aqueous ratio 1:10 was found to decrease from 175.5±8.47 to 142.1±3.54 nm. This may be due to surface stabilization of RSV-PLGA-BNPs by TPGS. During preparation, as the sonication energy was applied, organic phase was dispersed as minute globules in aqueous phase to form o/w emulsion. Blended nanoparticles were prepared using stabilizers in aqueous phase as reported in earlier

publications [30, 176]. In our formulations no other stabilizer was used in aqueous media to facilitate the presence of TPGS at RSV-PLGA-BNPs surface. Small fraction of TPGS molecules added in organic phase diffuses to surface of organic globules and stabilizes them as stable emulsion. The higher TPGS concentration in RSV-PLGA-BNPs 2 effectively stabilizes organic globules, prevents agglomeration during evaporation of organic solvent that resulted in lower particle size than RSV-PLGA-BNPs 1. Further increment in PLGA: TPGS blend ratio to 1:1 as in RSV-PLGA-BNPs 3, particle size was found to increase to 135.7±2.89 nm. However, this increase in particle size is statistically insignificant in comparison to the particle size of RSV-PLGA-BNPs 2 ($p>0.05$). This may be due to adequate stabilization achieved in RSV-PLGA-BNPs 2. Therefore, further increment in TPGS concentration in RSV-PLGA-BNPs 3 did not show significant decrease in particle size.

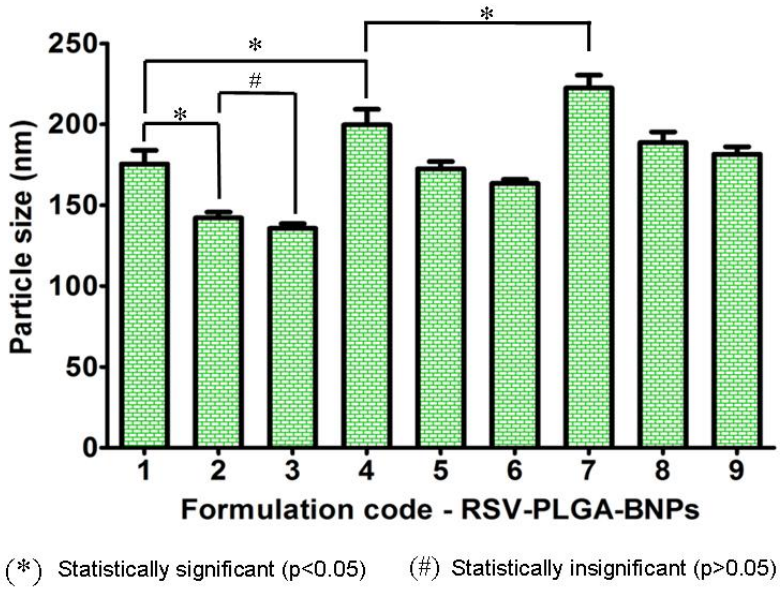

Figure 5.17. Particle size of various batches of RSV-PLGA-BNPs. Values are represented as mean±SD (n=3).

Particle size increased significantly with increase in organic to aqueous ratio at all levels of PLGA: TPGS blend ratios ($p<0.05$). For instance, particle size of RSV-PLGA-BNPs 1, 4 and 7 at organic to aqueous ratio 1:10, 2:10 and 3:10 was found to be 175.5±8.47, 199.7±9.56 and 222.5±7.89, respectively. As the organic solvent concentration is increased, the TPGS concentration used in our formulations may not be sufficient to emulsify/stabilize higher volume of organic phase that resulted in higher particle size. Polydispersity index of RSV-PLGA-BNPs varied from 0.147±0.09 to 0.462±0.11. Zeta potential varied from -8.54±2.51 to -16.86±1.59 mV as shown in Table 5.5. Both polydispersity index and zeta potential did not follow any pattern in varying PLGA: TPGS blend ratio and organic to aqueous ratio.

Table 5.5. Polydispersity index and zeta potential of various batches of RSV-PLGA-BNPs

Formulation code	Polydispersity index	Zeta potential (mV)
RSV-PLGA-BNPs 1	0.147±0.09	-16.86±1.59
RSV-PLGA-BNPs 2	0.462±0.11	-13.79±0.87
RSV-PLGA-BNPs 3	0.212±0.14	-11.55±2.17
RSV-PLGA-BNPs 4	0.157±0.08	-10.22±1.73
RSV-PLGA-BNPs 5	0.211±0.07	-9.70±1.49
RSV-PLGA-BNPs 6	0.312±0.11	-8.54±2.51
RSV-PLGA-BNPs 7	0.212±0.08	-10.72±1.56
RSV-PLGA-BNPs 8	0.134±0.10	-9.20±2.49
RSV-PLGA-BNPs 9	0.421±0.09	-9.54±1.02

5.3.2. Entrapment efficiency

Entrapment efficiency of various batches of RSV-PLGA-BNPs varied from 31.79±2.85 to 61.81±3.57% as shown in Figure 5.18. As increasing the concentration of TPGS in PLGA: TPGS blend ratio, entrapment efficiency was decreased at all levels of organic to aqueous ratio. For instance, RSV-PLGA-BNPs 1, 2 and 3 prepared using 1:0.5, 1:0.75 and 1:1 PLGA: TPGS blend ratio resulted in entrapment efficiency of 61.81±3.57, 53.53±1.25 and 46.38%, respectively ($p<0.05$). The decreasing entrapment efficiency may be related to particle size and solubilisation nature of TPGS. Particle size was observed to decrease upon increasing TPGS concentration. As particle size decreases, surface area of nanoparticles increases and entrapment volume decreases. Therefore, the number of RSV molecules accommodated inside nanoparticles decreases which ultimately resulted in decreasing entrapment efficiency. Moreover, partition of RSV molecule between nanoparticle matrix and bulk of dispersion media is altered upon increasing TPGS concentration. During preparation, TPGS (hydrophilic and water soluble molecule) diffuses from organic phase to aqueous phase. As increasing TPGS concentration, the number of TPGS molecules diffusing from organic to aqueous phase may be increased. Solubilisation nature of TPGS may increase the diffusion of RSV molecules from nanoparticle matrix to the bulk of dispersion media which resulted in decreasing entrapment efficiency.

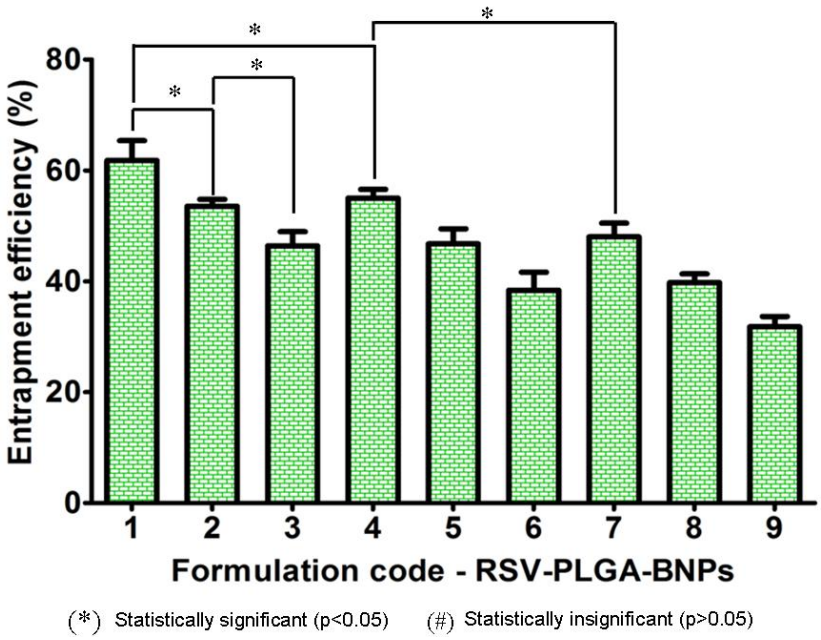

Figure 5.18. Entrapment efficiency of various batches of RSV-PLGA-BNPs. Values are represented as mean±SD (n=3).

Increasing organic to aqueous ratio was also showed similar trend of decreasing entrapment efficiency. For example, entrapment efficiency of RSV-PLGA-BNPs 1, 4 and 7 prepared using 1:10, 2:10 and 3:10 organic to aqueous ratio resulted in entrapment efficiency of 61.81±3.57, 55.07±1.56 and 48.06±2.5%, respectively, as shown in Figure 5.18. Ultra sonication energy was applied to form o/w emulsion during preparation. As increasing the organic phase volume, the number of globules formed during preparation is increased. As increasing the surface area of organic globules contacting the bulk of dispersion media, the number of RSV molecules diffusing in to aqueous phase (dispersion media) may be increased which resulted in decreasing entrapment efficiency.

5.3.3. Selection of best formulation

RSV-PLGA-BNPs 1 having lower particle size of 175.5±8.47 nm, narrow polydispersity index of 0.147±0.09 and larger entrapment efficiency of 61.81±3.57% with zeta potential value of -16.86±1.59 mV was selected for further investigations.

5.3.4. Shape of RSV-PLGA-BNPs

TEM micrographs of RSV-PLGA-BNPs showed spherical shape as shown in Figure 5.19. The mean particle size observed by TEM analysis was found to be 154 nm. This size was well correlated with the particle size obtained by dynamic laser light scattering technique (175.5±8.47 nm).

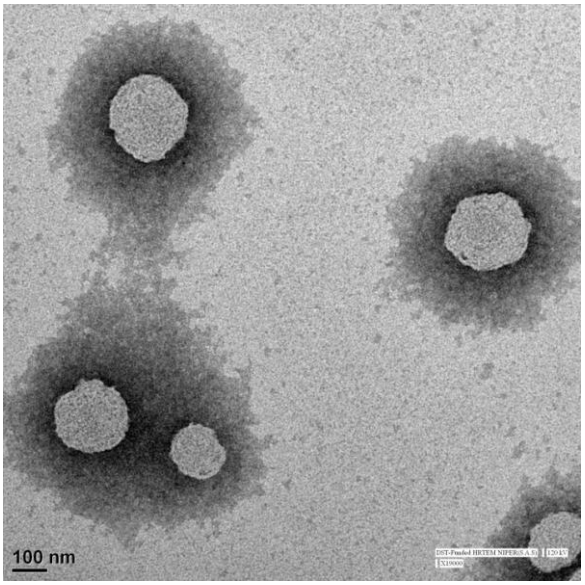

Figure 5.19. Transmission Electron Microscope (TEM) image of RSV-PLGA-BNPs

5.3.5. *In vitro* drug release

In vitro drug release profile of RSV-PLGA-BNPs is shown in Figure 5.20. RSV-PLGA-BNPs showed sustained release without any burst release. The cumulative percentage of drug release after 48 h was found to be only 49.52±4.91%. The absence of burst release may be due to lack of pristine RSV molecules at the surface of RSV-PLGA-BNPs. As the lipophilic RSV molecules housed at intermolecular spaces of polymer matrix, RSV release may be sustained. Correlation co-efficient (R^2) value of zero order, first order, Higuchi model and Korsmeyer–Peppas model were found to be 0.7943, 0.8679, 0.9620 and 0.9395, respectively. These results suggest that Higuchi kinetics is the best fit model for RSV-PLGA-BNPs. Hence, diffusion is the possible drug release mechanism. The release exponent (n) value calculated by Korse-Meyer Peppas model was found to be 0.6226. Therefore, the mechanism of drug release was concluded to be 'anomalous transport' which indicates non-linear diffusion of RSV molecules with respect to time.

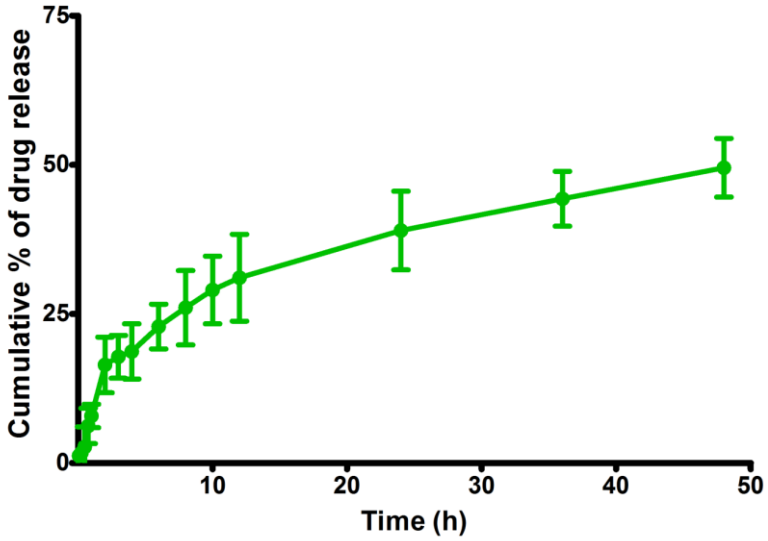

Figure 5.20. *In vitro* drug release profile of RSV-PLGA-BNPs. Values are represented as mean±SD (n=3).

5.3.6. Drug interaction analysis

FTIR analysis was carried out to evaluate possible chemical interaction of RSV with other components used in RSV-PLGA-BNPs. FTIR spectrum of RSV and lyophilized RSV-PLGA-BNPs are shown in Figure 5.21 (a) and (b). RSV showed its characteristic absorption bands at 3288.7 $cm^{-1}$for O-H stretching due to alcoholic group, 964.4 cm^{-1} for *trans* olefinic bond, 1153.4 cm^{-1} for C - O stretching, 1606.7 cm^{-1} for C-C stretching of olefinic group and 1442.8 cm^{-1} and 1587.4 cm^{-1} for C=C stretching of aromatic ring (Figure 5.21 (a)). RSV-PLGA-BNPs also showed all characteristic peaks of RSV with minor shift in absorption bands (Figure 5.21 (b)) which confirmed absence potential chemical interaction between RSV and other formulation excipients.

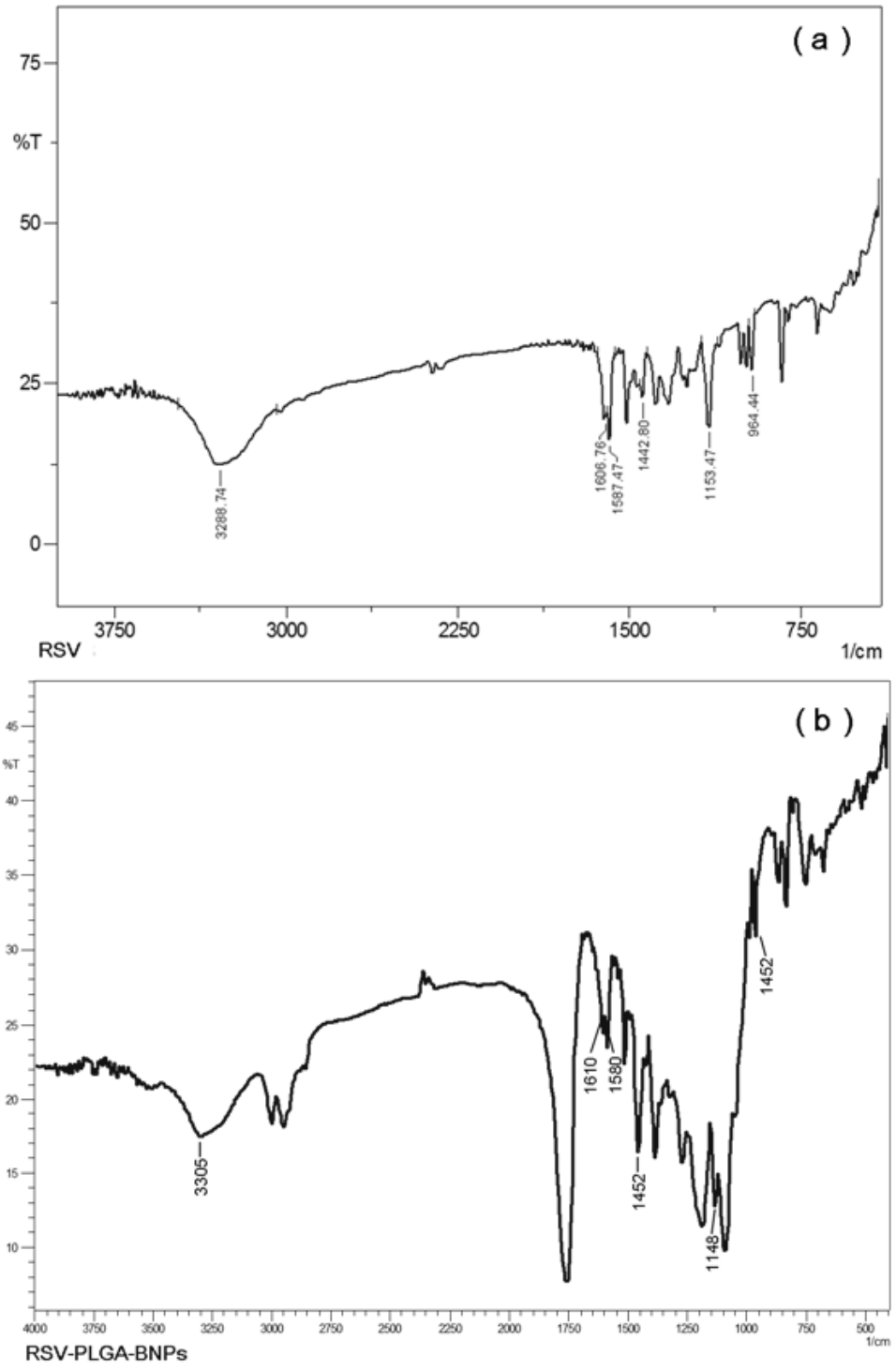

Figure 5.21. Fourier transform infra red (FTIR) spectra of (a) RSV and (b) RSV-PLGA-BNPs.

5.3.7. DSC analysis

DSC analysis was carried out to assess chemical interaction and dispersion pattern of RSV (amorphous or crystalline conversion). DSC thermograms of RSV, PLGA, TPGS and RSV-PLGA-BNPs are shown in Figure 5.22. RSV showed sharp endothermic peak at 267.71 °C which corresponds to its melting point. PLGA showed a peak at 88.12 °C which corresponds to its phase transition temperature. TPGS showed sharp endothermic peak at 35.11 ^{o}C, corresponding to its melting point. RSV-PLGA-BNPs showed two small blunt sharp peaks at 48.02 and 85.56 °C, which is corresponding to the peaks of TPGS and PLGA, respectively, with minor shift in their positions. These results suggest absence of potential chemical interaction between RSV and other formulation excipients. Absence of RSV melting peak at 267.71 °C in DSC thermogram of RSV-PLGA-BNPs suggest that RSV is dispersed in amorphous form.

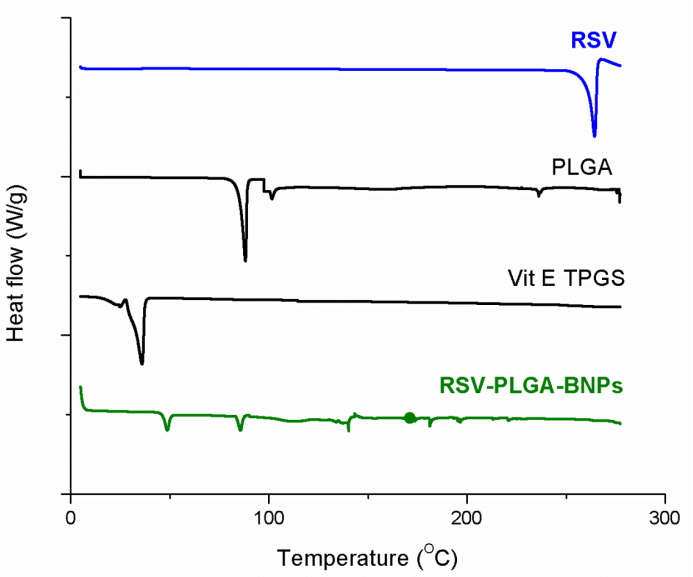

Figure 5.22. Differential scanning calorimetric (DSC) thermograms of RSV, PLGA, TPGS and RSV-PLGA-BNPs

5.3.8. X-Ray diffraction analysis

XRD pattern of RSV and RSV-PLGA-BNPs are shown in Figure 5.23. RSV showed sharp diffraction peaks at 6.62^{o}, 13.2^{o}, 16.36^{o}, 19.18^{o}, 22.28^{o}, 23.54^{o}, 25.18^{o}, 28.26^{o}, 31.6^{o}, 38.32^{o} and 45.18^{o} in 2θ scale. These results showed crystalline nature of RSV. In contrast, RSV-PLGA-BNPs did not show any characteristic intense sharp peaks of RSV. This observation suggest that RSV is converted from crystalline to amorphous form in RSV-PLGA-BNPs formulations. XRD results are well correlated with DSC results, which confirm the conversion of RSV from crystalline to amorphous form.

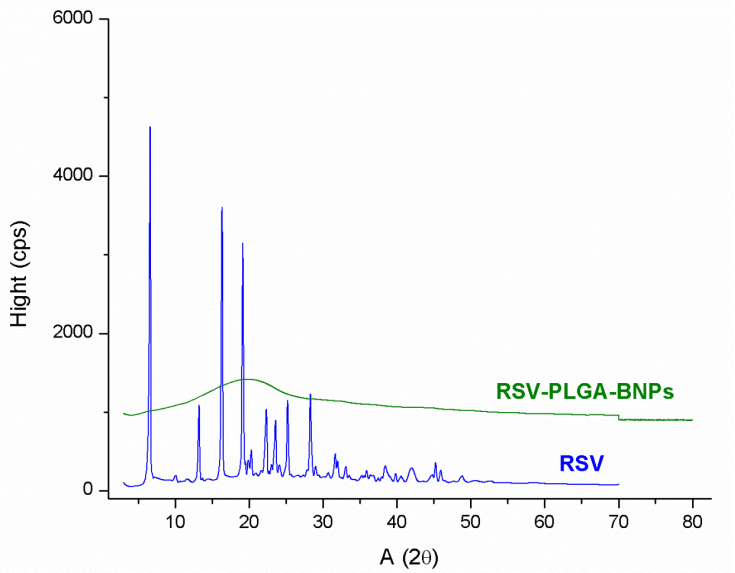

Figure 5.23. X-Ray diffraction pattern of RSV and RSV-PLGA-BNPs.

5.3.9. Cytotoxicity against C6 glioma cells

Cytotoxicity study was performed to compare the efficacy of RSV and RSV-PLGA-BNPs against C6 glioma cell lines. Cytotoxicity of pristine RSV, RSV-PLGA-BNPs and Placebo-PLGA-BNPs against C6 glioma cells is shown in Figure 5.24. Cellular toxicity

of RSV-PLGA-BNPs was found to be significantly higher than that of RSV in all individual concentrations ($p<0.05$). The additional cytotoxic potential of RSV-PLGA-BNPs can be explained from cytotoxic nature of placebo formulation. Placebo-PLGA-BNPs showed statistically significant increase in cytotoxicity in each increment of its concentrations ($p<0.05$) whereas PLGA concentration equivalent to Placebo-PLGA-BNPs dispersed in normal saline without TPGS did not show significant cytotoxicity (results not shown in figure). These results evidently indicated that the cytotoxicity of Placebo-PLGA-BNPs is due to presence of TPGS in the Placebo formulation. Cytotoxic potential of TPGS has been proved against several types of cancer both *in vitro* and *in vivo* as discussed in cytotoxicity of SLN formulations [185, 187, 188]. Therefore, the additional cytotoxicity potential of RSV-PLGA-BNPs in our study is due to presence of TPGS. The additive cytotoxic potential of RSV-PLGA-BNPs will be beneficial in the treatment of glioma.

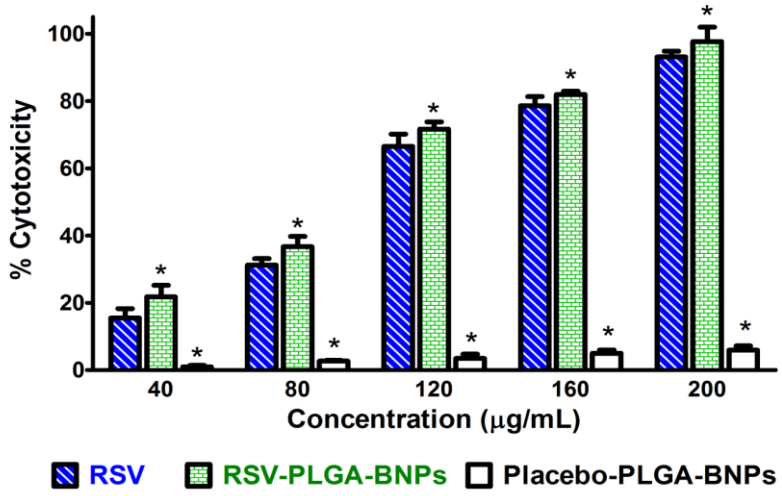

Figure 5.24. ***In vitro*** **cytotoxicity of RSV, RSV-PLGA-BNPs and Placebo-PLGA-BNPs. Values are represented as mean±SD (n=3). *Mark indicates significant difference from RSV ($p<0.05$).**

5.3.10. Cellular uptake

Figure 5.25 shows CLSM images of C6 glioma cells after treating with COU-PLGA-BNPs and counter stained by DAPI to visualize the nucleus. Green and blue are CLSM images of FITC and DAPI channels captured using suitable filters. Cellular uptake of images of COU-PLGA-BNPs (green colour) was visualized by superimposing the FITC channel and DAPI channel (blue colour) as shown in Figure 5.25 (c). COU-PLGA-BNPs showed excellent cell internalization in C6 glioma cells after 2 h of incubation. Nanoparticles were found to be highly concentrated at cytoplasm. According to earlier reported studies, cytoplasm is the major site of several apoptotic mechanisms of RSV as discussed in cellular internalization of SLN formulations [8]. Therefore, the present design of RSV loaded PLGA: TPGS blend nanoparticles can be applied as potential tool to exert its cytotoxic potential at cytoplasm.

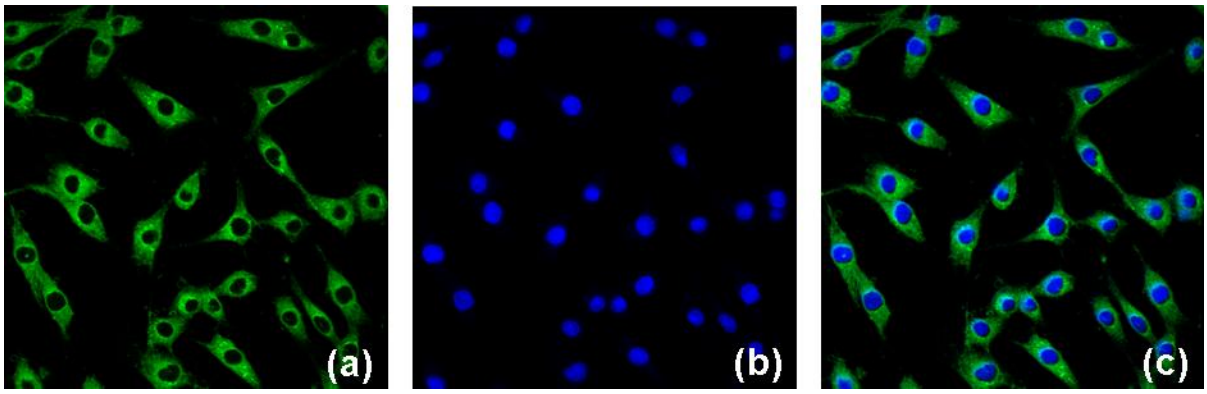

Figure 5.25. Cellular internalization of COU-PLGA-BNPs in C6 glioma cancer cells assessed by confocal laser scanning microscopy (CLSM) (a) FITC channel (green colour-showing COU-PLGA-BNPs localized within the cytoplasm); (b) DAPI channel (blue colour-showing stained nucleus); (c) superimposed image of FITC channel and DAPI channel.

5.3.11. Evaluation of haemolysis

As RSV-PLGA-BNPs is intended for *i.v.* administration, it should not cause haemolytic events during and after infusions. As per international standards, the spontaneous haemolysis limit is 10% to preserve the functionality of erythrocytes in blood [189]. Haemolysis results for 10, 50 and 100 µg/mL concentrations of test samples are shown in Figure 5.26 (a), (b) and (c), respectively. Despite RSV, RSV-PLGA-BNPs and Placebo-PLGA-BNPs showed disparate haemolysis values, haemolysis of all formulations are within the limits (<10%). Therefore, RSV-PLGA-BNPs is safe for *i.v.* administration in terms of haemolysis. Moreover, RSV is proved for protective effect on erythrocytes by decreasing malondialdehyde (MDA) level and protein carbonyl group content [7]. In addition, RSV is also reported for other antioxidative mechanisms such as reduction of

glutathione (GSH) and membrane sulphydryl groups (-SH) in erythrocytes which thereby strongly exhibit protective effect [7]. All these protective mechanisms of RSV might prevent the degradation of erythrocytes upon intravenous administration of RSV-PLGA-BNPs for glioma treatment.

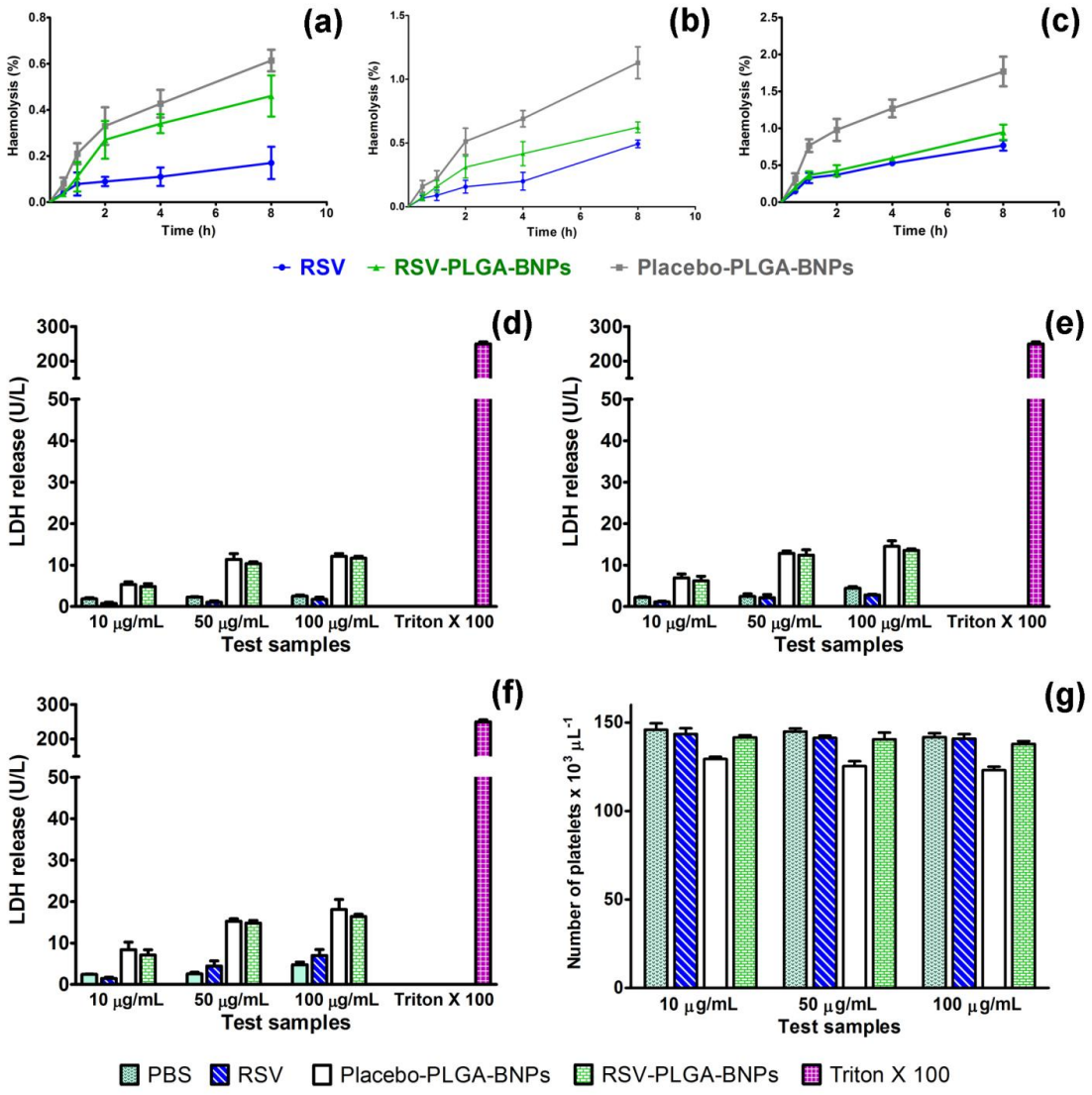

Figure 5.26. Percentage of haemolysis at different time intervals after treating with RSV, Placebo-PLGA-BNPs and RSV-PLGA-BNPs at (a) 10 (b) 50 and (c) 100 µg/mL; Amount of LDH release after treating with PBS, RSV, Placebo-PLGA-BNP

and RSV-PLGA-BNPs at (d) 1, (e) 4 and (f) 8 hours (g) Number of platelets after addition of PBS, RSV, Placebo-PLGA-BNPs and RSV-PLGA-BNPs. Values are represented as mean±SD (n=3).

5.3.12. Evaluation of erythrocyte membrane integrity

White blood cells and plasma were removed and only erythrocytes suspended normal saline solution were used in this study. Evaluation of membrane integrity was assessed by quantifying LDH enzyme. Structural disturbance in erythrocytes membrane integrity results in elevated level of LDH release. Amount of LDH release after treating 1 mL of erythrocyte suspension with RSV, RSV-PLGA-BNPs (equivalent to 10, 50 and 100 μg/mL of RSV) and Placebo-PLGA-BNPs (equal to the volume of RSV-PLGA-BNPs) are shown in Figure 5.26 (d), (e) and (f), respectively. RSV, RSV-PLGA-BNPs and Placebo-PLGA-BNPs did not show significant increase in LDH release in comparison to spontaneous enzyme release observed in PBS treated samples after 1, 4 and 8 h of incubation at all concentrations. These results suggest that membrane integrity of erythrocyte is not affected at these concentrations of test samples. Therefore, RSV or RSV-PLGA-BNPs formulations in blood at 10, 50 and 100 μg/mL concentrations will not damage erythrocyte membrane integrity. Thus, RSV and RSV-PLGA-BNPs are safe for *i.v.* administration in terms of safety of erythrocytes.

5.3.13. Platelet Aggregation

Excessive or inappropriate aggregation of platelets upon *i.v.* infusion of nanoparticulate fomulations may lead to thrombus formations in blood vessels that result in transient ischemia, myocardial infarction or stroke. Therefore, evaluation of platelet aggregation

upon *i.v.* administration of RSV-PLGA-BNPs formulation is essential. Platelet aggregation was carried out quantitatively using haematological counter after incubating with RSV, RSV-PLGA-BNPs and Placebo-PLGA-BNPs at three different concentrations (equivalent to 10, 50 and 100 μg/mL of RSV). PBS was served as spontaneous control to assess dilution effect. RSV treated samples did not show any significant difference in platelet count than that of PBS treated samples at all concentrations. These results suggest that RSV is not promoting platelet aggregation (Figure 5.26 (g)). Placebo-PLGA-BNPs showed significantly lower ($p<0.05$) platelet count than that of PBS treated samples in all concentration ranges; however, RSV-PLGA-BNPs treated samples showed statistically comparable platelet counts ($p>0.05$). Lower platelet count observed in Placebo-PLGA-BNPs may be due to the effect of its formulation components. Though all components of Placebo-PLGA-BNPs present in RSV loaded blended nanoparticulate formulations, RSV-PLGA-BNPs showed higher platelet count than that of its Placebo counterpart and similar platelet count as of PBS treated samples. This may be due to antiplatelet aggregation property of RSV. Systemic administration of RSV is proved to obstruct the increase in platelet aggregation in rabbits induced by hypercholesterolaemic diet [7]. Moreover, RSV is proved for anti platelet aggregation effect *in vitro* as discussed in platelet aggregation of SLN formulations [20].

In addition to platelet count, platelet aggregation in whole blood was also observed by optical microscope after incubation with test samples (PBS, RSV, Placebo-PLGA-BNPs and RSV-PLGA-BNPs) at three equivalent concentrations (10, 50 and 100 µg/mL). Erythrocytes, leucocytes and platelets were visualized using microscope and images were captured. Platelets are indicated by arrow marks in microphotographs (Figure 5.27).

Supportively, no platelet aggregation was seen in all test samples at three different concentrations. Though slight decrease in platelet count was observed with Placebo-PLGA-BNPs in quantitative measurements, platelets were distributed evenly throughout the blood smears in microscopic observations. All these observations suggest that RSV and RSV-PLGA-BNPs are nontoxic and haemocompatible in nature. All these haemocompatibility results suggest that both RSV and RSV-PLGA-BNPs are safe for *i.v.* administration.

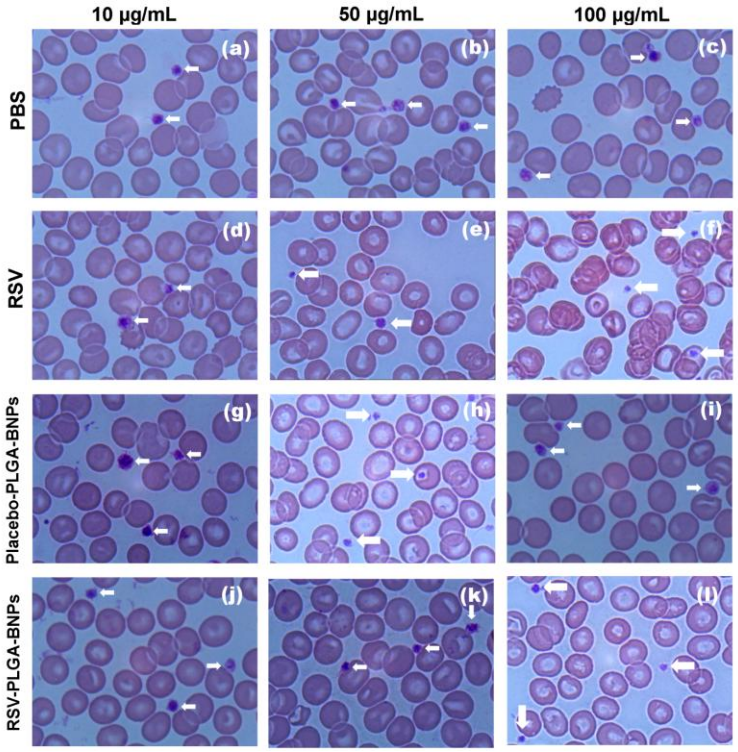

Figure 5.27. Light microscopy images of Leishman's stained whole blood samples after treating with (a) PBS equivalent volume to 10 µg/mL of test samples (b) PBS equivalent volume to 50 µg/mL of test samples (c) PBS equivalent volume to 100 µg/mL of test samples (d) 10 µg/mL RSV (e) 50 µg/mL RSV (f) 100 µg/mL RSV (g) 10 µg/mL Placebo-PLGA-BNPs (h) 50 µg/mL Placebo-PLGA-BNPs (i) 100 µg/mL

Placebo-PLGA-BNPs (j) 10 µg/mL RSV-PLGA-BNPs (k) 50 µg/mL RSV-PLGA-BNPs (l) 100 µg/mL RSV-PLGA-BNPs. Images were captured at magnification of 100x.

5.3.14. Pharmacokinetic studies

Comparative plasma concentration time profiles of RSV, RSV-PLGA-BNPs up to 48 h and 2 h (part of curve) are shown in Figure 5.28. Pharmacokinetic parameters analysed using WinNonlin 6.4 software is presented in Table 5.6. Pharmacokinetic profile of RSV solution showed rapid decline up to 0.5 h with the plasma concentration of 235.33±115.63 ng/mL. Plasma concentration was increased at 1 h (a small second peak) and declined again and was undetectable after 2 h. Similarly, RSV-PLGA-BNPs showed marked decline at 2 h with 493.65±294.51 ng/mL concentration and again rose to give second peak at 8 h with 828.19±270.03 ng/mL. Plasma concentration was continuously declined and was undetectable after 36 h. Formation of second peak (increment in plasma concentration) in RSV and RSV-PLGA-BNPs may be due enterohepatic circulation of drug. Enterohepatic circulation of RSV observed in our study was well correlated with the earlier publications [190]. Initial plasma concentration (C_0) of RSV and RSV-PLGA-BNPs was found to be 2625.33±366.74 and 2053.46±50.42 ng/mL, respectively. Area under the curve (AUC) and plasma half life ($t_{1/2}$) of RSV-PLGA-BNPs was found to be approximately 15.99 and 18.11 times higher than that of RSV solution, respectively. The higher AUC and $t_{1/2}$ may be due to presence of TPGS at the surface of RSV-PLGA-BNPs. Plasma half life ($t_{1/2}$) of RSV obtained in this study is well correlated with the calculated value of 0.55 h, calculated by Bayesian estimations in population

pharmacokinetic study at 2, 10 and 20 mg/kg [17]. The $t_{1/2}$ of RSV was found to be slightly higher than another reported value of 0.13±0.02 h at 15 mg/kg of RSV after *i.v.* administration in rats [18]. Clearance (CL) value of RSV-PLGA-BNPs was found to be 15.98 times lower than that of RSV solution. Short $t_{1/2}$ of RSV was well correlated with its higher clearance (CL) value (1894.84±382.46 mL/h/kg). Similarly, higher $t_{1/2}$ of RSV-PLGA-BNPs was in agreement with its lower CL value (118.53±33.35 mL/h/kg). Volume of distribution (V_d) of RSV and RSV-PLGA-BNPs were found to be statistically similar ($p>0.05$). V_d of RSV and RSV-PLGA-BNPs were found to be significantly higher than the total body water of a rat (150 mL/kg for a body weight of 0.25 kg) [17]. These results suggest that RSV and RSV-PLGA-BNPs undergo extensive tissue binding after *i.v.* administration. Mean residence time (MRT) of RSV-PLGA-BNPs was found to be approximately 12.52 times higher than that of RSV solution. TPGS present at the surface of RSV-PLGA-BNPs prevents adhesion of plasma proteins (opsonizaiton) due to stealth nature and thereby avoids recognition by reticulo endothelial system and eventually prolonged the systemic circulation. Pharmacokinetic study showed higher AUC, $t_{1/2}$ and MRT and lower CL of RSV-PLGA-BNPs than that of RSV solution. These results clearly suggest that PLGA: TPGS blend nanoparticle design will be a potential tool for improving systemic availability, prolonging systemic circulation and half life of RSV.

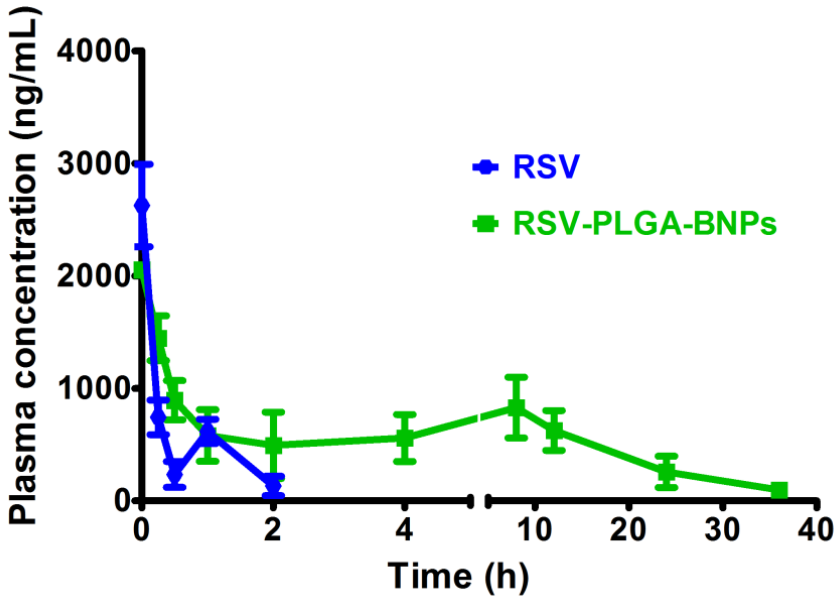

Figure 5.28. Comparative plasma concentration time profile of RSV and RSV-PLGA-BNPs up to 36 hours after *i.v.* administration of 2 mg/kg dose; Each data point is presented as mean±SD (n=6).

Table 5.6. Pharmacokinetic parameters of RSV and RSV-PLGA-BNPs after intravenous administration of 2 mg/kg dose.

Pharmacokinetic parameters	**RSV**	**RSV-PLGA-BNPs**
C_0 (ng/mL)	2463.5±334.46	2053.467±50.422*
AUC (ng*h/mL)	1013.56±194.54	16212.73±2646.026*
$t_{1/2}$ (h)	0.53±0.25	9.60±2.91*
CL (mL/h/kg)	1894.84±382.46	118.53±33.35*
V_d (mL/kg)	1431.82±220.73	1703.31±491.80
MRT (h)	0.58±0.18	12.48±0.69*

Data is presented as mean±SD (n=6); (*) Statistically significant difference from RSV ($P<0.05$).

5.3.15. Tissue distribution studies

Tissue distribution of RSV and RSV-PLGA-BNPs is shown in Figure 5.29. RSV-PLGA-BNPs showed highest accumulation in brain of 3.57±0.53 µg/g. Brain accumulation of RSV was found to be only 0.81±0.48 µg/g. Brain distribution of RSV-PLGA-BNPs was found to be approximately 4.41 times higher than that of RSV solution ($p<0.05$). RSV and RSV-PLGA-BNPs showed insignificant difference in their lung distributions. Liver accumulation of RSV and RSV-PLGA-BNPs was found to be 0.39±0.22 and 1.12±0.39 µg/g, respectively. RSV-PLGA-BNPs showed approximately 2.88 times lower liver distribution than that of RSV. In addition, spleen accumulation of RSV-PLGA-BNPs was also found to be approximately 2.18 times lower in comparison to RSV solution

($p<0.05$). Lower liver and spleen accumulation of RSV-PLGA-BNPs may be due to presence of TPGS at the nanoparticulate surface. The hydrophilic part of TPGS present at the surface of RSV-PLGA-BNPs reduces opsonisation and thus prevents recognition by monocytes, macrophages and Kupffer cells. This resulted in lower accumulation in liver and spleen and facilitated RSV-PLGA-BNPs to remain in blood pool for longer period of time. The reduction of liver distribution eventually minimizes the rate of biotransformation of RSV-PLGA-BNPs. Moreover, RSV molecules entrapped inside RSV-PLGA-BNPs will not readily available for glucuronidation or sulfonation like free RSV in liver which further delays biotransformation process. The lower liver and spleen accumulation in biodistribution study is well correlated with higher AUC and $t_{1/2}$ of RSV-PLGA-BNPs observed in pharmacokinetic studies. Kidney is the major elimination organ of RSV. Total renal excretion of RSV after *i.v.* administration was calculated to be 42.3 to 83.2% in previous publications [16]. Renal distribution of RSV-PLGA-BNPs was found be significantly lower than that of RSV solution. The lower distribution of RSV-PLGA-BNPs in kidney may be expected to decrease the elimination. Overall review of bio distribution results showed significantly higher brain distribution of RSV-PLGA-BNPs than that of RSV solution. Therefore, RSV-PLGA-BNPs can be applied as an effective tool to improve passive brain targeting potential of RSV useful in the treatment of glioma.

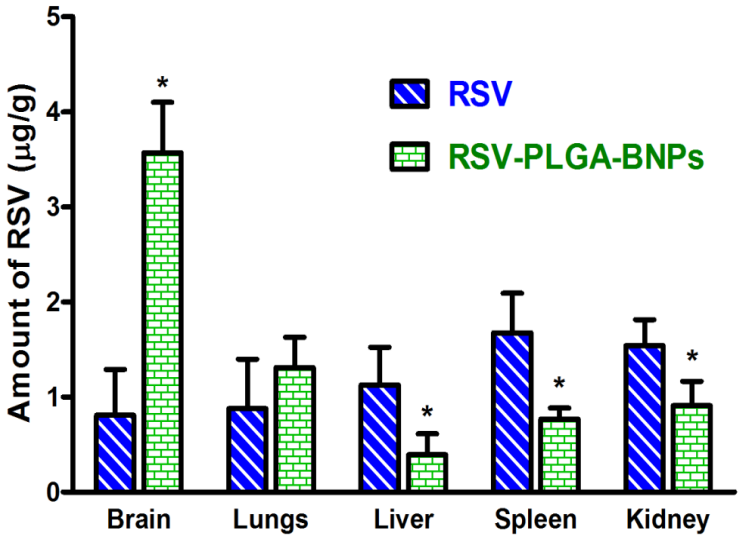

Figure 5.29. Comparative *in vivo* biodistribution of RSV and RSV-PLGA-BNPs in brain, lungs, liver, spleen and kidney after *i.v.* administration of 2 mg/kg dose; Values are presented as mean±SD (n=3), p<0.05. (*) Statistically significant difference from RSV (p<0.05).

5.3.16. Concluding results of RSV-PLGA-BNPs

Parameters	**Result for RSV-PLGA-BNPs**
Particle size	175.5±8.4 nm
Polydispersity index	0.147±0.09
Zeta potential	-16.86±1.59 mV
Shape	Spherical
Entrapment efficiency	61.81±3.57%
In vitro release studies	Sustained, Higuchi, anomalous
Interaction analysis (DSC/ FTIR)	No potential chemical interaction
Analysis of crystalinity (XRD)	Crystalline to amorphous
Cytotoxicity in C6 glioma cells (in comparison to RSV)	Higher cytotoxicity (due to TPGS)
Cellular uptake	Excellent cellular internalization
Haemolysis	Less than limit (10%), safe for *i.v.*
Erythrocyte membrane integrity	Less than limit (10%) , safe for *i.v.*
Platelet aggregation	No aggregation and safe for *i.v.*
Pharmacokinetic studies	Higher AUC, $t_{1/2,}$ MRT; present in blood up to 36 h
Tissue distribution studies	Higher brain; lower liver, spleen and kidney

5.4. Core-shell polymer-lipid hybrid nanoparticles

In our previous studies on solid lipid nanoparticles and PLGA:TPGS blend nanoparticles several pharmacokinetic parameters of RSV were improved. Among them, RSV-PLGA-BNPs showed significantly higher $t_{1/2,}$ MRT and systemic circulation in comparison to RSV-TPGS-SLN. RSV-PLGA-BNPs showed the $t_{1/2}$ of 9.60±2.91 h whereas RSV-TPGS-SLN showed only 5.53±0.55 h ($p<0.05$). MRT of RSV-PLGA-BNPs (12.48±0.69 h) was found to be increased twice in comparison to RSV-TPGS-SLN (6.84±0.23 h). Moreover, RSV was detected in blood up to 48 h when we administered RSV-PLGA-BNPs whereas RSV-TPGS-SLN was present in blood only up to 36 h. Though few pharmacokinetic parameters were improved with RSV-PLGA-BNPs in comparison to RSV-TPGS-SLN, the brain distribution was significantly decreased with the blend nanoparticles. Brain distribution of RSV-TPGS-SLN was found to be 7.48±1.69 µg/g whereas RSV-PLGA-BNPs showed only 3.57±0.53 µg/g. The higher lipophilic nature of SLN might be the reason for higher brain accumulation. Blend nanoparticles favour prolonged systemic circulation and solid nanoparticles support higher brain accumulation.

HNPs are novel drug delivery platform for higher drug entrapment, sustained drug release, stability in biological fluids and prolonged systemic circulation. Docetaxel loaded HNPs were prepared and proved for controlled release up to 4 days and better *in vitro* stability in phosphate buffered saline (PBS), plasma/heparin and foetal bovine serum (FBS) [179, 196]. Transferrin (Tf) conjugated HNPs were prepared for targeted delivery of aromatase inhibitor, 7α-(4'-amino) phenylthio-1,4-androstadiene-3,17-dione

(7α-APTADD) and proved for enhanced aromatase inhibition activity than that of non-targeted HNPs [197]. Vascular targeted HNPs were prepared for temporal antivasculature and anticancer activities and shown for efficient uptake by human umbilical vein endothelial cells [178]. siRNA loaded HNPs coated with targeting ligand (folate) and cell-penetrating peptides (penetratin) were also reported for synergistic action of dual-functionalization with increased cell surface avidity afforded by both ligands [198]. Paclitaxel loaded HNPs coated with collagen IV-targeting peptides were proved for lower neointima-to-media (N/M) scores at 2 wk and ∼50% reduction in arterial stenosis in comparison to sham-injury groups [199]. pH sensitive and magnetic field activated HNPs were proved for enhancing therapeutic efficacy and minimizing side-effects of chemotherapeutics by controllably releasing the encapsulated drug at the target site [200, 201]. Quantum dot loaded HNPs, co-delivery of chemotherapeutics and therapeutic radioisotopes (ChemoRad) HNPs and photothermal therapy HNPs were also reported for combining therapeutic and diagnostic functions [177, 202, 203]. Therefore, we developed RSV loaded TPGS and DSPE PEG 2000 coated core-shell polymer-lipid hybrid nanoparticles to improve the biological half life, prolonged systemic circulation, higher brain accumulation and therapeutic efficacy of RSV.

5.4.1. Particle size, poly dispersity index and zeta potential

Since TPGS is applied first time to prepare HNPs, formulation variables such as TPGS+Phospholipid concentration and volume of organic solvent were varied in order to get lower particle size and higher entrapment efficiency. With increase in the TPGS+Phospholipid concentration, the particle size decreased at all levels of volume of

organic solvent (1, 3 and 5 mL) as shown in Figure 5.30. The decreasing particles size may be due to stabilization effect of TPGS and phospholipid. TPGS is proved to be a best stabilizer in lower concentration (0.015% w/v) and having relatively low critical micelle concentration (CMC) of 0.02% w/w [22]. Therefore, TPGS in our formulation may effectively covers the surface of RSV-TPGS-HNPs and stabilize them to form lower particle size. Particle size was found to be significantly decreased as increasing the volume of organic solvent in 15+15 and 30+30 mg TPGS+Phospholipid concentrations. There was no marked change in particle size at 45+45 mg TPGS+Phospholipid concentration. Polydispersity varied from 0.208±0.05 to 0.388±0.12. Zeta potential of RSV-TPGS-HNPs varied from -6.42±0.75 to -48.35±2.34 mV. There was no trend observed in polydispersity index and zeta potential as changing formulation variables (Table 5.7).

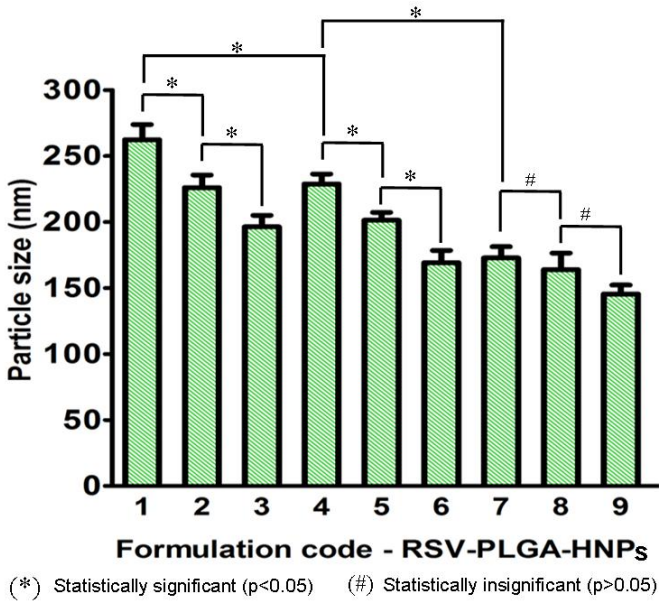

Figure 5.30. Particle size of various formulations of RSV-TPGS-HNPs. Values are represented as mean±SD (n=3).

Table 5.7. Polydispersity index and zeta potential of various batches of RSV-TPGS-HNPs

Formulation code	Polydispersity index	Zeta potential (mV)
RSV-TPGS-HNPs 1	0.190±0.082	-11.57±1.21
RSV-TPGS-HNPs 2	0.306±0.094	-14.94±0.59
RSV-TPGS-HNPs 3	0.388±0.078	-48.35±2.34
RSV-TPGS-HNPs 4	0.445±0.052	-13.97±1.24
RSV-TPGS-HNPs 5	0.351±0.081	-6.85±0.67
RSV-TPGS-HNPs 6	0.414±0.102	-9.57±1.59
RSV-TPGS-HNPs 7	0.462±0.086	-6.47±1.34
RSV-TPGS-HNPs 8	0.308±0.023	-6.42±0.75
RSV-TPGS-HNPs 9	0.217±0.110	-7.63±0.29

5.4.2. Entrapment efficiency

Entrapment efficiency of various batches of RSV-TPGS-HNPs is shown in Figure 5.31. Entrapment efficiency was found to be significantly increased with increasing phospholipid+TPGS concentration at all levels of organic solvent volumes. For an instance, entrapment efficiency of phospholipid+TPGS concentrations 15+15, 30+30 and 45+45 mg at 5 mL organic solvent was found to be 69.62±3.41, 77.46±2.67 and 84.31±1.46%, respectively. This may be due to combined effect of phospholipid and TPGS. As RSV is lipophilic in nature, the higher concentration of phospholid (lipophilic) may increase entrapment efficiency. TPGS was also proved to stabilize the lipophilic drug molecules inside the nanoparticle construct to result in higher entrapment efficiency

[22]. Increasing organic solvent did not result in significant change in entrapment efficiency in all concentration of phospholipid+TPGS.

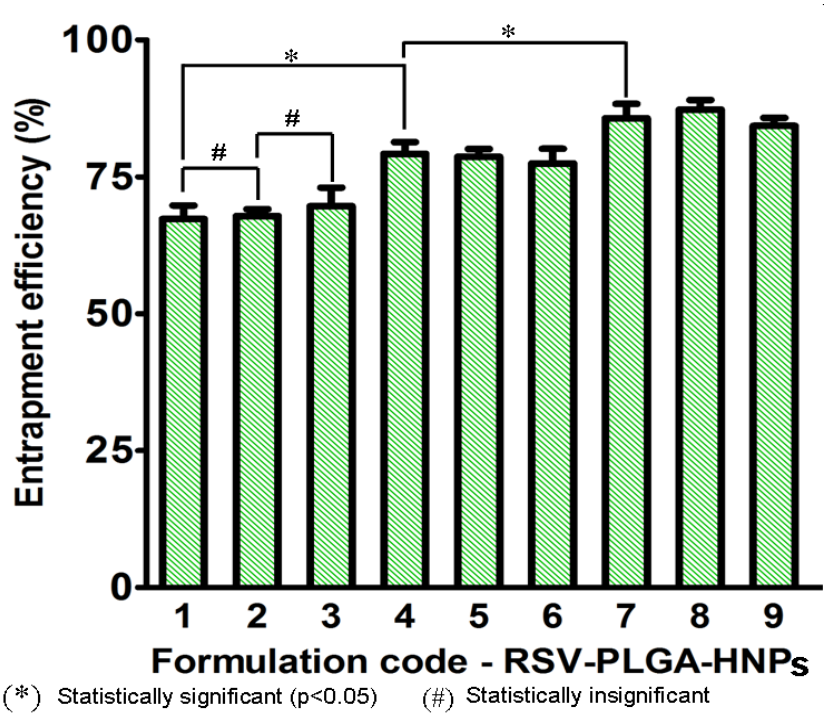

Figure 5.31. Entrapment efficiency of various batches of RSV-TPGS-HNPs. Values are represented as mean±SD (n=3).

5.4.3. Selection of best formulation

RSV-TPGS-HNPs 9 having particle size of 145.5±9.7 nm, PDI of 0.217±0.11, zeta potential of -7.63±0.29 mV and entrapment efficiency of 84.31±1.46% was selected as optimized formulation among TPGS coated HNPs. RSV-PEG-HNPs prepared using similar composition of RSV-TPGS-HNPs 9 by replacing TPGS with DSPE PEG 2000 showed the particle size of 238.4±12.6 nm, polydispersity index of 0.228±0.12 and

entrapment efficiency of 76.59±2.49%. Zeta potential of RSV-PEG-HNPs was found to be -15.46±2.34 mV.

5.4.4. Shape of HNPs

Shape of both RSV-TPGS-HNPs and RSV-PEG-HNPs was found to be spherical as shown in Figure 5.32 (a) and (b), respectively. The polymer core and lipid shell were clearly differentiated in both HNPs.

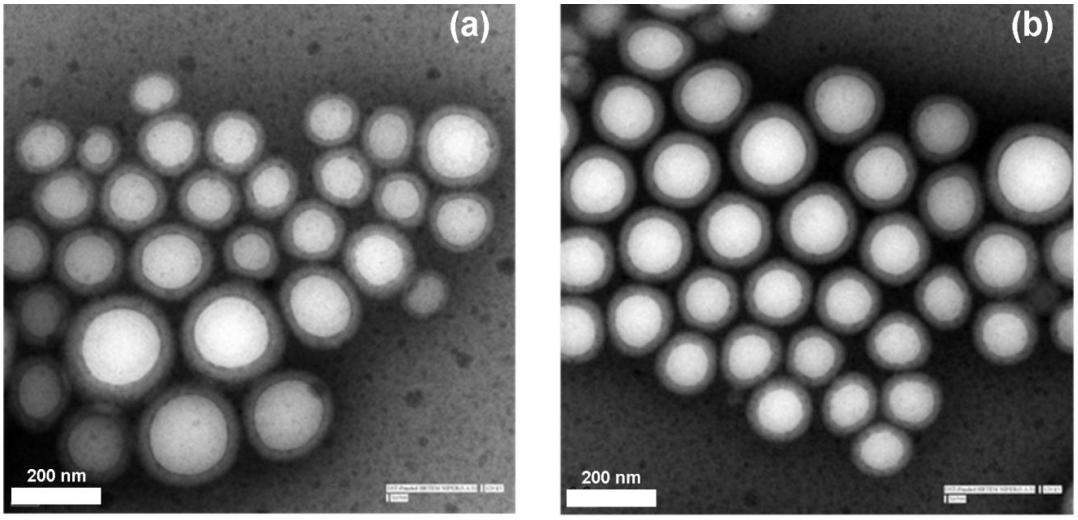

Figure 5.32. Transmission electron microscope images of (a) RSV-TPGS-HNPs and (b) RSV-PEG-HNPs.

5.4.5. *In vitro* drug release

The release of RSV from RSV-TPGS-HNPs and RSV-PEG-HNPs was found to be controlled throughout the study period of 48 h without any burst release (Figure 5.33). Correlation co-efficient (R^2) value of HNPs fitted in zero order, first order, Higuchi model and Korsmeyer–Peppas model is shown in Table 5.8. The results suggest that

Higuchi kinetics is the best fit model for both RSV-TPGS-HNPs and RSV-PEG-HNPs. Hence, diffusion is the possible drug release mechanism. The release exponent (n) value of RSV-TPGS-HNPs and RSV-PEG-HNPs calculated by Korse-Meyer Peppas model was found to be 0.6224 and 0.7160, respectively. Therefore, the mechanism of drug release from both HNPs was found to be 'anomalous transport' which indicates non-linear diffusion of RSV molecules with respect to time.

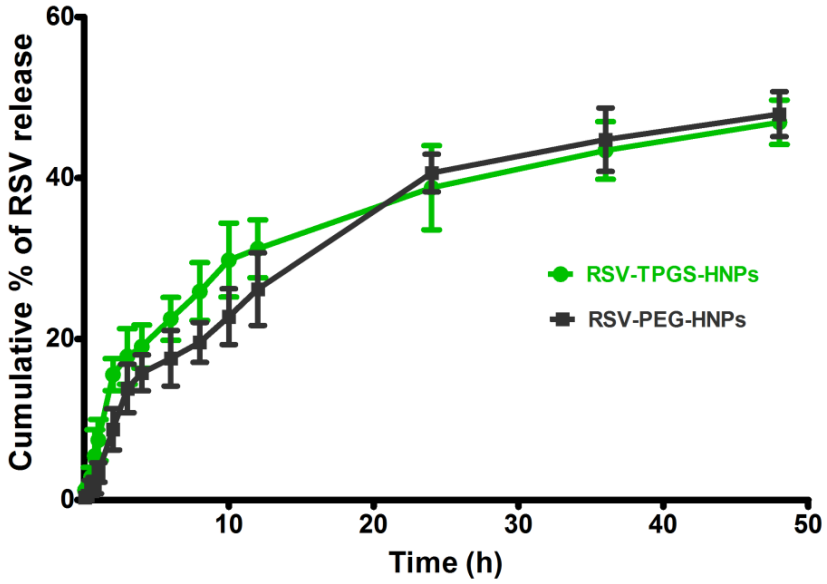

Figure 5.33. *In vitro* release profile of RSV-TPGS-HNPs and RSV-PEG-HNPs. Values are represented as mean±SD (n=3)

Table 5.8. Correlation co-efficient (R^2) and release exponent (n) value of *in vitro* drug release kinetics from RSV-TPGS-HNPs and RSV-PEG-HNPs

Kinetics/Parameters	**RSV-TPGS-HNPs**	**RSV-PEG-HNPs**
Zero order	0.7692	0.7661
First order	0.8388	0.8300
Higuchi model	0.9512	0.9497
Korsmeyer–Peppas model	0.9437	0.9315
Release exponent (n)	0.6224	0.7160
Best fit	**Higuchi kinetics**	
Mechanism of RSV release	**Anomalous transport**	

5.4.6. Drug-excipient interaction analysis

FTIR analysis was used to evaluate the potential chemical interaction of RSV with other formulation excipients of RSV-TPGS-HNPs and RSV-PEG-HNPs. FTIR spectrum of RSV and lyophilized RSV-TPGS-HNPs and RSV-PEG-HNPs are shown in Figure 5.34 (a), (b) and (c), respectively. RSV showed its characteristic absorption bands at 964.4 cm^{-1} for *trans* olefinic bond, 3288.7 $cm^{-1}$for O-H stretching of alcoholic group, 1606.7 cm^{-1}

for C-C stretching of olefinic group, 1153.4 cm^{-1} for C - O stretching and 1442.8 cm^{-1} and 1587.4 cm^{-1} for C=C stretching of aromatic ring. RSV-TPGS-HNPs showed all of these characteristic peaks of RSV at 964.44, 3288.74, 1606.76, 1153.47, 1442.80 and 1587.47 cm^{-1} and RSV-PEG-HNPs showed peaks at 966.37, 3200.01, 1635.69, 1147.68, 1464.02 and 1587.47 cm^{-1} with minor shift in absorption band positions which revealed the absence potential chemical interaction between RSV and other formulation components in both HNPs.

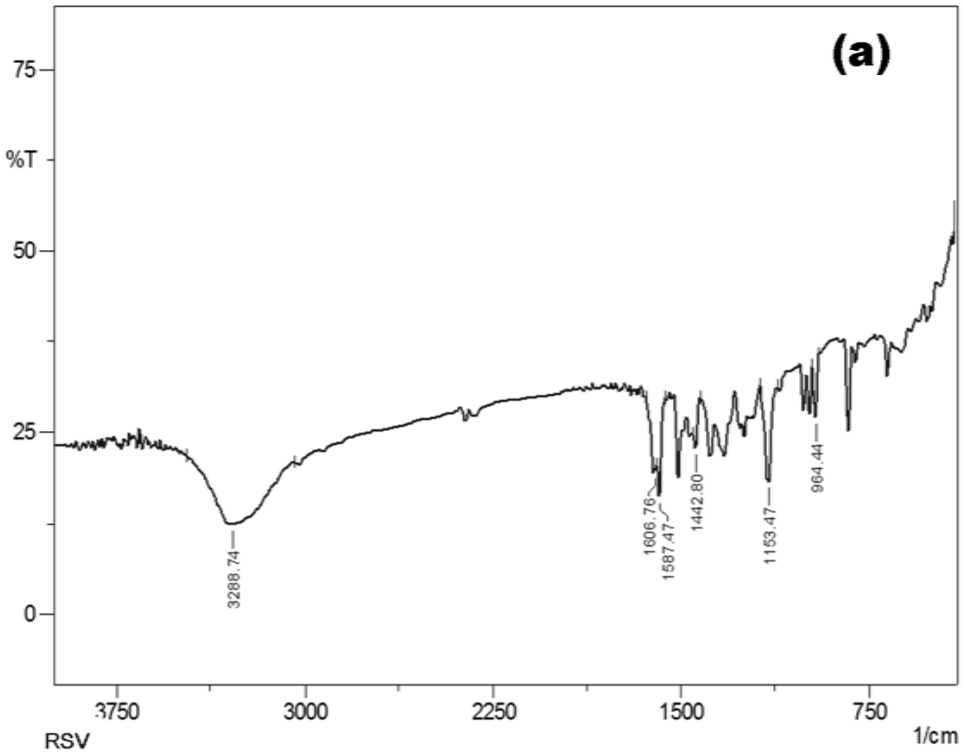

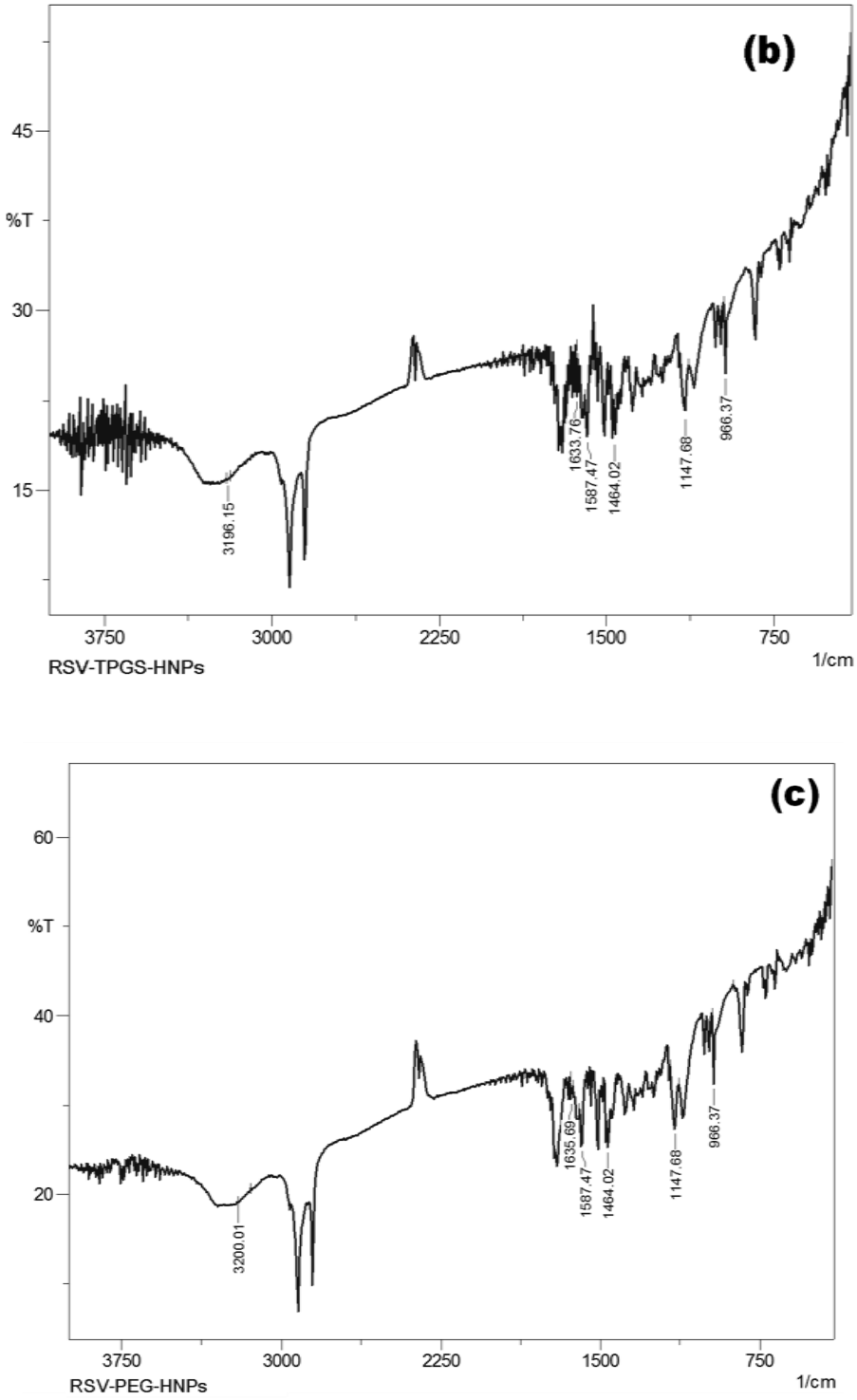

Figure 5.34. Fourier transform infra red (FTIR) spectra of (a) RSV (b) RSV-TPGS-HNPs and (c) RSV-PEG-HNPs

5.4.7. DSC analysis

DSC analysis was also carried out to study the potential chemical interaction and solid state behaviour of RSV after preparation of HNPs. DSC thermograms are shown in Figure 5.35. RSV showed sharp endothermic peak at 267.71 °C which corresponds to its melting point. PLGA showed a peak at 88.12 °C which corresponds to its phase transition temperature. Phosphatidylcholine showed two blunt peaks at 68.12 and 79.04 ^{o}C. TPGS and DSPE PEG 2000 showed their sharp endothermic peaks at 35.11 and 56.58 ^{o}C, respectively. RSV-TPGS-HNPs showed a small blunt sharp peak at 46.24 ^{o}C and a sharp peak at 75.66 °C which are corresponding to the peaks of TPGS and PLGA, respectively, with minor shift in their positions. Similarly, RSV-PEG-HNPs showed a small blunt sharp peak at 48.72 ^{o}C and a sharp peak at 75.89 ^{o}C which are corresponding to the peaks of DSPE PEG 2000 and PLGA, respectively, with minor shift in their positions. Absence of RSV melting peak at 267.71 °C in DSC thermogram of RSV-TPGS-HNPs and RSV-PEG-HNPs suggest the conversion of crystalline form of RSV to amorphous form in HNPs construct. All these results suggest the absence of potential chemical interaction between RSV and other excipients of both HNPs.

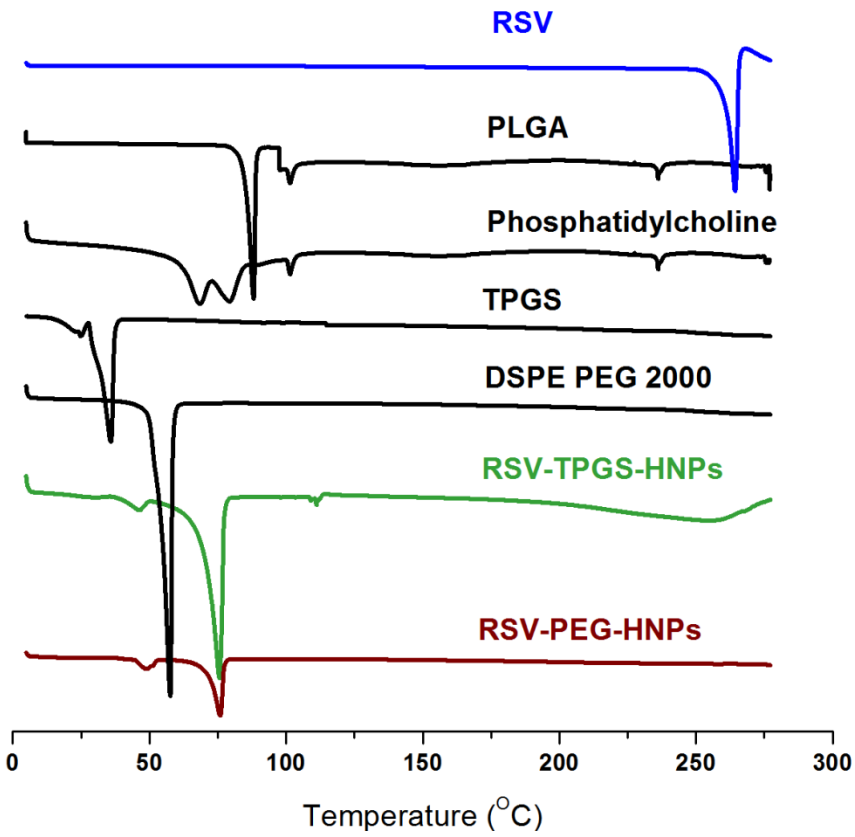

Figure 5.35. Differential scanning calorimetric (DSC) thermograms of RSV, phosphatidylcholine, TPGS, DSPE PEG 2000, RSV-TPGS-HNPs and RSV-PEG-HNPs.

5.4.8. Analysis of crystalinity

XRD pattern of RSV, RSV-TPGS-HNPs and RSV-PEG-HNPs are shown in Figure 5.36. RSV showed sharp diffraction peaks at 6.62°, 13.2°, 16.36°, 19.18°, 22.28°, 23.54°, 25.18°, 28.26°, 31.6°, 38.32° and 45.18° in 2θ scale. Presence of such sharp peak indicates crystalline nature of RSV. In contrast, RSV-TPGS-HNPs and RSV-PEG-HNPs did not show any characteristic sharp peaks. These results indicated the conversion of RSV from crystalline to amorphous form in RSV-TPGS-HNPs and RSV-PEG-HNPs formulations.

XRD results are well correlated with DSC results, which confirm the conversion of RSV from crystalline form to amorphous form in both HNPs.

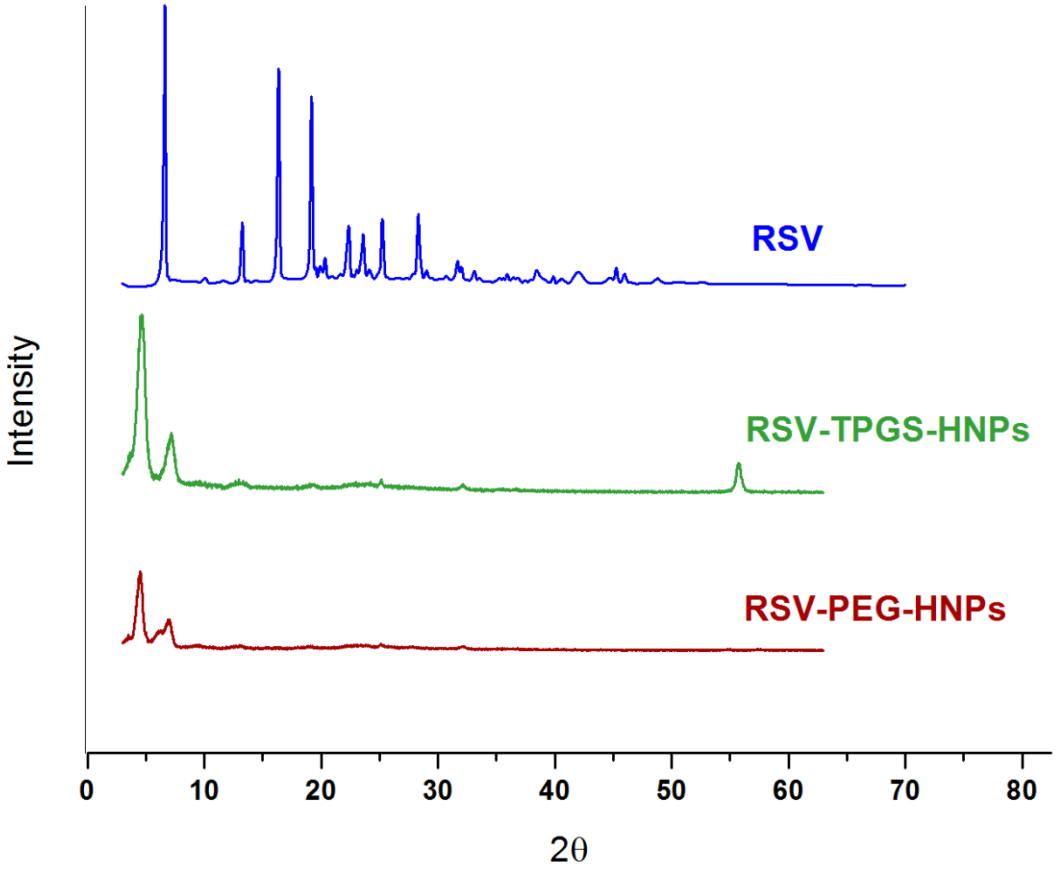

Figure 5.36. X-Ray diffraction (XRD) pattern of RSV, RSV-TPGS-HNPs and RSV-PEG-HNPs

5.4.9. Cytotoxicity studies

Cytotoxicity of pristine RSV, RSV-TPGS-HNPs, RSV-TPGS-HNPs, Placebo-TPGS-HNPs and Placebo-PEG-HNPs against C6 glioma cells is shown in Figure 5.37. RSV-TPGS-HNPs showed significantly higher cytotoxicity than RSV in all individual concentrations except 200 µg/mL, at which maximum cell death was reached in all

samples. The additional cytotoxic potential of RSV-TPGS-HNPs can be explained from the cytotoxicity of its placebo formulation. Placebo-TPGS-HNPs showed statistically significant increase in cytotoxicity in each increment of its concentrations ($p<0.05$) whereas equivalent concentration of lipid components of Placebo-TPGS-HNPs dispersed in water without TPGS did not show any cytotoxicity (not shown in figure). These results evidently indicate that the cytotoxicity of Placebo-TPGS-HNPs is due to TPGS. The cytotoxic potential of TPGS has been proved for several types of cancer types both *in vitro* and *in vivo* as explained in earlier chapters [185-188]. The additional cytotoxic potential of RSV-TPGS-HNPs will be more beneficial in the treatment of glioma without any toxicity to the normal cells. Cellular toxicity of RSV and RSV-PEG-HNPs was found to be statistically similar in all individual concentrations ($p>0.05$). Therefore, the cytotoxic potential of RSV is not changed upon entrapping in RSV-PEG-HNPs. Placebo-PEG-HNPs showed negligible cytotoxicity in all individual concentrations.

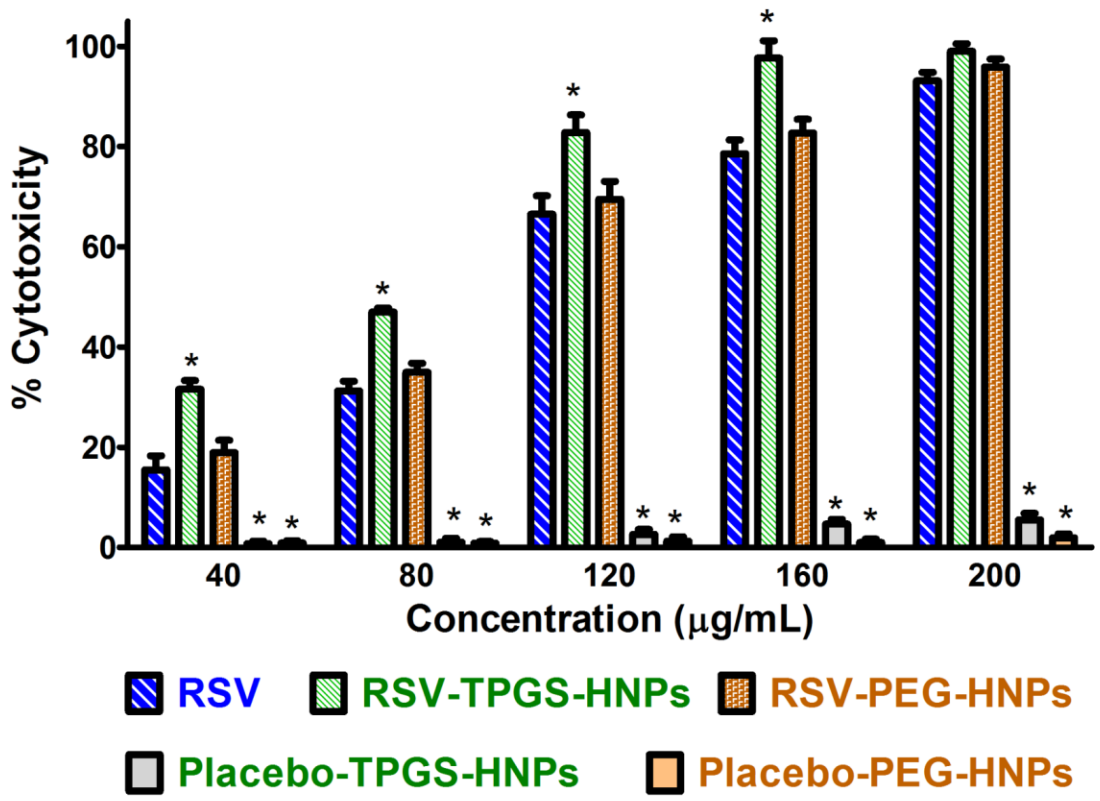

Figure 5.37. *In vitro* cytotoxicity of RSV, RSV-TPGS-HNPs, Placebo-TPGS-HNPs, RSV-PEG-HNPs and Placebo-PEG-HNPs. Values are represented as mean±SD (n=3). *Mark indicates significant difference from RSV ($p<0.05$).

5.4.10. Cellular uptake of HNPs

Figure 5.38 (a, b and c) shows CLSM images of C6 glioma cells after treating with COU-TPGS-HNPs and counter stained by DAPI to visualize the nucleus. Figure 5.38 (a) and (b) are showing CLSM images of FITC and DAPI channels captured using suitable filters, respectively. Cellular uptake of images of COU-TPGS-HNPs (green colour) was visualized by superimposing the FITC channel and DAPI channel (blue colour) as shown in Figure 5.38 (c). COU-TPGS-HNPs showed excellent cellular internalization in C6

glioma cells after 2 h of incubation. COU-TPGS-HNPs were found to be highly concentrated at cytoplasm. Similarly, Figure 5.38 (d, e and f) shows CLSM images of C6 glioma cells after treating with COU-PEG-HNPs and counter stained by DAPI to visualize the nucleus. Figure 5.38 (d) and (e) are showing CLSM images of FITC and DAPI channels captured using suitable filters, respectively. Cellular uptake of images of COU-PEG-HNPs (green colour) was visualized by superimposing the FITC channel and DAPI channel (blue colour) as shown in Figure 5.38 (f). COU-PEG-HNPs showed excellent cellular internalization in C6 glioma cells after 2 h of incubation. COU-PEG-HNPs were also found to be highly concentrated at cytoplasm. According to earlier reported studies, several cytotoxic mechanisms of RSV are taken place at cytoplasm [8]. Therefore, the present designs of RSV-TPGS-HNPs and RSV-PEG-HNPs can be applied as potential tool to exert its cytotoxic effect at cytoplasm.

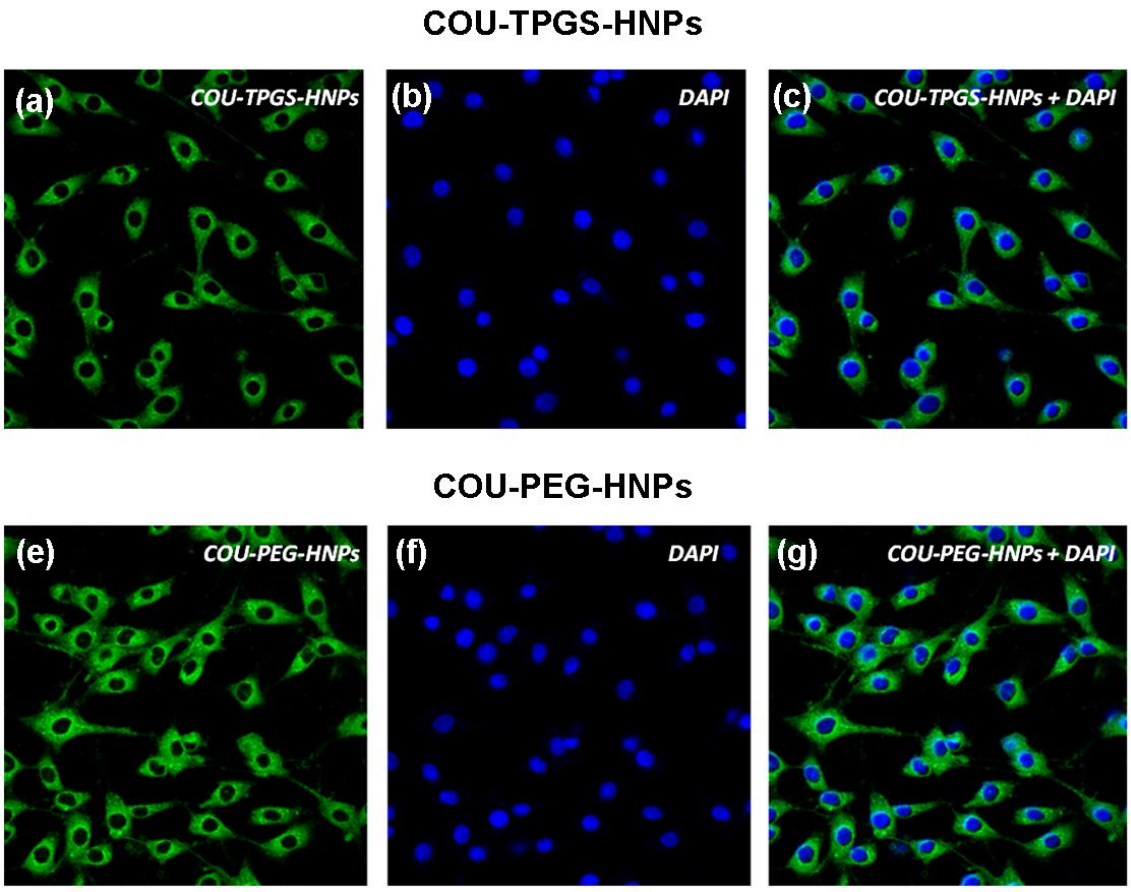

Figure 5.38. Cellular internalization of COU-TPGS-HNPs (a, b and c) and COU-PEG-HNPs (d, e and f) in C6 glioma cancer cells assessed by confocal laser scanning microscopy (CLSM).

5.4.11. Evaluation of haemolysis

As the RSV-TPGS-HNPs and RSV-PEG-HNPs are intended for *i.v.* administration, it should not cause haemolytic events during and after infusions and hence, the evaluation of haemolysis was carried out. As per international standards, the spontaneous haemolysis limit is 10% to preserve the functionality of erythrocytes in blood [189]. Haemolysis results of HNPs at 10, 50 and 100 µg/mL concentrations of test samples are

shown in Figure 5.39. Though RSV, RSV-TPGS-HNPs, RSV-PEG-HNPs, Placebo-TPGS-HNPs and Placebo-PEG-HNPs showed disparate percentage of haemolysis, all formulations are within the haemolysis limit of less than 10%. Therefore, RSV-TPGS-HNPs and RSV-PEG-HNPs are safe for *i.v.* administration in terms of haemolysis. Moreover, RSV is also reported for antioxidative mechanisms and protective effect on erythrocytes as explained in previous chapters. The protective nature of RSV may be expected to prevent the degradation of erythrocytes upon intravenous administration of RSV-TPGS-HNPs and RSV-PEG-HNPs for the treatment of glioma.

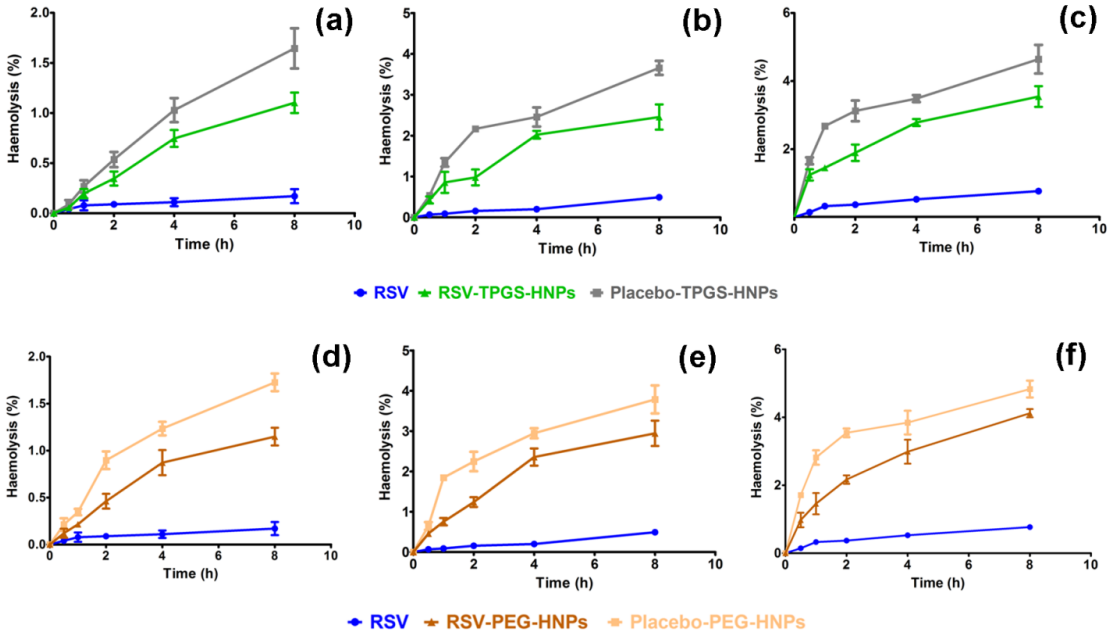

Figure 5.39. Percentage of haemolysis at different time intervals in whole blood samples after addition of (a) 10 (b) 50 (c) 100 µg/mL of RSV-TPGS-HNPs and (d) 10 (e) 50 (f) 100 µg/mL of RSV-PEG-HNPs. Values are represented as mean±SD (n=3).

5.4.12. Evaluation of erythrocyte membrane integrity

Any disturbance in structural integrity of erythrocytes membrane results in elevated level of LDH release. Therefore, evaluation of membrane integrity was assessed via quantifying lactate dehydrogenase enzyme by LDH assay. White blood cells and plasma were removed by centrifugation and only erythrocytes suspended normal saline was used in this study. Amount of LDH release after treating 1 mL of erythrocyte suspension with RSV, RSV-TPGS-HNPs and RSV-PEG-HNPs (equivalent to 10, 50 and 100 μg/mL of RSV), Placebo-TPGS-HNPs and Placebo-TPGS-HNPs (equal to the volume of respective HNPs) are shown in Figure 5.40. RSV, RSV-TPGS-HNPs, RSV-PEG-HNPs, Placebo-TPGS-HNPs and Placebo-PEG-HNPs also showed insignificant increase in LDH release in comparison to spontaneous enzyme release observed in PBS treated samples after 1, 4 and 8 h of incubation at all individual concentrations. Therefore, RSV and HNPs formulations in blood at 10, 50 and 100 μg/mL concentrations are safe for erythrocyte membrane integrity. All these results suggest that RSV, RSV-TPGS-HNPs and RSV-PEG-HNPs are safe for *i.v.* administration in terms of safety of erythrocytes.

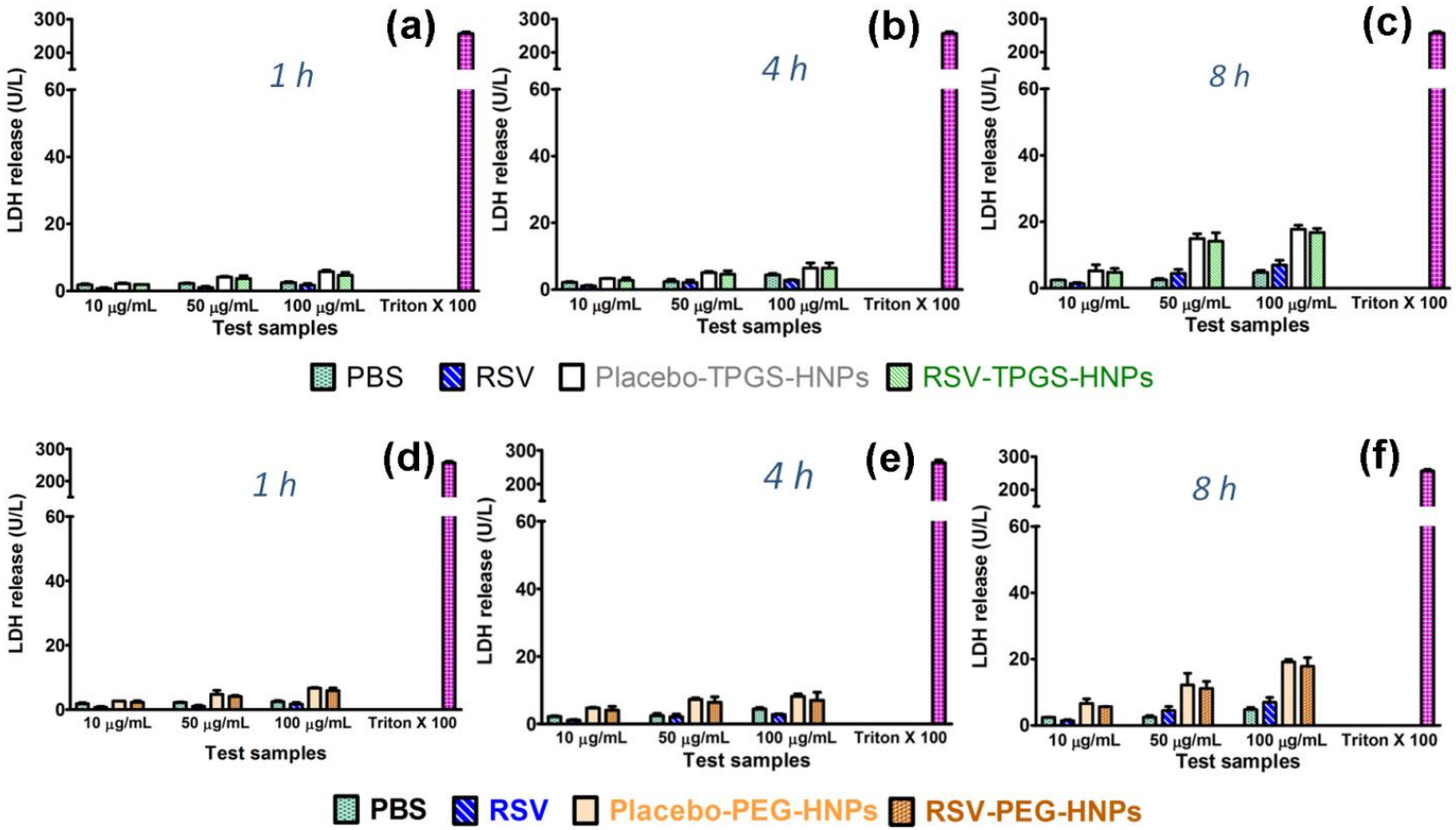

Figure 5.40. Amount of LDH release after treating with RSV-TPGS-HNPs at (a) 1, (b) 4 and (c) 8 hours and RSV-PEG-HNPs at (d) 1, (e) 4 and (f) 8 hours. Values are represented as mean±SD (n=3).

5.4.13. Platelet Aggregation

Aggregation of platelets upon *i.v.* infusion of nanoparticulate formulations may lead to thrombus formations in blood vessels which result in transient ischemia, myocardial infarction or stroke. Therefore, we evaluated *in vitro* platelet aggregation RSV, RSV-TPGS-HNPs and RSV-PEG-HNPs. Quantitative platelet aggregation was evaluated using haematological counter after incubating with RSV, RSV-TPGS-HNPs, RSV-PEG-HNPs, Placebo-TPGS-HNPs and Placebo-PEG-HNPs at three different concentrations (equivalent to 10, 50 and 100 μg/mL of RSV). PBS treated samples were used as spontaneous control. Quantitative platelet aggregation results are shown in Figure 5.41 (a) and (b). RSV treated samples did not show significant difference in platelet count than that of PBS treated samples at all concentrations. Therefore, RSV is not promoting platelet aggregation. RSV-TPGS-HNPs, RSV-PEG-HNPs, Placebo-TPGS-HNPs and Placebo-PEG-HNPs showed lesser platelet count in comparison to PBS and RSV ($p>0.05$). Lower platelet count may be due to the effect of formulation components. The percentage platelet count of RSV-TPGS-HNPs at 10, 50 and 100 μg/mL concentrations was calculated to be 95.72±2.46, 94.45±2.41 and 92.03±0.87%, respectively. Similarly, RSV-PEG-HNPs showed the percentage of platelet count of 93.89±2.46, 92.52±1.80 and 91.84±1.35% at 10, 50 and 100 μg/mL, respectively. The reduction of platelet in both HNPs was found to be less than 10%. Therefore, the reduction of platelet count upon RSV-TPGS-HNPs and RSV-PEG-HNPs is acceptable.

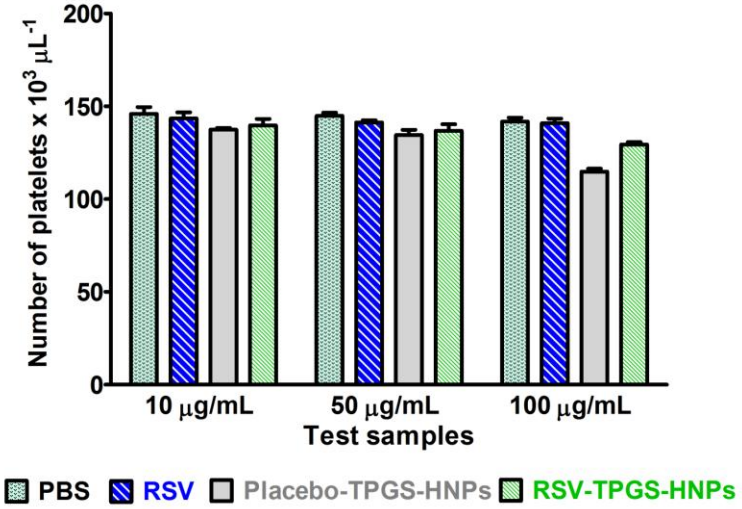

Figure 5.41. (a) Number of platelets after addition of PBS, RSV, Placebo-TPGS-HNPs and RSV-TPGS-HNPs at 10, 50 and 100 µg/mL. Values are represented as mean±SD (n=3).

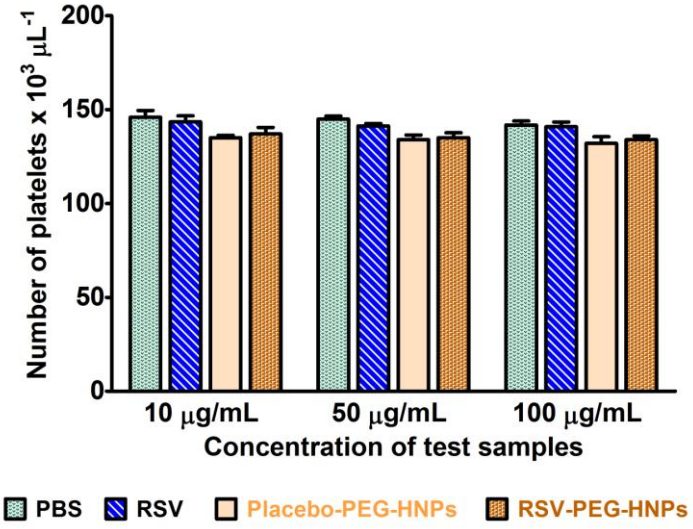

Figure 5.41. (b) Number of platelets after addition of PBS, RSV, Placebo-PEG-HNPs and RSV-PEG-HNPs at 10, 50 and 100 µg/mL. Values are represented as mean±SD (n=3).

Platelet aggregation in whole blood was also observed by optical microscope after incubation with test samples (PBS, RSV, Placebo-TPGS-HNPs, Placebo-PEG-HNPs, RSV-TPGS-HNPs and RSV-PEG-HNPs) at three equivalent concentrations (10, 50 and 100 µg/mL). Erythrocytes, leucocytes and platelets were visualized using microscope and images were captured. Platelets are pointed out by arrow marks in microphotographs (Figure 5.42). Though significant decrease in platelet count was observed with Placebo-TPGS-HNPs, Placebo-PEG-HNPs, RSV-TPGS-HNPs and RSV-PEG-HNPs in quantitative measurements, platelet aggregation was not observed in all three different concentrations of test samples and platelets were distributed uniformly throughout the blood smears of microphotographs. Therefore, RSV, RSV-TPGS-HNPs and RSV-PEG-HNPs are nontoxic and haemocompatible in nature and safe for *i.v.* administration.

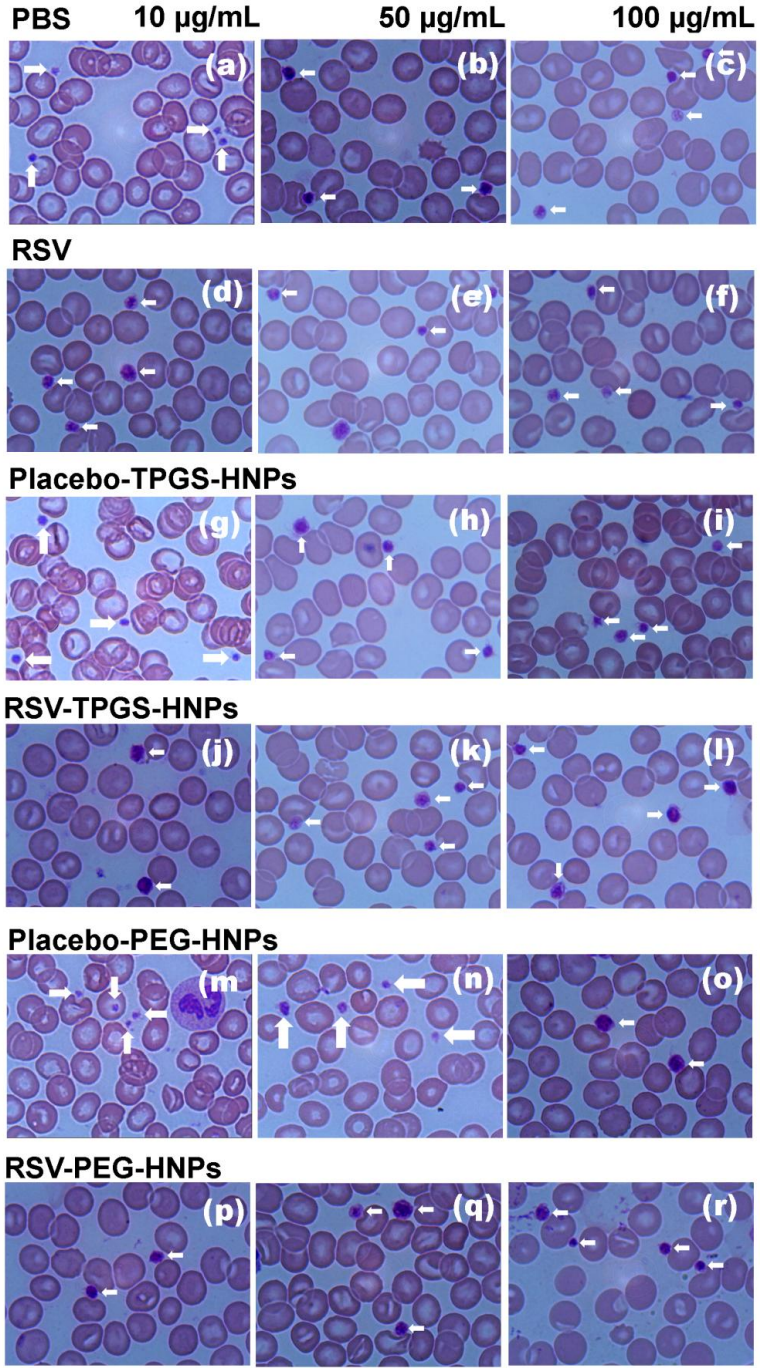

Figure 5.42. Light microscopy images of Leishman's stained whole blood samples after treating with (a) PBS equivalent volume to 10 µg/mL of test samples (b) PBS equivalent volume to 50 µg/mL of test samples (c) PBS equivalent volume to 100

µg/mL of test samples (d) 10 µg/mL RSV (e) 50 µg/mL RSV (f) 100 µg/mL RSV (g) 10 µg/mL Placebo-TPGS-HNPs (h) 50 µg/mL Placebo-TPGS-HNPs (i) 100 µg/mL Placebo-TPGS-HNPs (j) 10 µg/mL RSV-TPGS-HNPs (k) 50 µg/mL RSV-TPGS-HNPs (l) 100 µg/mL RSV-TPGS-HNPs (m) 10 µg/mL Placebo-PEG-HNPs (n) 50 µg/mL Placebo-PEG-HNPs (o) 100 µg/mL Placebo-PEG-HNPs (p) 10 µg/mL RSV-PEG-HNPs (q) 50 µg/mL RSV-PEG-HNPs (r) 100 µg/mL RSV-PEG-HNPs. Images were captured at magnification of 100x.

5.4.14. Pharmacokinetic studies

The comparative plasma concentration time profiles of RSV-TPGS-HNPs and RSV-PEG-HNPs with RSV up to 48 h are shown in Figure 5.43 (a) and (b), respectively. Pharmacokinetic parameters calculated by WinNonlin 6.4 software is presented in Table 5.9. RSV solution showed sudden decline up to 0.5 h, showed peak value at 1 h and declined again up to 2 h. The plasma concentration was undetectable after 2 h. Similarly, RSV-TPGS-HNPs showed marked decline at 4 h and again formed a peak at 24 h. Plasma concentration was continuously declined and was undetectable after 48 h. RSV-PEG-HNPs showed marked decline at 4 h and again formed a peak at 24 h. Plasma concentration was continuously declined and was undetectable after 48 h. The additional peaks (increment in plasma concentration) observed in RSV, RSV-TPGS-HNPs and RSV-PEG-HNPs may be due enterohepatic circulation. Enterohepatic circulation of RSV was explained in earlier publications by conversion of RSV into glucuronide/sulfate conjugates and secreted to small intestine via breast cancer resistance protein and multidrug resistance protein 2 [190]. Moreover, RSV undergoes sulphonation by

sulfotransferase enzyme to form *trans*-resveratrol-3-sulfate and glucuronidation by glucuronosyl transferase enzyme to form *trans*-resveratrol-C/O-diglucuronides. Enterohepatic circulation of RSV observed in our experiments was well correlated with the earlier publications [190]. Initial plasma concentration (C_0) of RSV, RSV-TPGS-HNPs and RSV-TPGS-HNPs was found to be 2517.44±254.28, 2051.45±130.44 and 2251.63±89.33 ng/mL, respectively. C_0 value of RSV was slightly higher than that of RSV-TPGS-HNPs and similar to that of RSV-PEG-HNPs. Area under the curve (AUC) and plasma half life ($t_{1/2}$) of RSV-TPGS-HNPs was found to be approximately 13.83 and 29.15 times higher than that of RSV solution, respectively. Similarly, $t_{1/2}$ and AUC of RSV-PEG-HNPs was found to be approximately 16.93 and 12.46 times higher than that of RSV solution, respectively. The higher $t_{1/2}$ and AUC of HNPs may be due to presence of TPGS or DSPE PEG 2000 at the surface of nanoparticles. Plasma half life ($t_{1/2}$) of RSV obtained in this study is well correlated with earlier publications calculated by Bayesian estimations in population pharmacokinetic study at 2, 10 and 20 mg/kg (0.55 h), [17]. Volume of distribution (V_d) of RSV-TPGS-HNPs were found to be significantly higher than that of RSV solution as well as RSV-PEG-HNPs ($p<0.05$). The V_d of RSV, RSV-TPGS-HNPs and RSV-PEG-HNPs were found to be significantly higher than the total body water of a rat (150 mL/kg for a body weight of 0.25 kg) [17]. These observations suggest that RSV as well as both HNPs undergo extensive tissue binding after *i.v.* administration. Clearance (CL) value of RSV-TPGS-HNPs and RSV-PEG-HNPs was found to be 14.75 and 12.60 times lower than that of RSV solution, respectively. Lower $t_{1/2}$ of RSV was well correlated with its higher clearance (CL) value. Similarly, higher $t_{1/2}$ of RSV-TPGS-HNPs and RSV-PEG-HNPs were in agreement with

its lower CL value. Mean residence time (MRT) of RSV-TPGS-HNPs and RSV-PEG-HNPs was found to be approximately 26.76 and 27.57 times higher than that of RSV solution, respectively ($p<0.05$). The higher AUC, $t_{1/2}$ and MRT of RSV-TPGS-HNPs and RSV-PEG-HNPs may be due to its stealth nature. TPGS or DSPE PEG 2000 present at the surface of HNPs prevents adhesion of plasma proteins (opsonisation), consequently avoids recognition by reticulo endothelial system (RES) and thereby prolonged the systemic circulation. Pharmacokinetic study showed lower CL and higher AUC, $t_{1/2}$ and MRT of HNPs than that of RSV solution. These results suggest that both HNPs will be the potential tool for improving systemic availability, prolonging systemic circulation and half life of RSV.

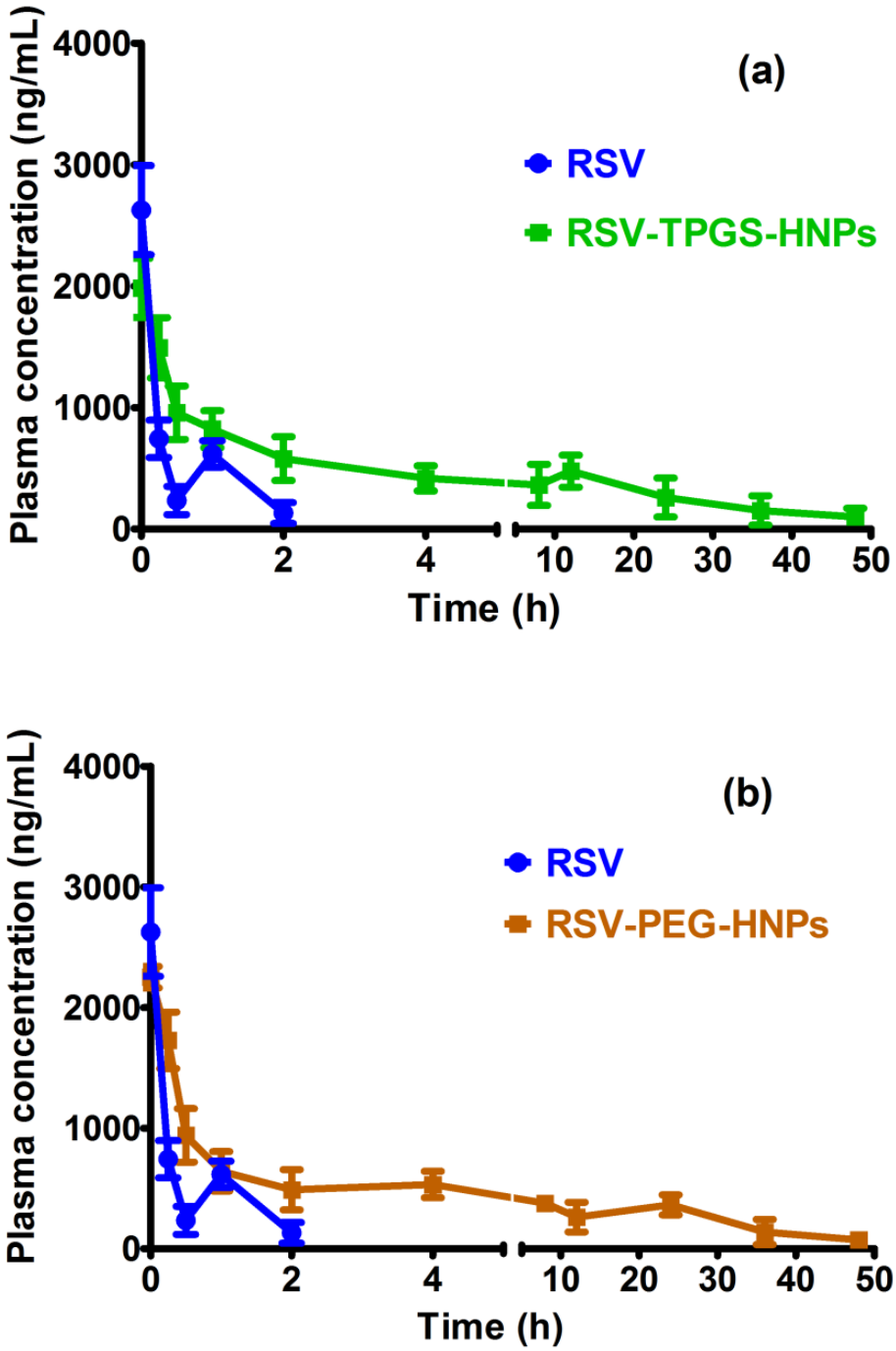

Figure 5.43. Comparative plasma concentration time profile of (a) RSV-TPGS-HNPs and (b) RSV-PEG-HNPs with RSV up to 48 hours after *i.v.* administration of 2 mg/kg dose; Each data point is the representation of mean±SD (n=6).

Table 5.9. Pharmacokinetic parameters of RSV, RSV-TPGS-HNPs and RSV-PEG-HNPs after intravenous administration of 2 mg/kg dose.

Pharmacokinetic parameters	**RSV**	**RSV-TPGS-HNPs**	**RSV-PEG-HNPs**
C_0 (ng/mL)	2517.44±254.28	2051.45±130.44*	2251.63±89.33
AUC (ng*h/mL)	1052.69±153.35	14554.34±2916.42*	13970.73±2708.24*
$t_{1/2}$ (h)	0.54±0.04	15.74±4.07*	10.33±4.15*
CL (mL/h/kg)	1823.05±297.66	123.55±34.37*	135.45±31.52*
V_d (mL/kg)	1415.61±158.58	2671.32±164.0*	1975.32±675.87
MRT (h)	0.59±0.02	15.79±2.99*	16.54±1.23*

Data is presented as mean±SD (n=6); *Mark indicates significant difference from RSV ($p<0.05$).

5.4.15. Tissue distribution studies

Tissue distribution of RSV and RSV-TPGS-HNPs is shown in Figure 5.44. RSV-TPGS-HNPs and RSV-PEG-HNPs showed highest accumulation in brain of 5.49±0.34 and 4.57±0.48 µg/g. Brain accumulation of RSV was found to be only 0.92±0.56 µg/g. Brain distribution of RSV-TPGS-HNPs and RSV-PEG-HNPs was found to be approximately 5.94 and 4.96 times higher than that of RSV solution, respectively ($p<0.05$). Several

drugs having higher molecular weights are not able to enter the brain due to presence of the blood-brain barrier (BBB) and therefore cannot be applicable in the treatment of brain diseases. Nanocarriers were developed to improve the delivery of drugs inside the brain. Colloidal nanocarriers having 200 and 250 nm are well reported for crossing blood brain barrier (BBB) [191-193]. Passive brain targeting efficiency of such nanoparticles is proved in healthy and diseased conditions both *in vitro* and *in vivo* experiments [191-194]. Therefore, RSV-TPGS-HNPs and RSV-PEG-HNPs having particle size of 145.5±9.7 and 238.4±12.6 nm can be expected to cross BBB effectively to deliver RSV in brain. Our findings are in conformation with the earlier reports [204, 205]. Both RSV-TPGS-HNPs and RSV-PEG-HNPs showed statistically similar lung distribution than that of RSV ($p>0.05$). Liver accumulation of RSV, RSV-TPGS-HNPs and RSV-PEG-HNPs was found to be 0.675±0.24, 0.24±0.02 and 0.14±0.12 µg/g, respectively. RSV-TPGS-HNPs and RSV-PEG-HNPs showed approximately 2.74 and 4.86 times lower liver distribution than that of RSV. In our case, the RSV-TPGS-HNPs and RSV-PEG-HNPs are coated with TPGS and DSPE PEG 2000, respectively. Hydrophilic part of the TPGS and DSPE PEG 2000 projected from the surface of HNPs reduces adhesion of opsonin proteins and thus prevents recognition by monocytes, macrophages and Kupffer cells. Thus resulted in lower accumulation of HNPs in liver and facilitated to remain in blood pool for prolonged period of time. The reduction of liver distribution consequently minimizes the biotransformation rate of RSV-TPGS-HNPs and RSV-PEG-HNPs. Moreover, RSV molecules entrapped inside the HNPs is not readily available for glucuronidation or sulfation like free RSV which further delays biotransformation process. The lower liver accumulation in biodistribution study is well correlated with

higher AUC, $t_{1/2}$ and MRT of both HNPs observed in pharmacokinetic studies. Spleen distribution of RSV, RSV-TPGS-HNPs and RSV-PEG-HNPs were found to be statistically similar ($p>0.05$). Kidney is the major elimination organ of RSV. Total renal excretion of RSV after *i.v.* administration reported in earlier publications was found to be in the range of 42.3 to 83.2% [16]. Renal distribution of RSV-TPGS-HNPs and RSV-PEG-HNPs was found be significantly lower (3.82 and 3.67 times, respectively) than that of RSV solution. The lower distribution of RSV-TPGS-HNPs in kidney can be expected to delay the elimination and prolong the systemic circulation. The higher brain distribution of RSV-TPGS-HNPs suggest that the present design of HNPs can be applied as an effective tool to improve passive brain targeting potential of RSV.

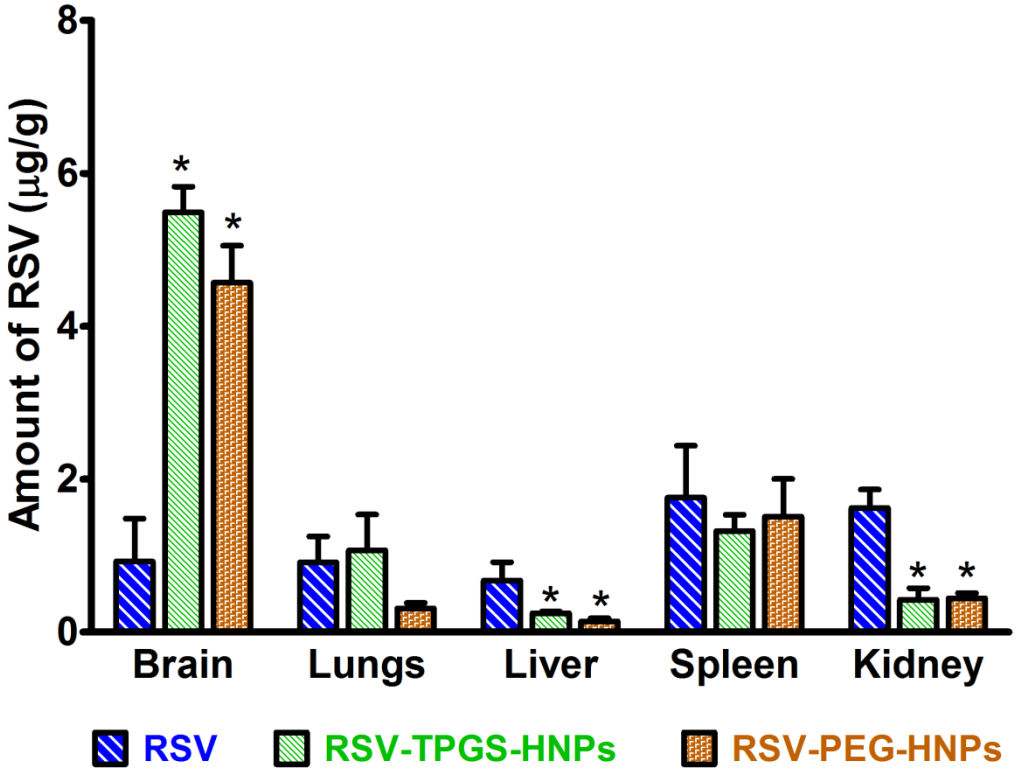

Figure 5.44. Comparative *in vivo* biodistribution of RSV, RSV-TPGS-HNPs and RSV-PEG-HNPs in brain, lungs, liver, spleen and kidney after *i.v.* administration of 2 mg/kg dose; Values are represented as mean±SD (n=3). *Mark indicates significant difference from RSV ($p<0.05$).

5.4.16. Comparative results of RSV-TPGS-HNPs and RSV-PEG-HNPs

Parameters	**RSV-TPGS-HNPs**	**RSV-PEG-HNPs**
Particle size	145.5±9.7 nm	238.4±12.6 nm
Polydispersity index	0.217±0.11	0.228±0.12
Zeta potential	-7.63±0.29 mV	-15.46±2.34 mV
Shape	Spherical	
Entrapment efficiency	84.31±1.46%	76.59±2.49%
In vitro release studies	Sustained, Higuchi, anomalous	
Interaction analysis (DSC/FTIR)	No potential chemical interaction	
Analysis of crystallinity (XRD)	Crystalline to amorphous	
Cytotoxicity in C6 glioma cells (in comparison to RSV)	Higher cytotoxicity (due to TPGS)	Similar cytotoxicity
Cellular uptake	Excellent cellular internalization	
Haemolysis	Less than limit (10%), safe for *i.v.*	
Erythrocyte membrane integrity	Less than limit (10%) , safe for *i.v.*	
Platelet aggregation	No aggregation and safe for *i.v.*	
Pharmacokinetic studies	Higher AUC, $t_{1/2}$ (10-15 h) (Up to 48 h)	
Brain distribution (than RSV)	5.94 times higher	4.96 times higher

5.5. Liposomes

Liposomes are lipid bilayer vesicles investigated for sustained/controlled delivery, improving plasma half life and higher brain accumulation. RSV and 5-fluorouracil loaded ultradeformable vesicles were prepared and reported for higher anticancer activity on non-melanoma skin cancer cells than free RSV [206]. The prepared liposomes were proposed to have synergistic action against lesions related to squamous cell carcinoma such as actinic keratosis, Bowen's disease and keratoacanthoma. Elastic liposomes of RSV co-encapsulated with quercetin was reported to induce synergic inhibition of adipogenesis and increase apoptosis in adipocytes which is useful in dissolving subcutaneous fat [207]. Chitosan-coated liposomes of RSV was found to exhibit stronger anti-oxidative and anti-inflammatory activities than RSV solution [208].

Stealth liposomes are attempted for prolonged systemic circulation of its therapeutic pay loads. PEGylation of liposomes reduces the interaction and adsorption of plasma proteins and thereby decreases RES uptake. Reduction of macrophage uptake or opsonisation ultimately favours prolonged systemic circulation and reduces the frequency of administration [34-36]. Moreover, the liposomal entrapped drug will not readily available for metabolism. In our case, the vigorous glucuronidation and sulphonation of RSV will be delayed until exposed to the metabolizing enzymes [37]. TPGS coated liposomes of docetaxel was reported for enhanced cellular uptake and cytotoxicity in brain cancer cells than that of Taxotere® [20]. IC_{50} value of TPGS coated liposomes was found to be 6.46 and 5.23 times higher than that of Taxotere® and uncoated liposomes, respectively. Folic acid receptor targeted multifunctional TPGS liposomes was prepared and qualitative

internalization of multifunctional liposomes by MCF-7 cells and cytotoxicity was assessed [58]. Qualitative cell internalization of multifunctional TPGS liposomes was found to be significantly higher than that of non-targeted liposomes. Trastuzumab-conjugated TPGS liposomes were proved for sustained and targeted delivery of docetaxel in HER2 overexpressing breast cancer cells [21]. TPGS molecule is comprised of hydrophilic poly ethylene glycol (PEG) and lipophilic alkyl chain. PEG chains of TPGS minimise the adsorption of opsonin proteins and thereby reduce the uptake of nanoparticles by reticulo endothelial system and prolong the systemic circulation. DSPE PEG 2000 is also a crucial molecule often reported for the preparation of stealth nanoparticles [34, 158]. Moreover, DSPE PEG 2000 and allied derivatives coated nanoparticles were well proved for prolonged systemic circulation and bioavailability enhancement of several therapeutic molecules [159, 160]. Attempts for prolongation of systemic circulation of RSV loaded liposomes were not reported in current literature. Moreover, liposomal formulations are presently manufactured in large scale and widely marketed for chemotherapeutic applications. This prompted us to investigate liposomes for improving the brain distribution as well as prolonged systemic circulation. Therefore, RSV-TPGS-Lipo and RSV-PEG-Lipo were developed to improve the biological half life, prolonged systemic circulation and passive brain accumulation of RSV after *i.v.* administration in rats.

5.5.1. Vesicular size, polydispersity index and zeta potential

Formulation variable (molar ratio of drug to other liposomal components) and process variable (sonication time) were varied to get smaller vesicular size and higher entrapment

efficiency. The effect of molar ratio of drug to other liposomal components and sonication time on vesicular size is shown in Figure 5.45. As increasing the molar ratio of drug to other liposomal components from 0.5:10 to 2:10, vesicular sizes were significantly increased at all levels of sonication time. For instance, vesicular sizes of liposomes having drug to liposomal component molar ratio 0.5:10, 1:10 and 2:10 were found to be 107.8±11.69, 212.5±24.23 and 262.3±17.28 nm, respectively ($p<0.05$; n=3). Coming to the effect of sonication time on vesicular size, a different kind of trend was observed. The liposomal batches prepared using drug to liposomal components ratio 0.5:10 and 1:10 showed decrease in vesicular size with increasing the sonication time from 1 to 3 min whereas a significant increase in size was observed with further increment in sonication time to 5 min ($p<0.05$; n=3). For instance, RSV-TPGS-Lipo 4, 5 and 6 prepared using drug to liposomal component ratio 1:10 at 1, 3 and 5 min sonication times showed the vesicular sizes of 212.5±24.23, 108±13.38 and 183.5±7.86 nm, respectively. The decrease in vesicular size upon increasing the sonication time from 1 to 3 min is due to breakdown of vesicles. The increase in vesicular size upon further increasing the sonication time from 3 to 5 min may be due to coalescence or aggregation of vesicles resulted from excessive sonication energy [183]. The liposomal batches prepared using drug to liposomal component ratio 2:10 (RSV-TPGS-Lipo 7, 8 and 9) did not show any significant difference in vesicular size ($p>0.05$; n=3). Polydispersity index and zeta potential of liposomal batches were varied from 0.121±0.051 to 0.631±0.107 and -2.1±0.76 to 1.76±0.83 mV, respectively. Both drug to liposomal components ratio and sonication time did not show any trend in polydispersity index and zeta potential (Table 5.10).

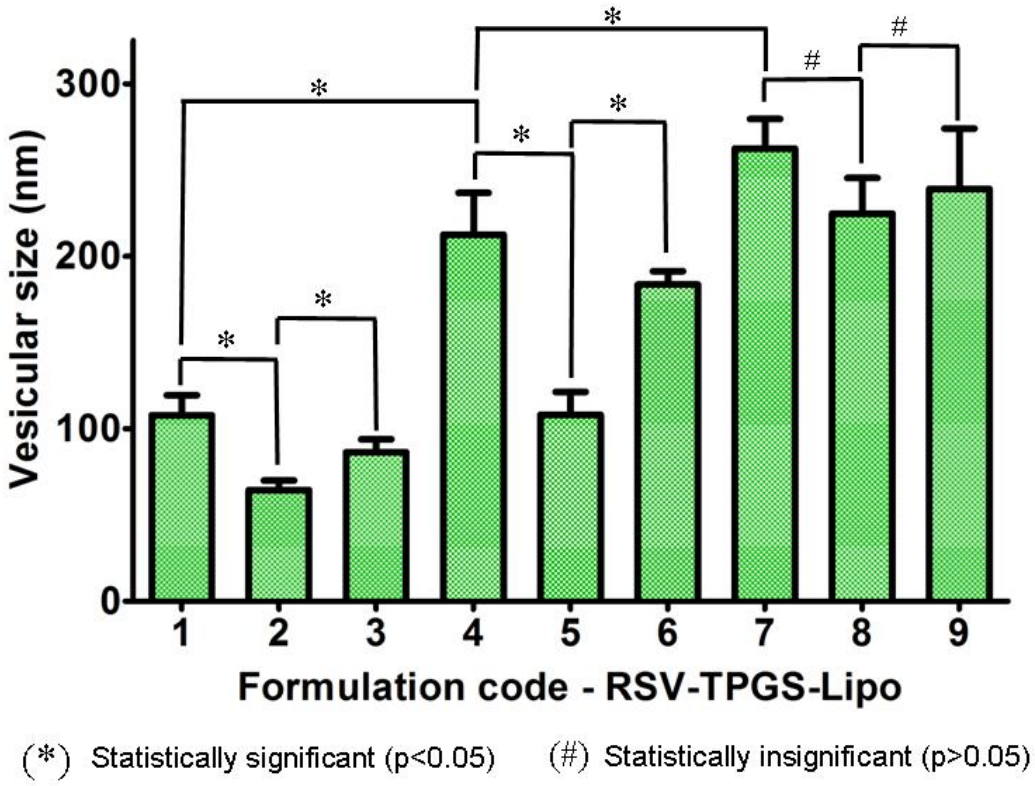

Figure 5.45. Vesicular size of various batches of RSV-TPGS-Lipo. Values are represented as mean±SD (n=3).

Table 5.10. Polydispersity index and zeta potential of various batches of RSV-TPGS-Lipo

Formulation code	Polydispersity index	Zeta potential (mV)
RSV-TPGS-Lipo 1	0.220±0.034	-2.1±0.76
RSV-TPGS-Lipo 2	0.398±0.021	-1.05±1.12
RSV-TPGS-Lipo 3	0.121±0.051	-1.83±0.97
RSV-TPGS-Lipo 4	0.433±0.075	-0.8±0.49
RSV-TPGS-Lipo 5	0.213±0.037	0.03±0.02
RSV-TPGS-Lipo 6	0.631±0.107	1.06±0.81
RSV-TPGS-Lipo 7	0.483±0.081	-0.04±0.01
RSV-TPGS-Lipo 8	0.537±0.101	0.79±0.29
RSV-TPGS-Lipo 9	0.496±0.083	1.76±0.83

5.5.2. Encapsulation efficiency

Entrapment efficiency of RSV-TPGS-Lipo formulations varied from 50.14±3.46 to 84.59±5.75% (Figure 5.46). When the ratio of RSV to liposomal components was increased, entrapment efficiency was significantly decreased at all levels of sonication time ($p<0.05$; $n=3$). For example, entrapment efficiency of RSV-TPGS-Lipo 1, 4 and 7 prepared by 1 min sonication time were found to be 84.19±5.75, 67.94±4.26 and 53.04±1.76%, respectively. This may be due to saturation of lipid interspaces and fails to accommodate the RSV molecules at higher concentrations. Increase in sonication time did not show any significant effect on entrapment efficiency.

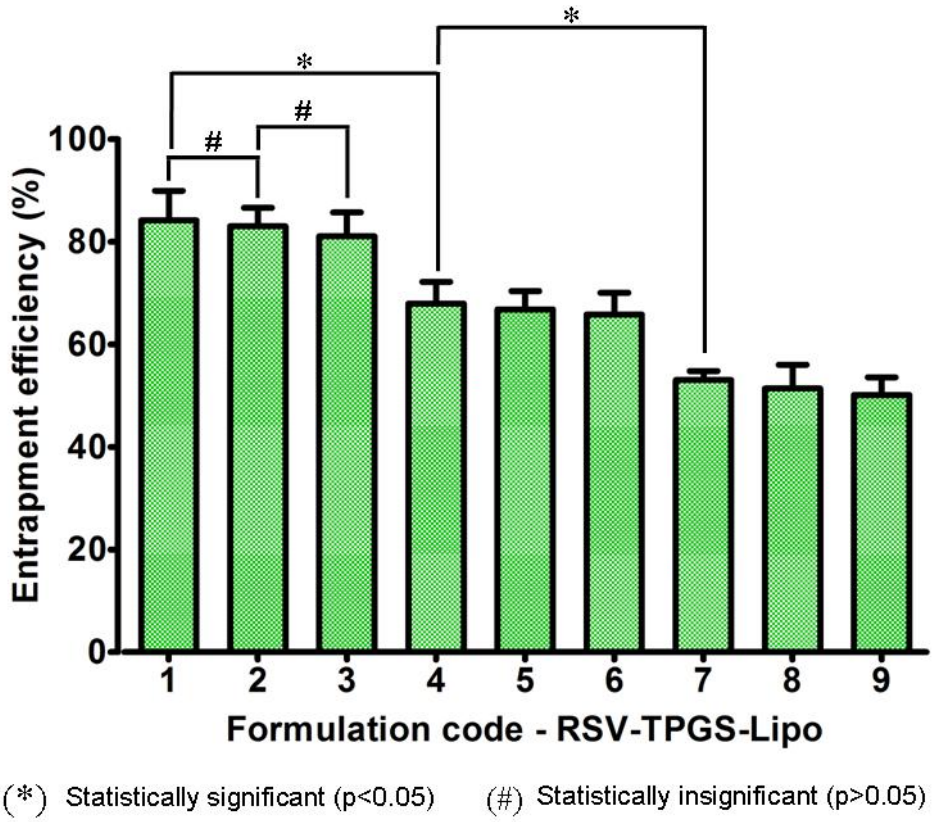

Figure 5.46. Entrapment efficiency of various batches of RSV-TPGS-Lipo. Values are represented as mean±SD (n=3).

5.5.3. Selection of optimized formulations

The liposomal formulation RSV-TPGS-Lipo 2 having lower vesicular size (64.5±5.56 nm) and higher entrapment efficiency (83.05±3.59%) was selected as best formulation and used for further evaluations. RSV-PEG-Lipo prepared using similar composition of RSV-TPGS-Lipo 2 by replacing TPGS with DSPE PEG 2000 showed particle size of 250.2±9.03 nm, polydispersity index of 0.196±0.010 and entrapment efficiency of 79.47±4.32%. Zeta potential of optimized RSV-TPGS-Lipo 2 and RSV-PEG-Lipo was found to be -1.05±1.12 and -26.47±0.75 mV, respectively. Similarly, liposomal

formulation prepared without TPGS or DSPE PEG 2000 showed particle size of 121.9±11.24 nm, polydispersity index of 0.321±0.019 and entrapment efficiency of 82.45±3.72%. Zeta potential of RSV-Lipo was found to be 3.47±0.97 mV.

5.5.4. Shape of liposomes

Shape of RSV-TPGS-Lipo, RSV-PEG-Lipo and RSV-Lipo was found to be spherical as shown in Figure 5.47 (a), (b) and (c), respectively. The mean vesicular size of RSV-TPGS-Lipo, RSV-PEG-Lipo and RSV-Lipo calculated by TEM was found to be 77.34±14.3, 235.7±19.2 and 132.4±9.4 nm, respectively. These sizes are well correlated with the vesicular size of corresponding liposomes obtained by dynamic laser light scattering technique.

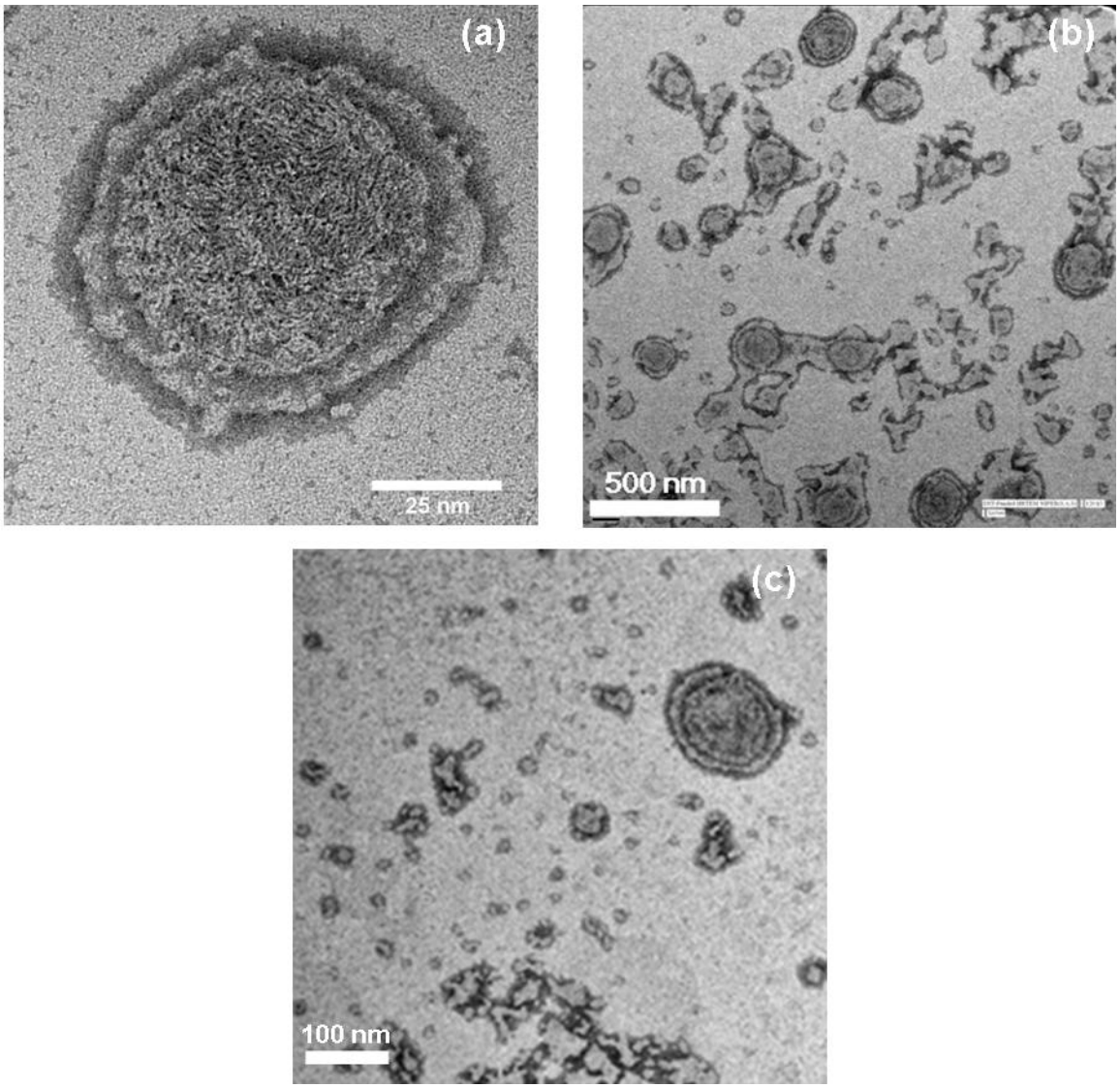

Figure 5.47. Transmission electron microscope images of optimized batch of (a) RSV-TPGS-Lipo (b) RSV-PEG-Lipo and (c) RSV-Lipo

5.5.5. *In vitro* drug release

In vitro drug release profile of RSV-Lipo, RSV-TPGS-Lipo and RSV-PEG-Lipo are shown in Figure 5.48. All liposomal formulations showed sustained release without any burst release. The cumulative percentage of drug release from RSV-Lipo, RSV-TPGS-

Lipo and RSV-PEG-Lipo after 48 h was found to be 51.46±3.75, 49.75±4.72 and 56.78±2.89%, respectively. The absence of burst release may be due to lack of RSV molecules at the surface of liposomal formulations. As the lipophilic RSV molecules housed at the intermolecular spaces of bilayer lipid membrane of liposomes, the drug release may be sustained. Correlation co-efficient (R^2) value of liposomes calculated from zero order, first order, Higuchi model and Korsmeyer–Peppas model is shown in Table 5.11. The results suggest that Higuchi kinetics is the best fit model for RSV-TPGS-Lipo and RSV-PEG-Lipo. Hence, diffusion is the possible drug release mechanism. Korsmeyer–Peppas model is the best fit model for RSV-Lipo. The release exponent (n) value of RSV-TPGS-Lipo, RSV-PEG-HNPs and RSV-Lipo calculated by Korse-Meyer Peppas model was found to be 0.4416, 0.8449 and 0.7661, respectively. Therefore, the mechanism of drug release of RSV-TPGS-Lipo was found to be 'Fickian'. The mechanism of drug release of RSV-PEG-HNPs and RSV-Lipo was found to be 'anomalous transport' which indicates non-linear diffusion of RSV molecules with respect to time.

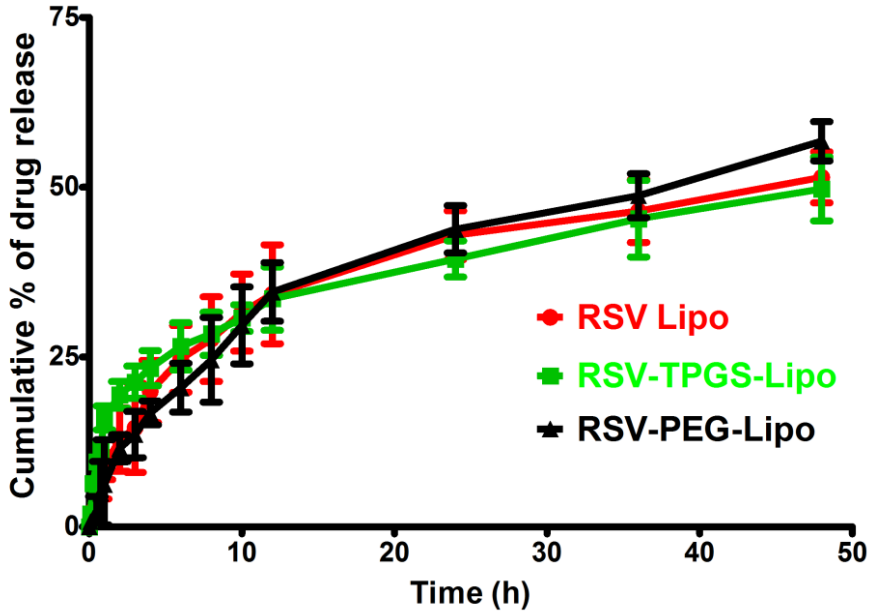

Figure 5.48. *In vitro* dug release of RSV-Lipo, RSV-TPGS-Lipo and RSV-PEG-Lipo. Values are represented as mean±SD (n=3).

Table 5.11. Correlation co-efficient (R^2) and release exponent (n) value of *in vitro* drug release kinetics from RSV-Lipo, RSV-TPGS-Lipo and RSV-PEG-Lipo

Kinetics/Parameter	RSV-Lipo	RSV-TPGS-Lipo	RSV-PEG-Lipo
Zero order	0.7661	0.7534	0.8449
First order	0.8300	0.8360	0.9042
Higuchi model	0.9497	0.9413	0.9797
Korsmeyer–Peppas model	0.9514	0.9195	0.9514
Release exponent (n)	0.7661	0.4416	0.8449
Best fit	Korsmeyer–Peppas model	Higuchi	Higuchi
Mechanism of RSV release	Anomalous	Fickian	Anomalous

5.5.6. Drug-excipient interaction analysis

FTIR spectrum of RSV and lyophilized RSV-TPGS-Lipo and RSV-PEG-Lipo are shown in Figure 5.49 (a), (b) and (c), respectively. FTIR spectrum of RSV showed its characteristic absorption bands at 964.4 cm^{-1} for *trans* olefinic bond, 1153.4 cm^{-1} for C-O stretching, 1442.8 cm^{-1} and 1587.4 cm^{-1} for C=C stretching of aromatic ring, 1606.7 cm^{-1} for C-C stretching of olefinic group and 3288.7 $cm^{-1}$for O-H stretching due to alcoholic group. RSV-TPGS-Lipo and RSV-PEG-Lipo showed all the characteristic peaks of RSV with minor shift in absorption bands. RSV-TPGS-Lipo showed *trans* olefinic band at 966.3 cm^{-1}, C-O stretching at 1147.6 cm^{-1}, C=C stretching of aromatic ring at 1464.0 cm^{-1}

and 1587.4 cm^{-1}, C-C stretching of olefinic group at 1635.6 cm^{-1} and O-H stretching of alcoholic group at 3190.3 cm^{-1}. Similarly, RSV-PEG-Lipo showed *trans* olefinic band at 966.3 cm^{-1}, C-O stretching at 1147.6 cm^{-1}, C=C stretching of aromatic ring at 1464.02 cm^{-1} and 1587.4 cm^{-1}, C-C stretching of olefinic group at 1635.6 cm^{-1} and O-H stretching of alcoholic group at 3169.1 cm^{-1}. The presence of all characteristic absorption bands of RSV in RSV-TPGS-Lipo and RSV-PEG-Lipo clearly indicates the absence of potential chemical interaction between drug and other liposomal components.

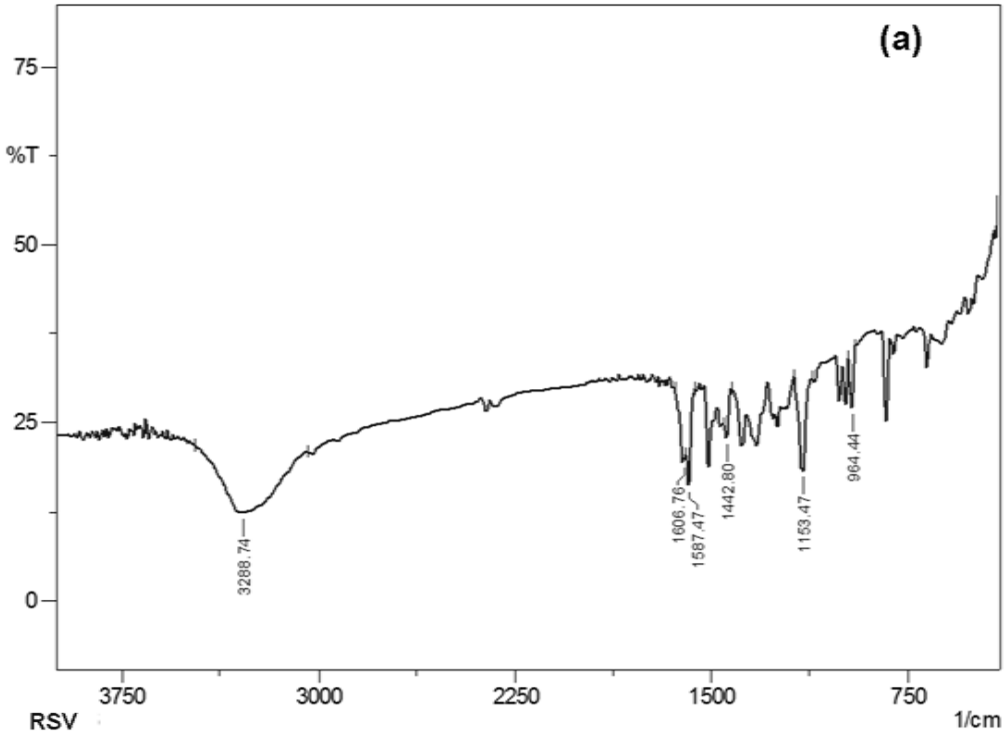

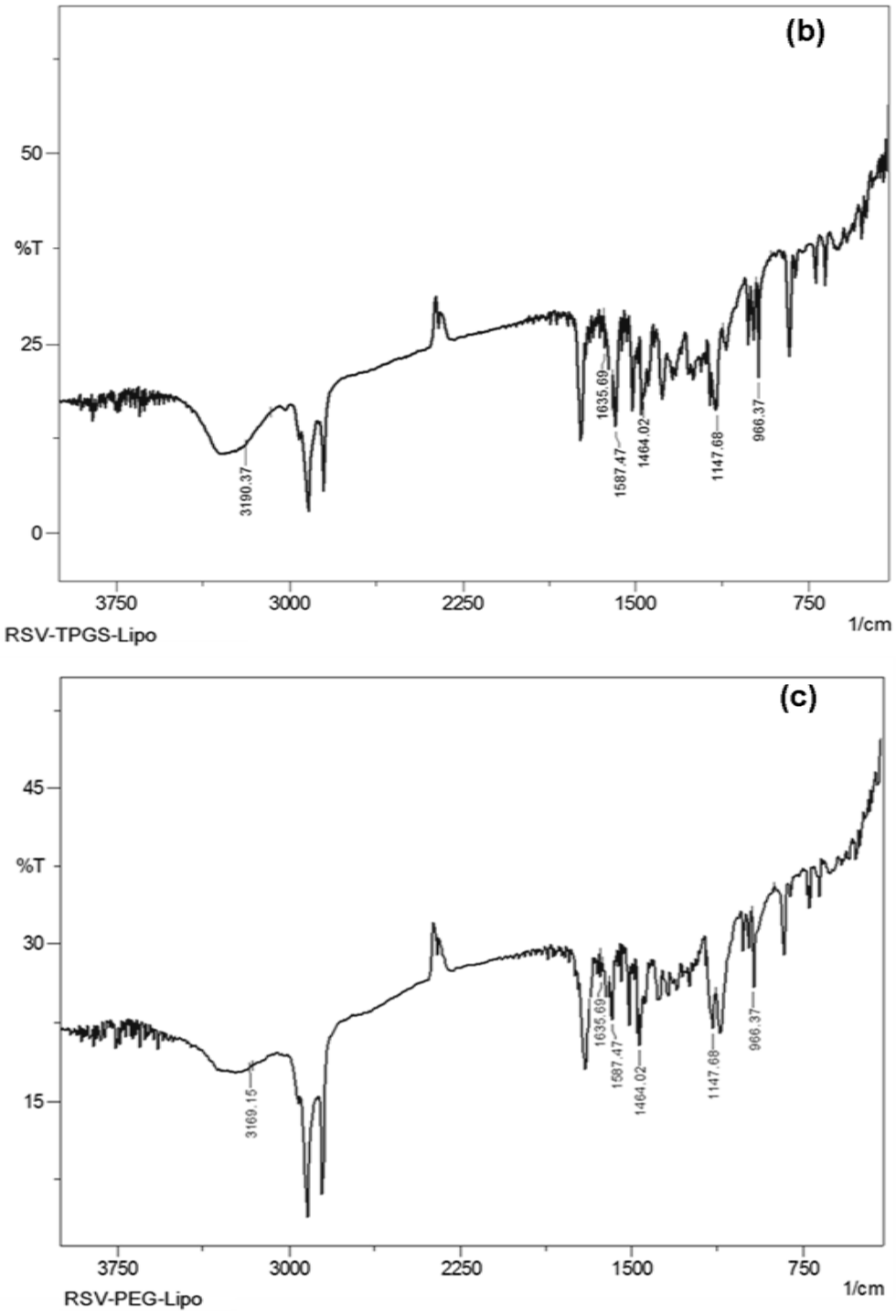

Figure 5.49. Fourier transformed infra red (FTIR) spectra of (a) RSV (b) RSV-TPGS-Lipo and (c) RSV-PEG-Lipo

5.5.7. DSC analysis

DSC thermograms of RSV, phosphatidylcholine, cholesterol, TPGS, DSPE PEG 2000, RSV-TPGS-Lipo and RSV-PEG-Lipo are shown in Figure 5.50. Pristine RSV showed a sharp endothermic peak at 267.71 ^{o}C which corresponds to its melting point. Phosphatidylcholine showed two blunt peaks at 68.12 and 79.04 ^{o}C. Cholesterol, TPGS and DSPE PEG 2000 showed sharp endothermic peaks at 147.4, 35.11 and 56.58 ^{o}C, respectively. RSV-TPGS-Lipo showed a sharp peak at 38.07 ^{o}C which corresponds to the peak of TPGS with minor shift in its position. Similarly, RSV-PEG-Lipo also showed a sharp peak at 62.16 ^{o}C which corresponds to the peak of DSPE PEG 2000 with minor shift in its position. Absence of RSV melting peak at 267.71 ^{o}C in both the liposomal formulations suggest that the drug was dispersed in amorphous form. All these results suggest the absence of potential chemical interaction between RSV and other components of both liposomal formulations.

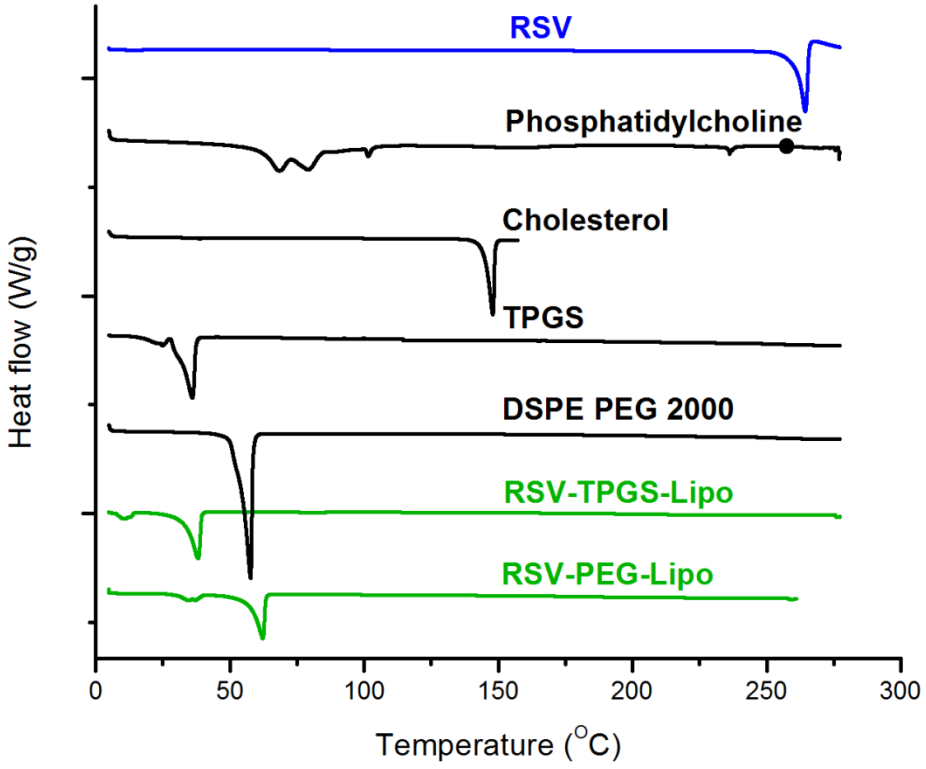

Figure 5.50. Differential scanning calorimetric thermograms of RSV, phosphatidylcholine, cholesterol, TPGS, DSPE PEG 2000, RSV-TPGS-Lipo and RSV-PEG-Lipo.

5.5.8. Crystalinity analysis

XRD pattern of RSV, RSV-TPGS-Lipo and RSV-PEG-Lipo are shown in Figure 5.51. RSV showed sharp diffraction peaks at 6.62°, 13.2°, 16.36°, 19.18°, 22.28°, 23.54°, 25.18°, 28.26°, 31.6°, 38.32° and 45.18° in 2θ scale. Presence of such sharp peak indicates crystalline nature of RSV. In contrast, RSV-TPGS-Lipo and RSV-PEG-Lipo did not show any characteristic intense sharp peaks. These results indicated the conversion of RSV from crystalline to amorphous form in both liposomal formulations. XRD results

are well correlated with DSC results, which confirm the conversion of RSV from crystalline to amorphous form in the liposomes.

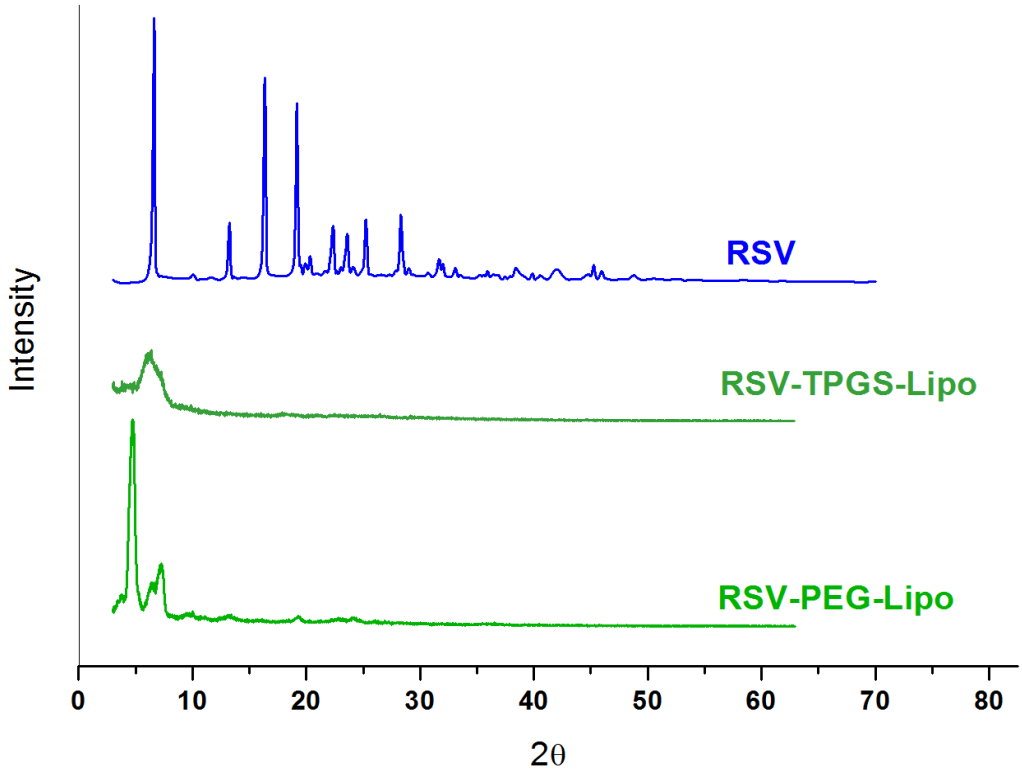

Figure 5.51. X-ray diffraction pattern of RSV, RSV-TPGS-Lipo and RSV-PEG-Lipo.

5.5.9. *In vitro* cytotoxicity studies

The comparative cytotoxicity of RSV, RSV-Lipo, RSV-TPGS-Lipo and RSV-PEG-Lipo against C6 glioma cell lines is shown in Figure 5.52. RSV-TPGS-Lipo showed significantly higher cytotoxicity than RSV, RSV-Lipo and RSV-PEG-Lipo at all levels of concentrations ($p<0.05$). The cytotoxic potential of RSV, RSV-Lipo and RSV-PEG-Lipo were found to be statistically similar ($p>0.05$). The additional cytotoxic potential of RSV-

TPGS-Lipo is due to presence of TPGS. *In vitro* and *in vivo* cytotoxic potential of TPGS was already proved against several types of cancer [185-188]. The additive cytotoxicity of RSV-TPGS-Lipo in our study will be more beneficial in the treatment of glioma. Cytotoxicity of RSV and RSV-PEG-Lipo was found to be statistically insignificant in all concentrations ($p>0.05$). Therefore, the cytotoxic potential of RSV is not changed upon entrapping in RSV-PEG-Lipo.

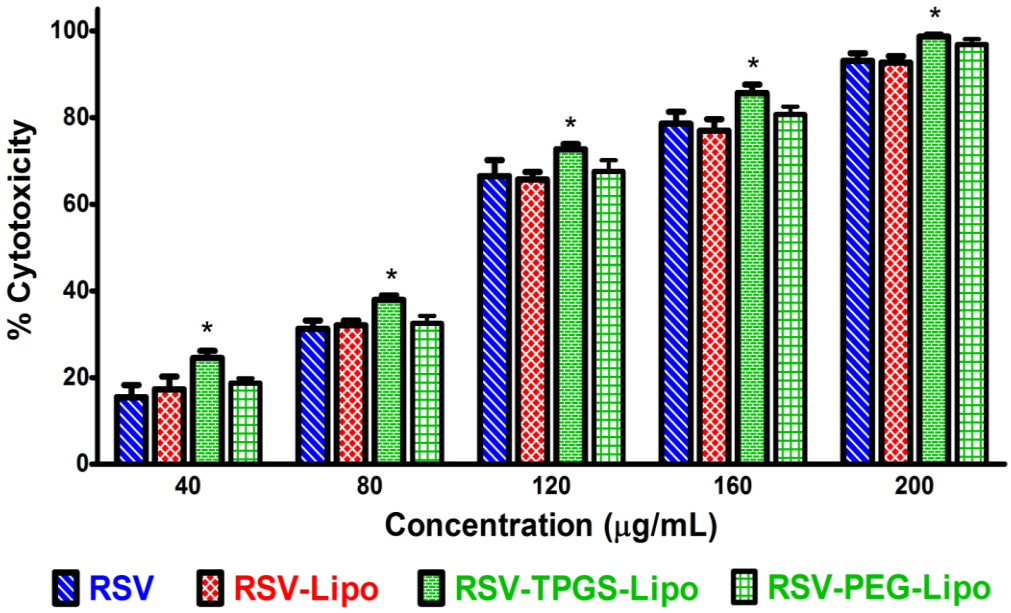

Figure 5.52. *In vitro* cytotoxicity of RSV, RSV-Lipo, RSV-TPGS-Lipo and RSV-PEG-Lipo. Values are represented as mean±SD (n=3). *Mark indicates significant difference from RSV ($p<0.05$).

5.5.10. Cellular uptake of Coumarin-6 loaded liposomes

CLSM images of COU-TPGS-Lipo and COU-PEG-Lipo treated C6 glioma cells are shown in Figure 5.53. The cells were counterstained by DAPI to visualize the nucleus.

Figure 5.53 (a) and (b) appearing green and blue colours are CLSM images of COU-TPGS-Lipo treated cells captured using FITC and DAPI filters, respectively. The cellular uptake of COU-TPGS-Lipo (green colour) was visualized by superimposing the images captured through FITC (green colour) over DAPI filters (blue colour) (Figure 5.53 (c)). Similarly, Figure 5.53 (d) and (e) are CLSM images of COU-PEG-Lipo taken using FITC (green colour) and DAPI filters (blue colour), respectively. Cellular uptake of COU-TPGS-Lipo is shown in the superimposed image (Figure 5.53 (f)). Both COU-TPGS-Lipo and COU-PEG-Lipo showed excellent cellular internalization and concentrated at cytoplasm in C6 glioma cells within 2 h of incubation.

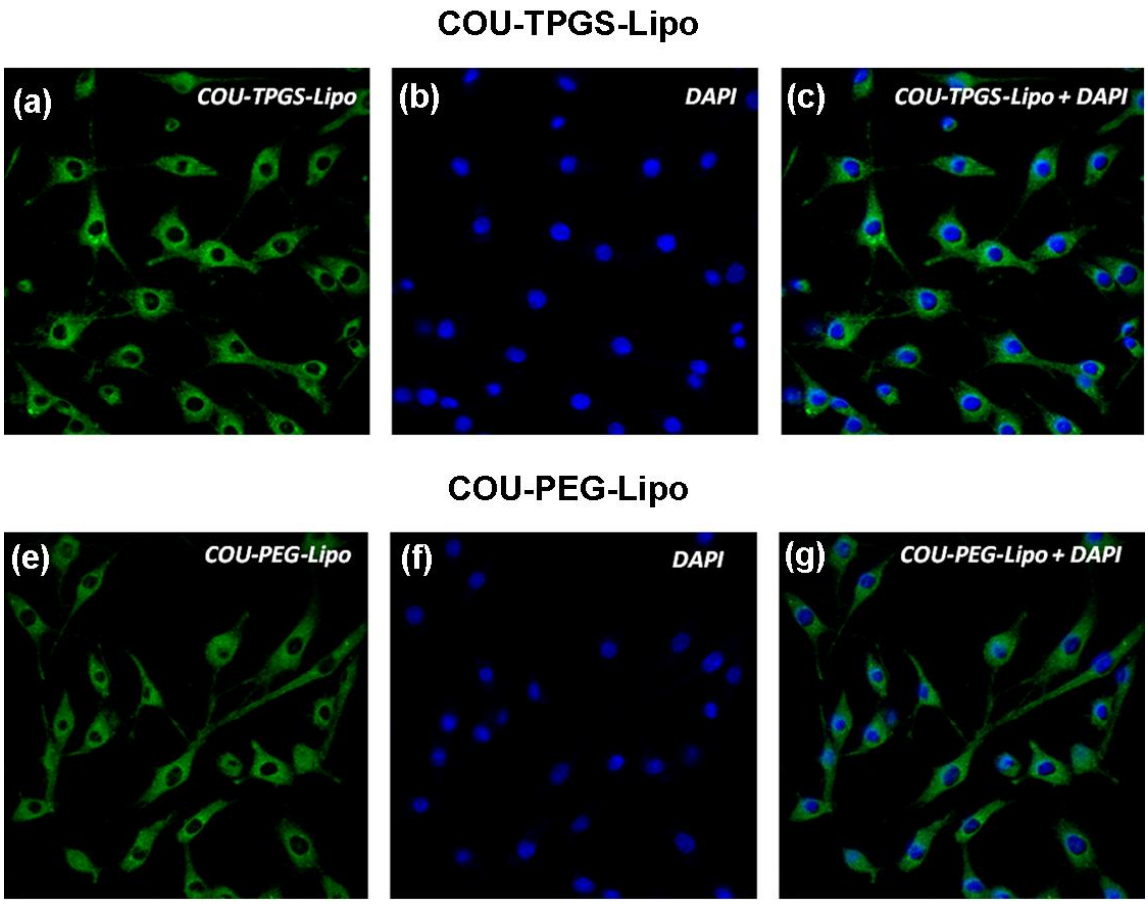

Figure 5.53. Cellular internalization of COU-TPGS-Lipo (a, b and c) and COU-PEG-Lipo (d, e and f) in C6 glioma cancer cells assessed by confocal laser scanning microscopy (CLSM).

5.5.11. Evaluation of haemolysis

Haemolysis of RSV, RSV-TPGS-Lipo and RSV-PEG-Lipo were assessed in three different concentrations (10, 50 and 100 µg/mL). Placebo-TPGS-Lipo and Placebo-PEG-Lipo were also included in the study to assess the effect of liposomal components on haemolysis. As per international standards, the spontaneous haemolysis limit is 10% to preserve the functionality of erythrocytes in blood [189]. Haemolysis results are shown in

Figure 5.54. RSV showed haemolysis within the prescribed limit at all levels of concentrations. Though RSV, RSV-TPGS-Lipo, RSV-PEG-Lipo, Placebo-TPGS-Lipo and Placebo-PEG-Lipo showed disparate percentage of haemolysis, all formulations showed less than 10% haemolysis. Therefore, RSV-TPGS-Lipo and RSV-PEG-Lipo are safe for *i.v.* administration in terms of haemolysis. Moreover, RSV is also reported for antioxidative mechanisms and protective effect on erythrocytes as explained in previous chapters. The protective nature of RSV may be expected to prevent the degradation of erythrocytes upon intravenous administration of RSV-TPGS-Lipo and RSV-PEG-Lipo for the treatment of glioma.

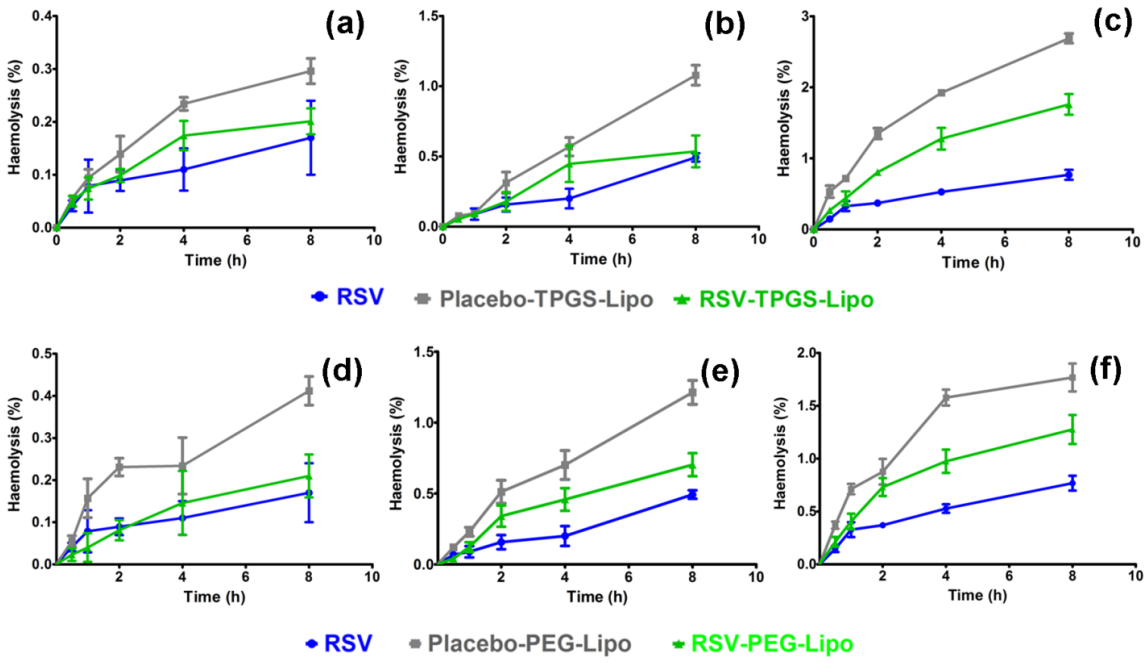

Figure 5.54. Percentage of haemolysis at different time intervals in whole blood samples after addition of (a) 10 (b) 50 (c) 100 µg/mL RSV-TPGS-Lipo and (d) 10 (e) 50 (f) 100 µg/mL of RSV-PEG-Lipo. Values are represented as mean±SD (n=3).

5.5.12. Erythrocyte membrane integrity

Erythrocytes suspended in normal saline was used to evaluate the membrane integrity in this study. Amount of lactate dehydrogenase (LDH) release is proportional to the structural disturbance in erythrocytes membrane. Therefore, evaluation of erythrocyte membrane integrity was studied by quantifying LDH enzyme. Amount of LDH release after treating 1 mL of erythrocyte suspension with test samples are shown in Figure 5.55. RSV, RSV-TPGS-Lipo, RSV-PEG-Lipo, Placebo-TPGS-Lipo and Placebo-PEG-Lipo did not show significant increase in LDH release in comparison to spontaneous enzyme release observed in PBS treated samples after 1, 4 and 8 h of incubation ($p>0.05$). These results suggest that membrane integrity of erythrocyte is not affected at all concentrations of test samples. Therefore, RSV, RSV-TPGS-Lipo and RSV-PEG-Lipo in blood at 10, 50 and 100 μg/mL equivalent concentrations will not damage erythrocyte membrane integrity significantly. Therefore, RSV-TPGS-Lipo and RSV-PEG-Lipo are safe for *i.v.* administration in terms of erythrocytes safety.

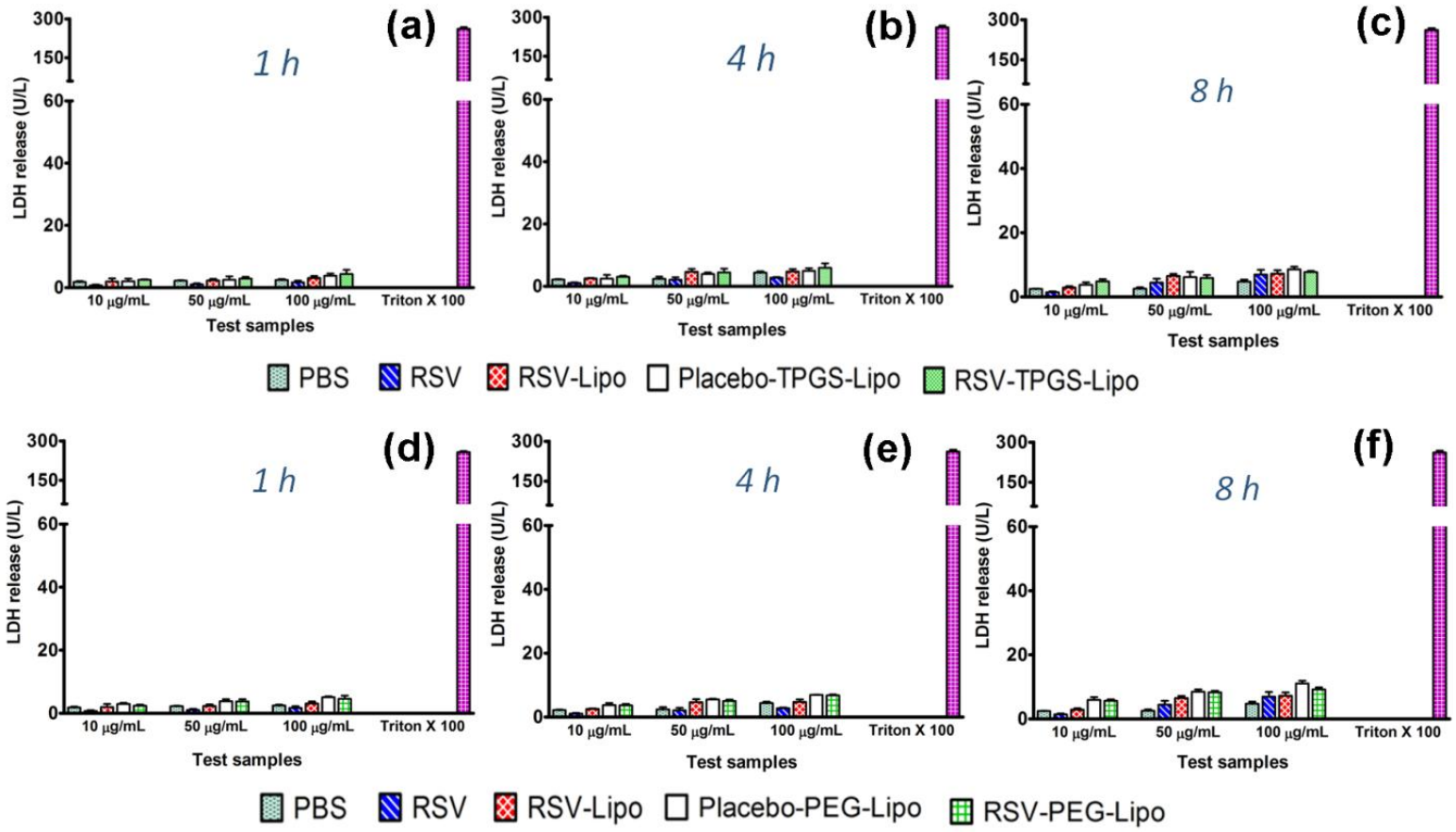

Figure 5.55. Amount of LDH release after treating with RSV-TPGS-Lipo at (a) 1, (b) 4 and (c) 8 hours and RSV-PEG-Lipo at (d) 1, (e) 4 and (f) 8 hours. Values are represented as mean±SD (n=3).

5.5.13. Platelet aggregation

Platelet aggregation forms thrombus in blood vessels which causes ischemia, myocardial infarction or stroke. Intravenous infusion of liposomal formulations should not cause platelet aggregation. Therefore, assessment of platelet aggregation is an essential study before *i.v.* administration of RSV, RSV-TPGS-Lipo and RSV-PEG-Lipo. Placebo liposomal formulations were also included in the study to assess effect of liposomal components on platelet aggregation. PBS was used as spontaneous control to assess the dilution effect. Quantitative platelet aggregation results of RSV-TPGS-Lipo and RSV-PEG-Lipo are shown in Figure 5.56 (a) and (b), respectively.

RSV treated samples did not show significant difference in platelet count than that of PBS treated samples at all concentrations. Therefore, RSV is not promoting platelet aggregation. RSV-TPGS-Lipo, RSV-PEG-Lipo, Placebo-TPGS-Lipo and Placebo-PEG-Lipo showed lesser platelet count in comparison to PBS ($p>0.05$). Lower platelet count may be due to the effect of formulation components. Despite RSV-TPGS-Lipo showed lower platelet count, the percentage of platelet count at 10, 50 and 100 μg/mL concentrations was calculated to be 95.81±2.99, 93.69±1.60 and 92.37±1.87%, respectively. Similarly, RSV-PEG-Lipo showed the percentage of platelet count of 95.13±1.89, 94.37±1.14 and 93.06±1.98% at 10, 50 and 100 μg/mL, respectively. The reduction of platelet in both liposomes was found to be less than 10%. Therefore, the reduction of platelet count of RSV-TPGS-Lipo and RSV-PEG-Lipo is acceptable. Though all components of Placebo-TPGS-Lipo are present in RSV-TPGS-Lipo, it showed higher platelet count. This may be due to antiplatelet aggregation property of

RSV. RSV was already proved for anti platelet aggregation effect *in vitro* as discussed in platelet aggregation of SLN formulations [20].

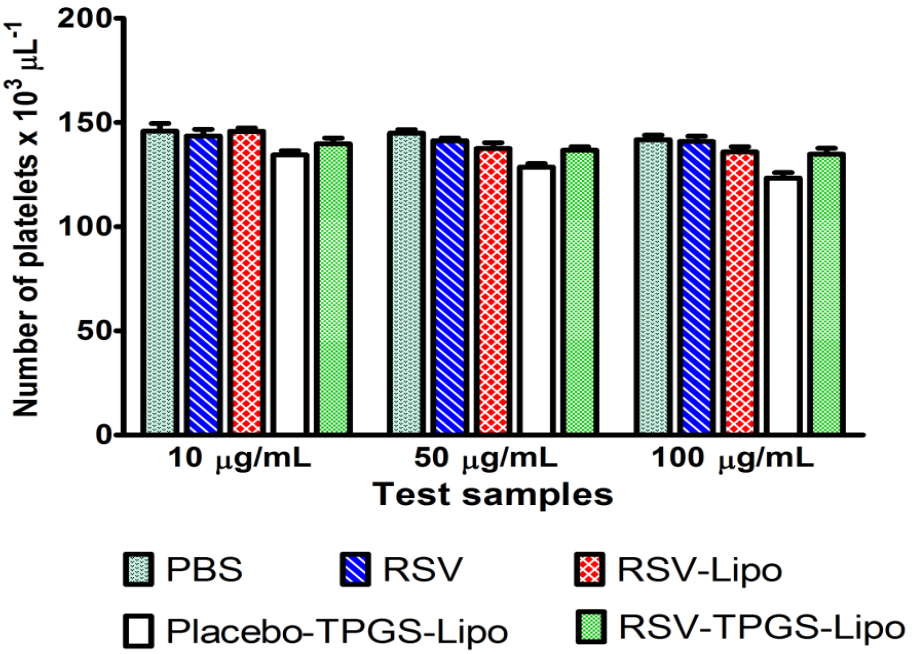

Figure 5.56. (a) Number of platelets after addition of PBS, RSV, RSV-Lipo, Placebo-TPGS-Lipo and RSV-TPGS-Lipo at 10, 50 and 100 µg/mL. Values are represented as mean±SD (n=3).

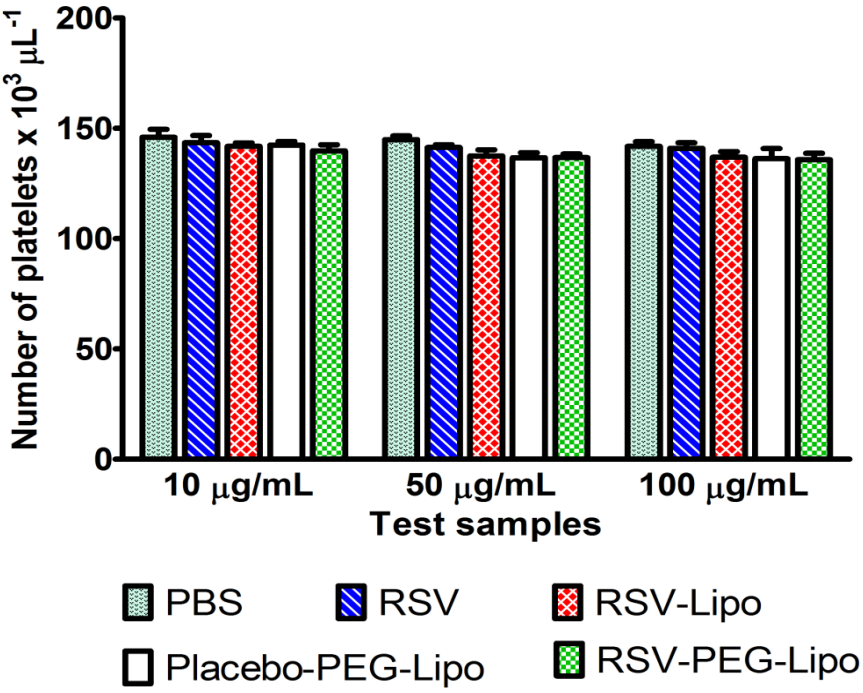

Figure 5.56. (b) Number of platelets after addition of PBS, RSV, RSV-Lipo, Placebo-PEG-Lipo and RSV-PEG-Lipo at 10, 50 and 100 µg/mL. Values are represented as mean±SD (n=3).

As a qualitative support, platelet aggregation in whole blood was also observed by optical microscopy after incubation with the test samples (PBS, RSV, RSV-TPGS-Lipo, Placebo-TPGS-Lipo, RSV-PEG-Lipo and Placebo-PEG-Lipo) at 10, 50 and 100 μg/mL concentrations. Platelets are indicated by arrow marks on microphotographs (Figure 5.57). Supportively, no platelet aggregation was seen in all the samples at all concentrations of test samples. Though slight decrease in platelet count was observed with Placebo-TPGS-Lipo in quantitative measurements, the platelets were distributed evenly throughout the blood smears upon microscopic observations. Both quantitative

and qualitative observations indicated that RSV, RSV-TPGS-Lipo and RSV-PEG-Lipo are haemocompatible and safe for *i.v.* administration.

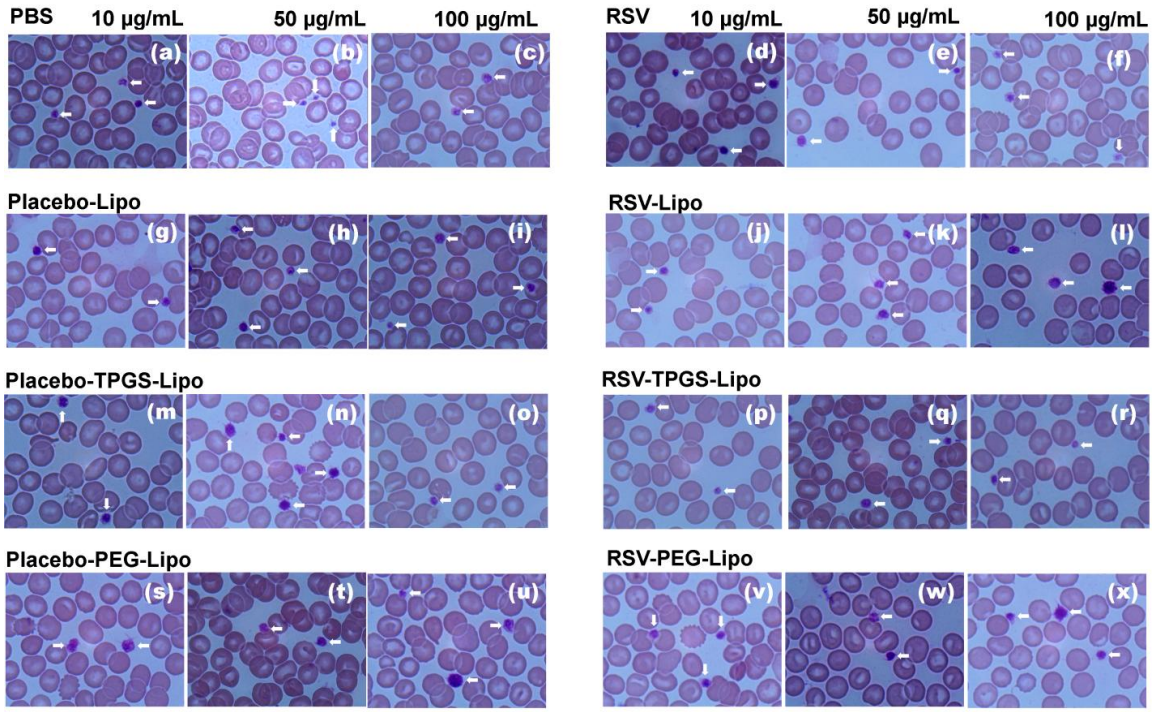

Figure 5.57. Light microscopy images of Leishman's stained whole blood samples after treating with (a) PBS equivalent volume to 10 µg/mL of test samples (b) PBS equivalent volume to 50 µg/mL of test samples (c) PBS equivalent volume to 100 µg/mL of test samples (d) 10 µg/mL RSV (e) 50 µg/mL RSV (f) 100 µg/mL RSV (g) 10 µg/mL Placebo-Lipo (h) 50 µg/mL Placebo-Lipo (i) 100 µg/mL Placebo-Lipo (j) 10 µg/mL RSV-Lipo (k) 50 µg/mL RSV-Lipo (l) 100 µg/mL RSV-Lipo (m) 10 µg/mL Placebo-TPGS-Lipo (n) 50 µg/mL Placebo-TPGS-Lipo (o) 100 µg/mL Placebo-TPGS-Lipo (p) 10 µg/mL RSV-TPGS-Lipo (q) 50 µg/mL RSV-TPGS-Lipo (r) 100 µg/mL RSV-TPGS-Lipo (s) 10 µg/mL Placebo-PEG-SLN (t) 50 µg/mL Placebo-PEG-SLN (u) 100 µg/mL Placebo-PEG-SLN (v) 10 µg/mL RSV-PEG-SLN (w) 50

µg/mL RSV-PEG-SLN (x) 100 µg/mL RSV-PEG-SLN. Images were captured at magnification of 100x.

5.5.14. Pharmacokinetic studies

The comparative plasma concentration time profiles of RSV-TPGS-Lipo and RSV-PEG-Lipo with RSV and RSV-Lipo up to 48 h is shown in Figure 5.58 (a) and (b), respectively. Pharmacokinetic parameters analysed using WinNonlin 6.4 is presented in Table 5.12. As described in previous chapters, plasma concentration time curve of RSV showed a rapid decline up to 0.5 h, slight increment at 1 h (a small second peak), declined again up to 2 h and remain undetectable after 2 h. RSV-Lipo showed declining plasma concentration up to 2 h slightly increased at 4 h and showed continuous decline up to 12 h, after which the concentration was undetectable. RSV-TPGS-Lipo showed marked decline up to 1 h, rose to give slightly increasing mean concentration at 2 h. The mean plasma concentration increased again to small extent at 8 h and showed continuous decline up to 48 h. Similarly, RSV-PEG-Lipo showed marked decline up to 2 h, again rose to give second peak at 8 h and continued up to 48 h. Multiple increment (peaks) in mean plasma concentrations of RSV, RSV-Lipo, RSV-TPGS-Lipo and RSV-PEG-Lipo may be due enterohepatic circulation of drug. Enterohepatic circulation observed in our study is well correlated with earlier publication on population pharmacokinetics of RSV by linked rat model [18]. Enterohepatic circulation phenomenon of RSV was further demonstrated by the conversion of drug into glucuronide/sulfate conjugates and secreted to small intestine via breast cancer resistance protein and multidrug resistance protein 2 [190]. Initial plasma concentration (C_0) of RSV, RSV-Lipo, RSV-TPGS-Lipo and RSV-

PEG-Lipo after *i.v.* administration was found to be statistically similar (P>0.05). AUC and $t_{1/2}$ of RSV-TPGS-Lipo was found to be approximately 29.94 and 29.66 times higher than RSV and 5.73 and 6.71 times higher than RSV-Lipo, respectively. Similarly, and $t_{1/2}$ of RSV-TPGS-Lipo was found to be approximately 29.94 and 29.66 times higher than RSV and 5.73 and 6.71 times higher than RSV-Lipo, respectively. Higher AUC and $t_{1/2}$ value of RSV-TPGS-Lipo and RSV-PEG-Lipo in comparison to RSV-Lipo is due to presence of TPGS and DSPE PEG 2000 at the surface of liposomes. Moreover, AUC and $t_{1/2}$ value of RSV-Lipo was found to be 5.23 and 4.42 times higher than RSV. This may be due to sustained release and protection of liposomal entrapped RSV from the metabolic enzymes. The plasma half life ($t_{1/2}$) of pristine RSV obtained in this study was higher than earlier reported value (0.13±0.02 h) at 15 mg/kg and well correlated with the value (0.55 h, calculated by Bayesian estimations) estimated in population pharmacokinetic study at 2, 10 and 20 mg/kg of RSV after *i.v.* administrations in rats [17, 18]. Short $t_{1/2}$ of RSV was in agreement with its higher clearance (CL) value of 1894.84±382.46 mL/h/kg. In contrast, higher half life of RSV-TPGS-Lipo and RSV-PEG-Lipo was correlated well with their lower CL values (33.01 and 40.64 times, respectively). The CL value of RSV-TPGS-Lipo and RSV-PEG-Lipo was found to be 6.44 and 7.92 times lower than RSV-Lipo. V_d of RSV-TPGS-Lipo was found to be statistically similar with RSV whereas RSV-PEG-Lipo showed significantly lower V_d than RSV ($p<0.05$). Noticeably, V_d of RSV, RSV-Lipo, RSV-TPGS-Lipo and RSV-PEG-Lipo were found to be higher than the total body water of rat (150 mL/kg for a body weight of 0.25 kg) [17]. These results suggest that RSV, RSV-Lipo, RSV-TPGS-Lipo and RSV-PEG-Lipo are undergoing extensive tissue binding. MRT of RSV-TPGS-Lipo

and RSV-PEG-Lipo was 29.48 and 29.24 times higher than RSV and 5.36 and 5.31 times higher than RSV-Lipo, respectively. The higher MRT values of RSV-TPGS-Lipo and RSV-PEG-Lipo confirmed the prolonged systemic circulation potential. This may be due to presence of TPGS and DSPE PEG 2000 at the liposomal surface. TPGS and DSPE PEG 2000 molecules prevent the adhesion of plasma proteins (by stealth nature) and thereby avoid recognition by reticulo endothelial system which ultimately enhanced systemic circulation time. MRT of RSV-Lipo was found to be 5.5 times higher than RSV, which may be due to delayed metabolism of liposomal entrapped drug. The overall observation of higher AUC, $t_{1/2}$ and MRT and lower V_d and CL of RSV-TPGS-Lipo and RSV-PEG-Lipo than pristine RSV and RSV-Lipo evidently indicate that the present liposomal design will be the potential tools for enhancing systemic availability and prolonged systemic circulation of RSV.

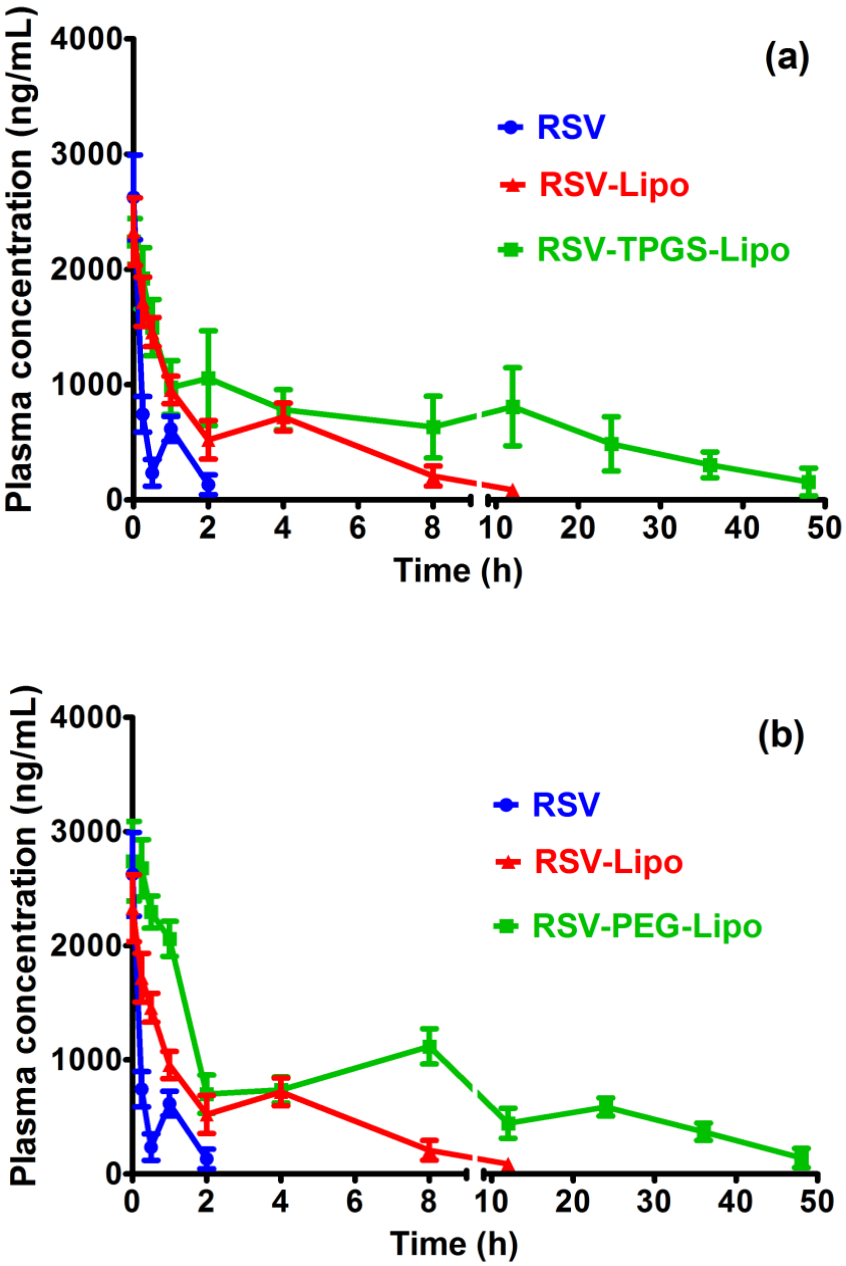

Figure 5.58. Comparative plasma concentration time profile of (a) RSV-TPGS-Lipo and (b) RSV-PEG-Lipo with RSV and RSV-Lipo up to 48 hours after *i.v.* administration of 2 mg/kg dose; Each data point is the representation of mean±SD (n=6).

Table 5.12. Pharmacokinetic parameters of RSV, RSV-Lipo, RSV-TPGS-Lipo and RSV-PEG-Lipo after intravenous administration of 2 mg/kg dose.

PK parameters	**RSV**	**RSV-Lipo**	**RSV-TPGS-Lipo**	**RSV-PEG-Lipo**
C_0 (ng/mL)	2463.5±334.46	2187±226.27	2357.51±14.14	2783.27±276.28
AUC (ng*h/mL)	1013.56±194.54	5296.38±943.28*	30349.73±4850.28*	27044.36±4617.33*
$t_{1/2}$ (h)	0.53±0.31	2.34±0.35*	15.72±2.96*	11.47±3.93*
CL (mL/h/kg)	1894.84±382.46	369.48±72.16*	57.40±7.59*	46.63±10.22*
V_d (mL/kg)	1431.82±220.73	1228.79±58.03	1318.45±417.23	683.11±103.93*
MRT (h)	0.58±0.18	3.19±0.20*	17.10±0.28*	16.96±0.81*

Data is presented as mean±SD (n=6); *Mark indicates significant difference from RSV ($p<0.05$).

5.5.15. Tissue distribution studies

Tissue distribution results are shown in Figure 5.59. RSV-Lipo, RSV-TPGS-Lipo and RSV-PEG-Lipo showed highest tissue accumulation in brain (6.95±0.97, 8.87±0.91 and 7.30±0.65 µg/g, respectively). The brain accumulation value of RSV-Lipo, RSV-TPGS-Lipo and RSV-PEG-Lipo was found to be approximately 9.01, 10.95, and 8.58 times higher than RSV ($P<0.05$). RSV-Lipo showed similar brain distribution like RSV-TPGS-Lipo and RSV-PEG-Lipo ($P>0.05$). Higher molecular weight drugs are not able to enter the brain due to presence of blood-brain barrier (BBB) and therefore cannot be useful in the treatment of brain diseases. Several nanocarriers were developed to improve the brain delivery of drugs. Liposomes are bilayer vesicles having lipophilic in nature. Several liposomal formulations were reported for higher brain accumulation. Our findings are well correlated with the earlier reports on brain accumulation of liposomes [204, 205]. Breviscapine loaded uncoated liposomes were showed 5 times higher brain distribution than pristine drug solution after intravenous injection in rats [205].

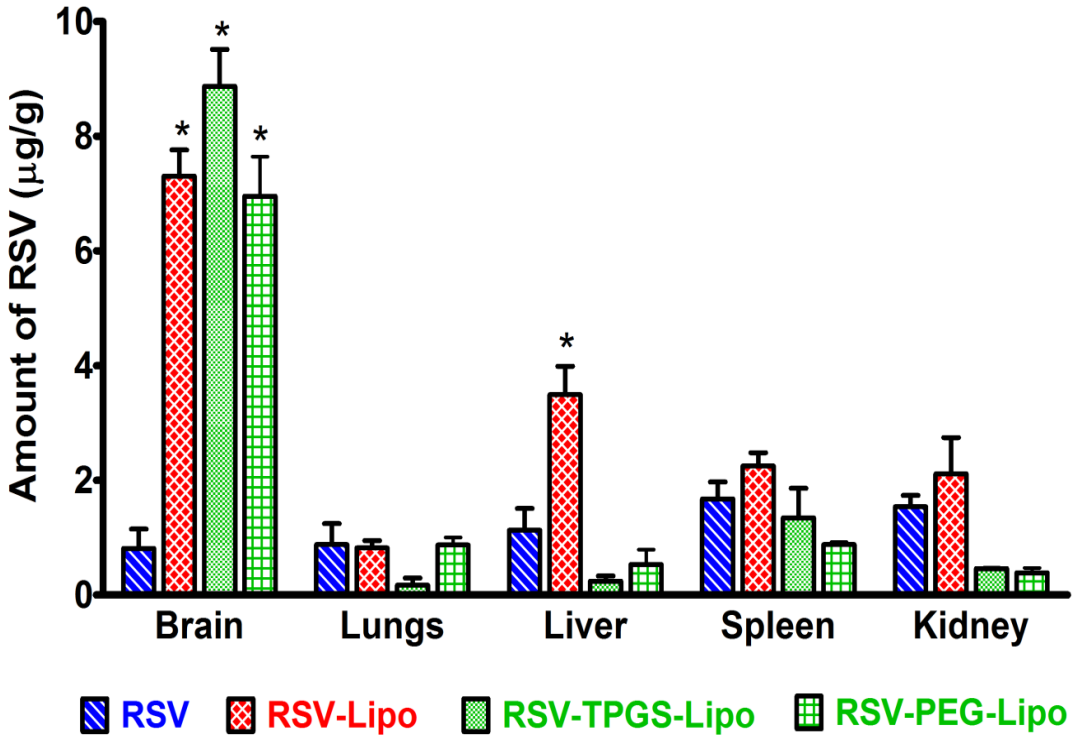

Figure 5.59. Comparative *in vivo* biodistribution of RSV, RSV-Lipo, RSV-TPGS-Lipo and RSV-PEG-Lipo in brain, lungs, liver, spleen and kidney after *i.v.* administration of 2 mg/kg dose; Values are represented as mean±SD (n=3). * Mark indicates statistically significant difference from RSV ($p<0.05$).

Distribution of RSV-Lipo, RSV-TPGS-Lipo and RSV-PEG-Lipo in lungs, spleen and kidney were found to be statistically similar with RSV. Liver is reported to be the major biotransformation site of RSV as well as major organ of reticulo endothelial system. RSV-TPGS-Lipo and RSV-PEG-Lipo showed 4.70 and 2.12 times lower accumulation than RSV and 14.56 and 6.58 times lower than RSV-Lipo in liver, respectively. RSV-Lipo showed 3.10 times higher liver distribution than RSV. The higher liver accumulation of RSV-Lipo is due to lipophilic nature of its components which can be

further explained by the physiology of reticulo endothelial system. This system comprised of macrophages and monocytes, liver kupffer cells, lymphatic vessels and spleen to remove foreign material from the body. RSV-Lipo comprised of hydrophobic molecules such as RSV, phospholipid and cholesterol. All these components render hydrophobic nature to the surface of the vesicles. Hydrophobic particles are more vulnerable to the RES uptake. When hydrophobic materials present in systemic circulation, plasma (opsonin) proteins are adsorbed at the surface of the materials. Consequently, phagocytic cells engulf the material and transport it to liver or spleen for degradation and excretion. RSV-Lipo is highly susceptible for opsonisation, engulfed by macrophages or monocytes and transported to the liver and spleen. Moreover, additional phagocytic macrophages permanently located in liver (also known as Kupffer cells) might trap more RSV-Lipo in the liver. The lower liver accumulation of RSV-TPGS-Lipo and RSV-PEG-Lipo is due to hydrophilic nature of the vesicles. TPGS and DSPE PEG 2000 molecules present at the surface of liposomes reduce opsonization process and thereby prevents the recognition by monocytes, macrophages and Kupffer cells. This resulted in lower liver accumulation and facilitated RSV-TPGS-Lipo and RSV-PEG-Lipo to remain in blood pool for prolonged period of time [210, 211]. The reduction of liver distribution obviously minimizes the rate of biotransformation of RSV in liposomal formulations. Moreover, liposomal encapsulated RSV present in the liver will not readily available for glucuronidation or sulfation like free RSV which further delays biotransformation process [37]. The higher liver accumulation of RSV-Lipo (naked or non-PEGylated liposomes) and lower uptake of RSV-TPGS-Lipo (PEGylated liposomes) is well correlated with earlier publications [212-214]. PEGylated liposomal doxorubicin

showed lesser liver accumulation in comparison to uncoated liposomes (LipoDox) in mice [212]. 7-Ethyl-10-hydroxy-camptothecin loaded PEGylated liposomes showed lower distribution in liver, spleen and kidney and two times higher plasma concentration in comparison to non-PEGylated liposomes [213]. In conclusion, biodistribution results showed that brain distribution RSV-Lipo, RSV-TPGS-Lipo and RSV-PEG-Lipo was found to be significantly higher than the RSV solution. Therefore, RSV-Lipo, RSV-TPGS-Lipo and RSV-PEG-Lipo can be effective tool for brain targeting of RSV for the treatment of glioma. The lower distribution of RSV-TPGS-Lipo and RSV-PEG-Lipo in liver (related to reticulo endothelial system) may suppress the biotransformation and prolongs systemic circulation. Therefore, both RSV-TPGS-Lipo and RSV-PEG-Lipo would be the best tool for prolonged systemic circulation and passive brain targeting.

5.5.16. Comparative results of RSV-TPGS-Lipo and RSV-PEG-Lipo

Characteristics	**RSV-TPGS-Lipo**	**RSV-PEG-Lipo**
Vesicular size	64.5±5.56 nm	250.2±9.03 nm
Polydispersity index	0.398±0.021	0.196±0.010
Zeta potential	-1.05±1.12 mV	-26.47±0.75 mV
Shape	Spherical	
Entrapment efficiency	83.05±3.59%	79.47±4.32%
In vitro release studies	Higuchi, anomalous	Higuchi, Fickian
Interaction analysis (DSC/FTIR)	No potential chemical interaction	
Analysis of crystallinity (XRD)	Crystalline to amorphous	
Cytotoxicity in C6 glioma cells (in comparison to RSV)	Higher cytotoxicity (due to TPGS)	Similar cytotoxicity
Cellular uptake	Excellent cellular internalization	
Haemolysis	Less than limit (10%), safe for *i.v.*	
Erythrocyte membrane integrity	Less than limit (10%) , safe for *i.v.*	
Platelet aggregation	No aggregation and safe for *i.v.*	
Pharmacokinetic studies	Higher AUC, $t_{1/2}$ (11-15 h)**;** present in blood up to 48 h	
Brain distribution (than RSV)	8.27 times higher	6.64 times higher